6. SITE 874[1]

Shipboard Scientific Party[2]

HOLE 874A

Date occupied: 12 June 1992

Date departed: 12 June 1992

Time on hole: 6 hr, 30 min

Position: 12°00.216′N, 164°56.388′E

Bottom felt (rig floor, m; drill-pipe measurement): 1386.0

Distance between rig floor and sea level (m): 11.1

Water depth (drill-pipe measurement from sea level, m): 1374.9

Total depth (rig floor, m): 1392.0

Penetration (m): 7.0

Number of cores (including cores with no recovery): 1

Total length of cored section (m): 7.00

Total core recovered (m): 1.50

Core recovery (%): 21

Oldest sediment cored:
Depth (mbsf): 174.0
Nature: limestone
Age: Maastrichtian

HOLE 874B

Date occupied: 13 June 1992

Date departed: 15 June 1992

Time on hole: 2 days, 12 hr, 43 min

Position: 12°00.228′N, 164°56.388′E

Bottom felt (rig floor, m; drill-pipe measurement): 1386.0

Distance between rig floor and sea level (m): 11.1

Water depth (drill-pipe measurement from sea level, m): 1374.9

Total depth (rig floor, m): 1579.5

Penetration (m): 193.5

Number of cores (including cores with no recovery): 24

Total length of cored section (m): 193.50

Total core recovered (m): 32.31

Core recovery (%): 16.7

Oldest sediment cored:
Depth (mbsf): 168.0
Nature: clay and claystone
Age: Campanian

Hard rock:
Depth (mbsf): 177.7
Nature: altered basalt
Measured velocity (km/s): 2.8–3.4

Basement:
Depth (mbsf): 187.0
Nature: basalt
Measured velocity (km/s): 4.5–5.6

Principal results: A local pre-site seismic survey was conducted on 12 June 1992 on the northeastern side of Wodejebato Guyot, across the two perimeter ridges that partly encircle the summit area of Wodejebato platform. Seven parallel seismic lines, spaced about 0.25 nmi apart and 1.6 nmi in length, were shot perpendicular to the axis of the ridges. These northeast-southwest transects along the rim and flank of the guyot, were intended to characterize the detailed features of these perimeter ridges. An 80-in.^{3} water gun was used as the seismic source. Coring began at Site 874 on 12 June 1992 and was completed on 15 June, after 2.7 days. Upon completion of the drilling, a logging program, including the geophysical and geochemical tool strings and the Formation MicroScanner (FMS) tool, was undertaken. After obtaining our drilling objectives and logging in Hole 874B, we departed Site 874 on 15 June 1992.

Site 874 is located at 12°00.76′N, 164°55.22′E, in 1374 m water depth, on the inner perimeter ridge near proposed Site SYL-4. The inner perimeter ridge appears as a constructional feature in the seismic profiles. The specific objectives at Site 874 were (1) to determine the constructional nature of the inner perimeter ridge, (2) to establish the characteristics of the facies and to evaluate their distribution in time, (3) to determine the nature of the acoustic basement reflector beneath the inner perimeter ridge, and (4) to interpret the subsidence history of the platform relative to sea-level fluctuations.

Two holes, Holes 874A and 874B, were drilled at Site 874 on the seaward side of the inner ridge crest. A reconnaissance of the seafloor was conducted with the vibration-isolated television (VIT); then Hole 874A was spudded in a shallow depression, <1 m deep, on bare rock with the rotary core barrel (RCB). After coring 10 mbsf, this first attempt failed. After another seafloor survey with the VIT, Hole 874B was successfully spudded on bare rock and cored with the RCB to a total depth (TD) of 193.5 msbf. Typical recovery was 19.7%, with poor recovery (0%–1.6%) in the skeletal packstone, which decreases the overall average recovery for the hole to 16.7%.

Four lithologic units were recognized at Site 874, using a combination of visual core descriptions, smear-slide and thin-section data, and downhole logging data. The age of these units was based on the identification of larger benthic foraminifers and macrofossils (rudists), and subordinately by calcareous plankton. The recognized units are, from top to bottom:

Unit I (0–0.11 mbsf) consists of a manganese-encrusted and phosphatized limestone conglomerate of late middle Eocene age. The conglomerate was cemented by phosphatized pelagic sediments of late middle Eocene, early Eocene, and late Paleocene age. Clasts of Maastrichtian foraminifer rudist grainstone are embedded in the crust.

Unit II (0.11–162.82 mbsf) consists of a sequence of white to light brown bioherms and associated facies of Maastrichtian to possibly late Campanian age. Lithologies are predominantly grainstone, but boundstone, packstone, rudstone, and wackestone were also recovered. The average carbonate content in Unit II is 95%. Major components include rudists (caprinids and radiolitids), red algae (corallinaceans, squamariaceans), foraminifers (*Sulcoperculina, Asterorbis,* miliolids), molluscan molds, corals, stromatoporoids, and echinoids. Unit II is divided into six subunits on the basis of depositional texture, skeletal constituents, and color. The porosity is mostly moldic, interparticle, or vuggy with a few solution-enlarged interparticle

[1] Premoli Silva, I., Haggerty, J., Rack, F., et al., 1993. *Proc. ODP, Init. Repts.,* 144: College Station, TX (Ocean Drilling Program).
[2] Shipboard Scientific Party is as given in the list of participants preceding the contents.

pores; estimated porosity typically ranges from 2% to 20%. Irregular solution cavities are partially filled with banded isopachous crusts of calcite cement and geopetal internal sediments. Cavities in the upper part of the sequence are filled with pelagic sediments of Maastrichtian to late Paleocene age.

Unit III (162.82–177.7 mbsf) consists of ferruginous clay and claystone of Campanian age, to an older, indeterminate age. The main lithologies include black clay, rich in woody material (TOC > 5%) and pyrite (30% sulfur), with a thin basal bed rich in larger foraminifers; and bluish gray to dusky red clay, with relict structures of vesicular, plagioclase-phyric basalt. Calcareous nannofossils of Campanian age occur in the upper part of the clay unit. Unit III is virtually carbonate free except for a single level in which carbonate content reaches 0.8%; this corresponds to the nannofossils and benthic foraminifer-bearing layer.

Unit IV (177.7–193.5 mbsf) consists of a single flow of altered ankaramitic basalt. The groundmass is alkali olivine basalt, similar to those recovered at the other sites on Wodejebato Guyot.

Magnetic measurements were undertaken on a few discrete samples of basalt. The range of inclination of all the samples is from +9.6° to +23.1°, which is slightly lower than that sampled at Site 873 (+17° to +27°). These data may be tentatively interpreted as representing a reversed polarity magnetization acquired at a low southern latitude (~9°S).

In Hole 874B, the lower 130 m of the carbonate platform was successfully logged with the FMS, and the geophysical and geochemical tool strings. Near the base of Unit II at 143 mbsf, the top of the rhodolith-rich, algal grainstone facies is associated with a well-cemented surface that is overlain by a uranium-concentration horizon. This association suggests the possibility of a condensed interval and perhaps a hiatus in sedimentation. The overlying reddish yellow grainstone (Subunit IIE) also has a uranium-concentration horizon at its upper limit at 123 mbsf. Between 80 and 38 mbsf, a series of upward-increasing resistivity cycles occur that are interpreted to be shallowing-upward sequences associated with Subunit IIC. These cycles become thinner and better cemented toward the top of this facies; the irregular sharp tops of the higher cycles may be exposure surfaces.

BACKGROUND AND OBJECTIVES

For a discussion of the geologic history of Wodejebato Guyot and previous studies, see the "Background and Objectives" section, "Site 873" chapter (this volume).

Previous drilling at Site 873, located in the central portion of Wodejebato Guyot, recovered Upper Cretaceous lagoonal strata composed of skeletal packstone, grainstone, and wackestone. Overall recovery by rotary core barrel (RCB) drilling in Hole 873A was 20.1%, but recovery was very low in the Upper Cretaceous platform limestones (2.5% for the uppermost 34 m). The motor-driven core barrel (MDCB) was used in Hole 873B, in an attempt to recover the upper 11 m of platform sediments; this yielded 39.1% recovery, although six times the length of time was needed to core these 11 m in comparison to RCB coring at Hole 873A.

The skeletal wackestone to grainstone recovered at Site 873 contained reef debris, but boundstone from a reef or biostrome was not recovered at Site 873 and logging results did not reveal any evidence that a reef or biostrome had been encountered. Therefore, in an attempt to acquire reef limestones with a more pronounced signature of sea-level change, the drilling objective was focused on investigating the perimeter ridges (associated with proposed Site Syl-4) that encircle the summit area of Wodejebato platform. On seismic profiles and SeaMarc II imagery, there are two perimeter ridges along the north and east rims of this guyot, but only the inner perimeter ridge is consistently present around the west rim of the guyot. These ridges appear as constructional features in the seismic profiles. The inner perimeter ridge was chosen as a first target because it had a distinct acoustic basement reflector beneath it and a thicker carbonate sequence (on the basis of the two-way traveltime) than the outer perimeter ridge.

The specific objectives at Site 874 were (1) to verify the nature of the inner perimeter ridge, (2) to determine if it was built with reefal facies and to evaluate their distribution in time, and (3) to interpret the subsidence history of the atoll relative to sea-level fluctuations and tectonic subsidence.

Drilling and logging at Site 874 were very successful. The primary objectives associated with this site are addressed with the preliminary shipboard studies and additional shore-based studies.

OPERATIONS

Transit to Site 874

The ship departed Site 873 with the 200-in.^{3} water gun streamed for a seismic survey and soundings being made with the 3.5-kHz echo sounder. At approximately 6 nmi from Site 873, a series of seven crossings over two narrow (≤0.5 nmi wide) perimeter ridges along the north-northeast rim of Wodejebato Guyot were made to characterize these perimeter ridges and select the location of Site 874. After 5 hr of surveying, the positioning beacon was launched at 0615L (L = local time) on 12 June 1992.

Site 874—Wodejebato Guyot, Inner Perimeter Ridge

The perimeter ridges appear to be constructional features, potentially reefs, on the basis of the site survey geophysical profiles. The inner perimeter ridge ponds sediment on the summit of Wodejebato Guyot; however, the surfaces of both the inner and outer ridges are typically devoid of any significant pelagic sediment cover.

Hole 874A

The vibration-isolated television (VIT) was deployed during the initial pipe trip. When the bottom-hole assembly (BHA) and VIT were in position, just above the bare-rock seafloor, the top drive was picked up and the drill string was spaced out so that a core could be cut and retrieved without an additional connection.

A reconnaissance of the seafloor was conducted by moving the ship on automatic-station-keeping (ASK) offsets. After a 45-min search, a small depression was located that could potentially supply lateral containment of the bit for spudding. The bit was set into the depression and held there by means of the drill-string motion compensator while the VIT was recovered to the ship. On the basis of drill-pipe measurement (DPM), the seafloor was 1386.0 m below the dual-elevator stool (DES) or 1374.9 m below sea level.

Hole 874A was spudded at 1330L on 12 June 1992 when rotation of the drill string began. Irregular torque occurred during the initial spudding of the hole; a minimal weight on bit (WOB) of 6,000–10,000 lb and a rotating speed of about 40 rpm were maintained to prevent the bit from skating on the seafloor or stalling. The ROP was relatively slow; approximately 2.5 hr were required to cut a 7-m core. The 7-m depth of the hole was sufficient to enable retrieval of a core without pulling the bit above the seafloor and to provide a sample for determination of the limestone facies.

The drill string began torquing and sticking in the hole while the first core was being recovered. Because no connection was to be made, the inner barrel was recovered and the replacement barrel dropped through the traveling block and the full-diameter oil saver. This permitted the pipe to be held lower in the hole and allowed minimum interruption of rotation and circulation. A 1.5-m core of limestone was recovered, and a second core of 3 m was cut in 1 hr. Hole conditions seemed normal during the coring operation, but severe torquing and sticking occurred as soon as the bit was lifted off bottom for the wireline trip.

A viscous mud sweep was circulated while the pipe was "worked" in the hole to free it. The drill string needed to be sufficiently free before it could be stopped for insertion of the wireline retrieving

assembly. Those measures failed to improve the situation and the string eventually became firmly stuck, apparently by chunks of limestone above the bit wedging it in the bit-sized hole. After approximately 30 min of attempting to free the string, both mud pumps were put on-line at full circulation. With strong overpull and pump assistance, the bit began to move up the hole, only to stick again. As the maximum intended overpull was reached, the ship heaved and overpull jumped to about 310,000 lb. The string suddenly came free, jolting the ship. When circulation was reduced to the normal rate, it was noted that about 150 psi of circulation pressure had been lost and that there was an apparent slight loss of drill-string weight.

A failure had occurred low in the BHA, possibly at the bit sub. A wireline run was made to attempt to retrieve the inner core barrel and core before the string was raised enough to clear the hole. The pulling tool encountered an obstruction in the pipe at the proper depth for the inner core barrel, but the barrel could not be engaged. The drill string then was recovered to assess the damage and replace the lost components.

Upon recovery of the BHA, it was observed that the connection between the top sub of the outer core barrel (OCB) assembly and the OCB drill collar had failed, leaving the drill collar, bit sub, and bit in the hole. In addition, the inner barrel assembly had parted at the connection between the barrel tube and the swivel. The latch and swivel were trapped in the failed and deformed connection with the swivel extending about 40 cm below the pin. The failure of the rotary-shouldered connection was typical of buckling failures that occur when unsupported drill collars are put into compression. The pin of the connection was partially collapsed and the threads were stripped out of the box. Apparently, the damage occurred during attempts to free the stuck and unsupported pipe by applying weight. The overpull triggered the final parting.

Hole 874B

The new BHA was given an electromagnetic inspection as it was run through the rotary table, in case other connections were damaged. No other damage was found. As at Hole 874A, the VIT was run and the string was spaced out for coring. Before starting the search for a new site, Hole 874A was videotaped with the OCB extending about 2 m above the seafloor. Following this, the new drilling location was determined by a survey of the seafloor topography that lasted about 1 hr.

About 50 m west of Hole 874A, a sediment chute was located adjacent to an outcrop that stood about 1 m above the sediment surface. By landing the bit on the side opposite the outcrop and then in the chute, the chute was estimated to be about 1.5 m wide and 0.5 m deep. The bit was kept in the middle of the chute with the motion compensator while the VIT was recovered. The seafloor was 1384.9 m below the DES on the basis of the drill-pipe measurement or 1373.8 m below sea level.

Rotation of the drill string began at 0645L on 13 June 1992. The first few meters of limestone were denser than at Hole 874A, with ROP averaging less than 1 m/hr for the uppermost 3.5 m. An 8-m interval of softer limestone then permitted burial of the core barrel before another hard layer was penetrated. Core recovery averaged 14.9% over the first 86.2 m, but a trend toward higher ROP with depth was accompanied by a trend toward reduced recovery (Table 1). The interval from 86.2 to 116.8 mbsf, cored at up to 100 m/hr, produced a total of 20 cm of skeletal coral packstone in the upper 15.5 m, and no recovery in the lower 15.1 m. The underlying grainstone displayed an increase in recovery above the contact (162.8 mbsf) with clay. Core recovery was good in the 14.9 m of clay and claystone (162.8–177.7 mbsf; recovery = 58.3%), and in the 15.8 m of altered basalt (177.7–193.5 mbsf TD; recovery = 44.7%). In the basalt, ROP fell to 1 m/hr at times.

A wiper trip was made in preparation for logging; the pipe began to stick near the top of the trip and a solid ledge was met as the bit was lowered back to 68 mbsf. The ledge was reamed away with the top drive. The bottom of the hole contained 8 m of fill. A 20-bbl sweep of viscous mud was circulated to clean the hole, and the bit subsequently

Table 1. Coring summary, Site 874.

Core no.	Date (June 1992)	Time (Z)	Depth (mbsf)	Cored (m)	Recovered (m)	Recovery (%)
144-874A-						
1R	12	0530	0.0–7.0	7.0	1.50	21.4
Coring totals				7.0	1.50	21.4
144-874B-						
1R	13	0100	0.0–9.7	9.7	1.40	14.4
2R	13	0500	9.7–19.2	9.5	1.89	19.9
3R	13	0800	19.2–28.7	9.5	3.00	31.6
4R	13	0935	28.7–38.1	9.4	0.60	6.4
5R	13	1110	38.1–47.6	9.5	2.46	25.9
6R	13	1320	47.6–57.2	9.6	1.34	13.9
7R	13	1420	57.2–66.9	9.7	0.59	6.1
8R	13	1520	66.9–76.6	9.7	0.31	3.2
9R	13	1620	76.6–86.2	9.6	1.25	13.0
10R	13	1700	86.2–91.2	5.0	0.08	1.6
11R	13	1755	91.2–96.2	5.0	0.06	1.2
12R	13	1835	96.2–101.7	5.5	0.06	1.1
13R	13	1915	101.7–107.2	5.5	0.00	0.0
14R	13	2025	107.2–112.0	4.8	0.00	0.0
15R	13	2110	112.0–116.8	4.8	0.00	0.0
16R	13	2200	116.8–126.4	9.6	0.44	4.6
17R	13	2245	126.4–136.0	9.6	0.92	9.6
18R	13	2335	136.0–143.5	7.5	0.57	7.6
19R	14	0115	143.5–153.1	9.6	1.38	14.4
20R	14	0205	153.1–162.8	9.7	0.22	2.3
21R	14	0340	162.8–172.4	9.6	3.60	37.5
22R	14	0545	172.4–177.7	5.3	5.08	95.8
23R	14	1115	177.7–184.0	6.3	2.70	42.8
24R	14	1620	184.0–193.5	9.5	4.36	45.9
Coring totals				193.5	32.31	16.7

was released with no problem. The mechanical bit release (MBR) top connector was pulled to 36 mbsf and logging preparations were made.

A standard suite of Schlumberger logs was run. The geophysical tool string was stopped by an apparent bridge at 176 mbsf in the clay zone. Because competent sediment extended up to the seafloor, it should have been possible to raise the drill string and log the open hole to within a few meters of the seafloor. However, the weight indicator showed that the pipe was not completely free in the hole, and therefore the blocks were not raised to expose additional hole. If this was done and difficulty had been encountered in lowering the string after passage of the tool, the drill string and the additional logs would have been jeopardized. The FMS and geochemical logs were recorded successfully; both tools recorded data as deep as 171 and 168 mbsf, respectively (see Table 2). After logging was completed, the backup geochemical tool was picked up and run down the pipe to 100 m for in-pipe calibration checks. The tool was determined to be operational and was recovered after logging ended. The test required an additional hour of operating time.

While logging operations were in progress, the VIT frame was lowered to check the top of the hole. The cuttings pile and apparent hole size were noted, videotaped, and compared with the pre-spud videotape. The consensus was that reentry could be made into Hole 874B without the aid of any seafloor hardware, if reentry was needed.

With the logging sheaves rigged down, the pipe trip out of the hole began. With the MBR top connector at 3 mbsf, the drill string became stuck and 100,000-lb overpull was required to pull it free. During the pipe trip, the two positioning beacons were recovered and the rig began offsetting toward Site 875.

UNDERWAY AND SITE GEOPHYSICS

Introduction

Sites 874 through 877 all lie on the perimeter ridges along the northeast rim of Wodejebato Guyot (Figs. 1–2). Before drilling, existing data over this region included SeaMARC II side-scan images and bathymetry, single-channel and six-channel seismic records, and echo-sounder profiles from the 1988 *Moana Wave* Cruise (MW8805). In addition, the 1991 *Thomas Washington* Cruise (TUNE06) collected

Table 2. Well-log data recorded from Hole 874B.

Log type	Depth (mbsf)
Natural gamma ray	35–173
Sonic	35–173
Neutron porosity (AmBe neutron source)	35–173
Lithodensity (Ce gamma-ray source)	35–173
Resistivity	35–173
Aluminum clay (Ca neutron source)*	0–168
Gamma-ray spectrometry*	0–168
Formation MicroScanner	40–171

Notes: Log data assume that the seafloor is at 1374.0 m, with all logs correlated and depths shifted to the gamma-ray log from the geochemical tool string.

*These logs were recorded in pipe from 0 to 40 mbsf.

Sea Beam multibeam bathymetry over these ridges (H. Staudigel, pers. comm.). This section focuses on describing the area across which the perimeter ridges are found. A more thorough overview of the regional geology of Wodejebato Guyot is located in the "Underway and Site Geophysics" section, "Site 873" chapter (this volume).

Site Survey—*Moana Wave* and *Thomas Washington* Cruises

The two perimeter ridges on the northeast side of Wodejebato Guyot were first identified in the side-scan images collected during MW8805 (Fig. 3). In these images, the ridges appear as high backscatter (dark) bands along the northeast perimeter of the summit. Two ridges are present across areas where a shelf exists (e.g., adjacent to the volcanic ridges extending away from the flanks of the edifice) and both become more distinct across areas where the shelf widens. In areas where a shelf is not present, the outer ridge presumably eroded away (Fig. 3).

The inner ridge is slightly inset from the upper slope and, on the basis of the side-scan and seismic data, is more continuous along the perimeter of the summit than the outer ridge. The inner ridge identified in the seismic data exists primarily as an acoustically massive unit against which horizontal reflectors (presumably lagoonal sediments) truncate. Figure 3 shows a representative example of the seismic data. In this profile, the inner ridge consists of a packet of strong reflectors overlying a more acoustically massive unit. The packet of strong reflectors in this profile is 0.03 s two-way traveltime (TWT) thick. The maximum thickness of the inner ridge above the reflector interpreted as basement is 0.16 s TWT. Along the southern flank, faulting presumably removed the inner ridge.

As mentioned previously, the outer ridge is most distinct along the north and northeast sides of the guyot where the volcanic lobes extending away from the edifice form relatively wide shelves (Fig. 1). At some time in the past, the outer ridge may have extended along the entire north-northeast side of Wodejebato Guyot, as suggested by the two high-backscatter bands along the volcanic ridge attaching Wodejebato Guyot to Pikinni Atoll (Fig. 1). The outer ridge adjacent to the northeastern spur loses relief toward the edge of the shelf (Fig. 2). It exhibits a maximum thickness above the basement reflector of 0.12 s TWT.

A small trough separates the outer ridge from the inner ridge (Fig. 2). Relief on the inner ridge, measured from the axis of the trough to the top of the mound, is ~98 m; relief on the outer ridge is ~135 m (Fig. 3). The inner ridge extends ~45 m shallower than the outer ridge. Pelagic sediments do not cover the ridges in the area where the six-channel seismic line crosses.

Site Survey—Leg 144

Bathymetric coverage over the two perimeter ridges of Wodejebato Guyot was quite sparse, especially across the inner ridge northwest of the Sea Beam area shown in Figure 4. To address this inadequacy, we conducted a 3.5-kHz survey over the ridges. We departed from Site 873 on Julian Day (JD) 163 at ~1400Z (GMT time) and began collecting single-channel seismic and echo-sounder data at 1415Z using a 200-in.^{3} water gun as a source. The survey pattern consisted of seven northeast-southwest passes over the perimeter ridges (ship heading of 060°and 240°). The lines were run ~0.5 km apart at a ship speed of ~6 kt. A suitable location for Site 874 was identified on Line G–G′, and the beacon was dropped on a return pass over this line at 1915Z, along Profile F–F′. We recovered the seismic gear at ~1925Z, and the ship went on station at ~1945Z. Site 874 was moved ~0.3 km southwest of the beacon drop to drill a thicker section of the presumed reef sediments; this location corresponds to the coordinates of 1805Z on Line G–G′. Site 875 is located on the outer ridge in the area crossed by the six-channel seismic line; it lies ~0.95 km north of Site 874 (Figs. 3–4). Sites 876 and 877 are located on the outer and inner ridges, respectively. They lie approximately 1–2 km northwest of Sites 874 and 875 (Fig. 4). Profile A–A′ in Figure 5 shows their position with respect to the ridges in the 3.5-kHz echo-sounder records.

As stated previously, both ridges are only present along areas where a shelf extends from the summit. The echo-sounder bathymetry collected during this survey provides information on how the perimeter ridge morphology changes in response to shelf widening. As suggested by the side-scan images and the Sea Beam bathymetry, both ridges broaden to the northwest coincident with the increase in shelf width. The inner ridge doubles in width, from 0.9 km in Profile H–H′, to 1.8 km in Profile A–A′. Its gradient decreases from ~6° to ~2° over the same distance, and the landward side of the ridge becomes more hummocky. The outer ridge also increases in width to the northwest, from <0.5 km in Profile H–H′ to 1.6 km in Profile A–A′. Where the shelf ends along the north flank of the guyot, the outer ridge disappears, apparently through erosion. Pelagic sediment, contained behind the inner ridge in Profile H–H′, begins to lap over this topographic high by the position of Profile C–C′ and creates a thin cover over the outer ridge by Profile B–B′.

Figure 6 shows the location of Sites 874, 876, and 877 with respect to the seismic profiles collected during Leg 144. The seismic data over the ridges shows a pair of reflector packets similar to those identified in the six-channel data. Across the inner ridge, a packet of strong reflectors 0.09 s TWT thick overlies a more acoustically massive unit. On the outer ridge, the packet of strong reflectors thins to 0.06 s TWT. Each of these thicknesses is greater than that shown in the six-channel seismic line. This suggests either that these units vary along the strike of the ridge or that the data requires additional processing to remove the source pulse. The reflector interpreted as basement lies 0.20 s TWT beneath the top of the inner ridge for both Sites 874 and 877, and 0.14 s TWT beneath Site 876 on the outer ridge. These thicknesses compare favorably with those observed on the six-channel profile for the inner and outer ridges (0.16 and 0.14 s, respectively). Velocity pull-up of the reflector precludes any detailed analysis of its variance along-strike.

LITHOSTRATIGRAPHY

Drilling results obtained in the two holes at Site 874 on Wodejebato Guyot are summarized in a single lithostratigraphic framework (Fig. 7 and Table 3). Lithologic units are identified by characteristics such as color, carbonate and clay content, fossil and particle constituents, lithification, sedimentary structures, and log characteristics. The four major lithologies identified at this site are (1) manganese crust and manganese-phosphate coated limestone conglomerate (Hole 874A, 0–0.14 mbsf; Hole 874B, 0–0.11 mbsf); (2) rudist algal foraminifer limestone (Hole 874A, 0.14–7 mbsf; Hole 874B, 0.11–162.8 mbsf); (3) ferruginous clay, claystone, and extremely altered vesicular basalt (Hole 874B, 162.8–177.7 mbsf); and (4) basalt (177.7–193.5 mbsf). The lithologic units and subunits are summarized in Figure 7 and Table 3, as well as being described below.

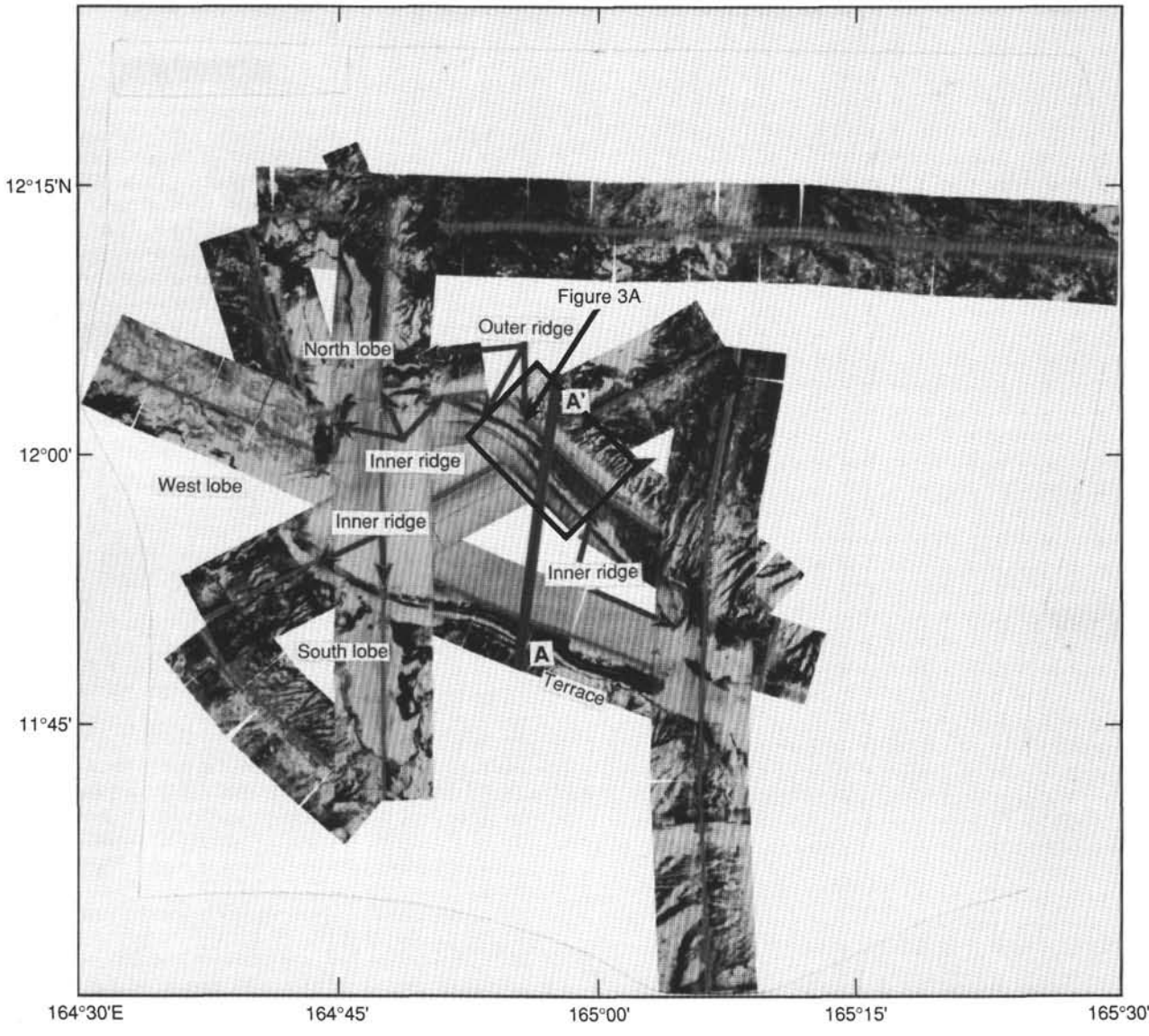

Figure 1. Side-scan images over Wodejebato Guyot during Cruise MW8805. In these images, dark tones represent high backscatter features, and light gray to white tones represent low backscatter features. The inner ridge appears as a dark band extending around three-fourths of the summit perimeter. The outer ridge is present along the northern and northeastern flank ridges, and possibly along the volcanic ridge attaching Wodejebato Guyot and Pikinni Atoll.

Unit I

Intervals: Hole 874A, Interval 144-874A-1R-1, 0–14 cm; Hole 874B, Interval 144-874B-1R-1, 0–11 cm
Depths: Hole 874A, 0–0.14 mbsf; Hole 874B, 0–0.11 mbsf
Age: Maastrichtian to middle Eocene

In Hole 874A, Unit I is comprised of a dense manganese crust, up to 1 cm thick, overlying well-cemented foraminifer rudist grainstone and commonly underlying a manganese-phosphate-coated limestone conglomerate (Fig. 8).

The upper few centimeters of the foraminifer rudist grainstone are recrystallized, scalloped, and red stained (2.5YR 5/8); manganese dendrites and threads grow inward. The manganese crust is black (2.5YR N2.5/0) and up to 1 cm thick; it includes multiple generations of digitate and laminated accretions. Thin red to yellow coatings, probably phosphatic, occur at the top of the manganese dendrites. Clasts of foraminifer rudist grainstone, 2–3 mm in size, are embedded in the crust. Pores between the manganese accretions are filled with several generations of pelagic limestone rich in planktonic foraminifers and nannofossils; similar yellow (10YR 7/6) to white (10YR 8/2) pelagic limestone infills irregular cavities in the encrusted foraminifer rudist grainstone. The manganese has clearly replaced some of the original lithology and cuts grains of the pelagic infillings.

The dense manganese crust is overlain in some samples by a manganese-phosphate-coated limestone conglomerate made of clasts of yellow to very pale brown limestones with planktonic foraminifers and nannofossils. The outer edges of clasts are stained red to reddish yellow by phosphate. These clasts support bulbous to dendritic manganese accretions that grow in every direction. Several infillings of very pale brown limestone with planktonic foraminifers occur in this limestone conglomerate.

In Hole 874B, manganese encrusts two pebbles of planktonic foraminifer limestone at the top of Core 144-874B-1R. Crusts are up to 15 mm thick, black (N2), and structureless to botryoidal. Dendrites with tiny laminated hemispheres (botryoids or digitate accretions) extend up to 20 mm into the planktonic foraminifer limestone.

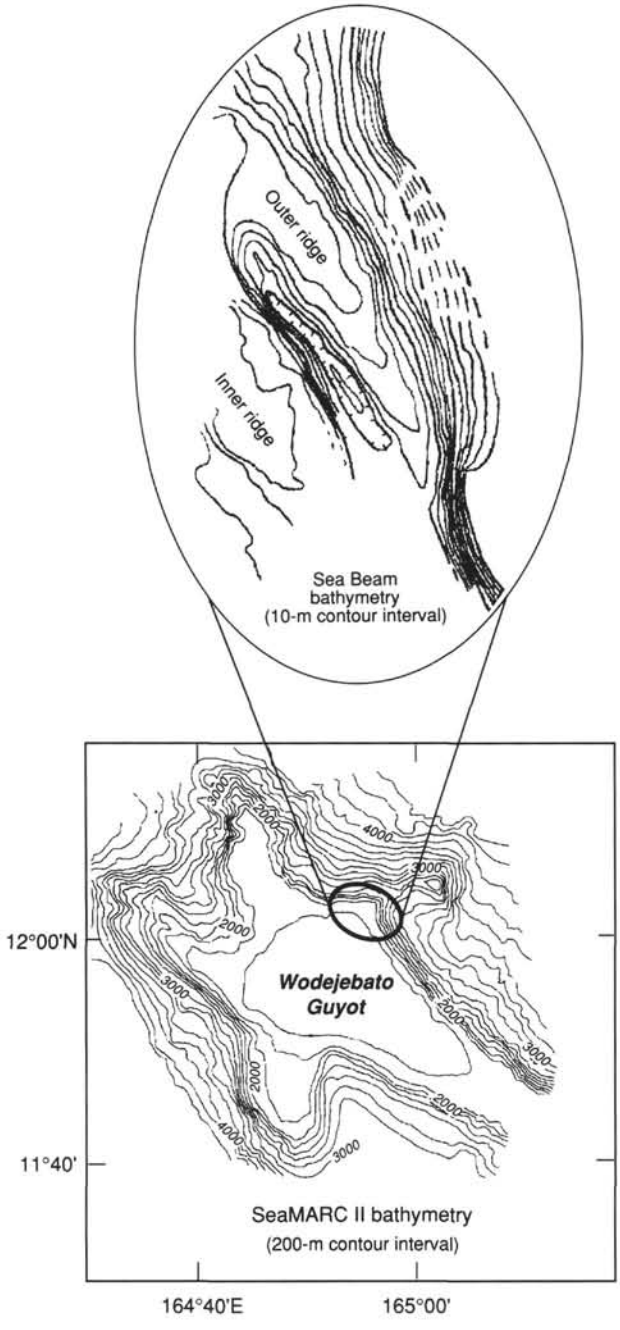

Figure 2. SeaMARC II and Sea Beam bathymetric coverage over Wodejebato Guyot and the perimeter ridges, respectively. The Sea Beam bathymetry requires additional processing to correct for depth inconsistencies with the echo-sounder bathymetry collected during Leg 144; the data set as a whole, however, shows the relative morphology of the ridges better than the hand-contoured map shown in Figure 4. Use of Sea Beam data courtesy of Hubert Staudigel at Scripps Institution of Oceanography.

Replacement appears to follow no pattern although some foraminifers may be selectively impregnated; other surfaces (e.g., burrow margins, clast boundaries) appear to have been conduits for manganese. Phosphate occurs as a patchy brownish yellow (10YR 6/6) stain through the limestone; many grains (including pellets?) up to 1 mm in diameter, are phosphorite. The planktonic foraminifer limestone also contains a few millimeter-size lithoclasts with echinoderms and molluscan fragments, several fish(?) bone or tooth fragments(?), and grains of manganese oxide (up to 2 mm in diameter). Burrows are common. They are 0.2 to 1 mm in diameter, straight, branching or networks, and they are filled by gray mud with sparse planktonic foraminifers.

In Hole 874B, clasts of pelagic limestone embedded in the manganese crust include nannofossils and planktonic foraminifers of late Paleocene age. Several generations of pelagic infillings (Fig. 9), including both nannofossils and planktonic foraminifers, are recorded. They range in age from the late Paleocene to middle Eocene (see "Biostratigraphy" section, this chapter).

In Hole 874A, the base of Unit I is placed at a depth of 0.14 mbsf, in contact with the underlying unit. In Hole 874B, the contact with the underlying unit was recovered at a depth of 0.11 mbsf. Unit I could be as thin as 10 or 11 cm in the two holes, or it could be thicker. The slow accretion rates of such manganese crusts (a few millimeters per million year) argues against a significantly greater thickness.

Unit II

Intervals: Hole 874A, Sections 144-874A-1R-1, 14 cm, through -1R-2, 26 cm; Hole 874B, Section 144-874B-1R-1, 11 cm, through -21R-1, 2 cm
Depths: Hole 874A, 0.14–1.74 mbsf; Hole 874B, 0.11–162.82 mbsf
Age: Maastrichtian to late Campanian?

Unit II is a 162.7-m-thick sequence of white (10YR 8/1, 10YR 8/2), very pale brown (10YR 7/3, 10YR 7/4, 10YR 8/3), light brown (10YR 8/4), light gray (10YR 7/2), yellow (10YR 7/8), and reddish yellow (5YR 7/8) platform carbonates that are dominated by grainstone but that also include boundstone, packstone, rudstone, and wackestone. Major components include rudists (caprinids and radiolitids), red algae (corallinaceans and squamariaceans), benthic foraminifers (mostly larger foraminifers and miliolids), common molluscan molds (bivalves and gastropods), corals, stromatoporoids, and a few echinoids. These limestones contain a rich assemblage of larger foraminifers, including *Sulcoperculina, Asterorbis*, and *Omphalocyclus*(?), indicating a Maastrichtian age (see "Biostratigraphy" section, this chapter).

Pelagic limestones that infill irregular cavities in the Maastrichtian platform limestones have been dated as Maastrichtian (probable), early late Paleocene in Interval 144-874B-3R-1, 114–118 cm, and late early Eocene in Interval 144-874B-1R-1, 47–50 cm (see "Biostratigraphy" section, this chapter).

Unit II is divided into six subunits on the basis of depositional texture, variations in skeletal constituents, and color (Table 4). Relationships between lithology and measured porosities for Unit II (see "Physical Properties" section, this chapter) are shown in Figure 10. All of the cores recovered from Unit II are shown in composite photographs in Figures 11–13. Average recovery in the interval from 0.1 to 162.82 mbsf was 8.84%; core recovery was nil between 101.7 and 123.5 mbsf (see "Operations" section, this chapter).

Subunit IIA

Intervals: Hole 874A, Section 144-874A-1R-1, 14 cm, through -1R-2, 26 cm; Hole 874B, Section 144-874B-1R-1, 11 cm, through -2R-1, 140 cm
Depths: Hole 874A, 0.14–1.74 mbsf; Hole 874B, 0.11–11.1 mbsf
Age: Maastrichtian

Subunit IIA consists of 11 m of skeletal grainstone and rudstone with intervals of boundstone. The color is very pale brown (10YR 7/4, 10YR 8/2 to 10YR 8/4), light gray (10YR 7/2) to white (10YR 8/2) with local patches of reddish yellow (7.5YR 6/8). The average carbonate content in Subunit IIA is 98.6%, and the total organic carbon content is 0.14% (see "Organic Geochemistry" section, this chapter). The average recovery in the interval from 0.11 to 11.1 mbsf was 17.15% (see "Operations" section, this chapter).

Skeletal grainstone and rudstone are generally poorly sorted and medium coarse to very coarse grained, with various amounts of gravel-sized fragments. Rudist fragments (mostly caprinids, but also some radiolitids; Fig. 14) are abundant throughout the subunit; as are

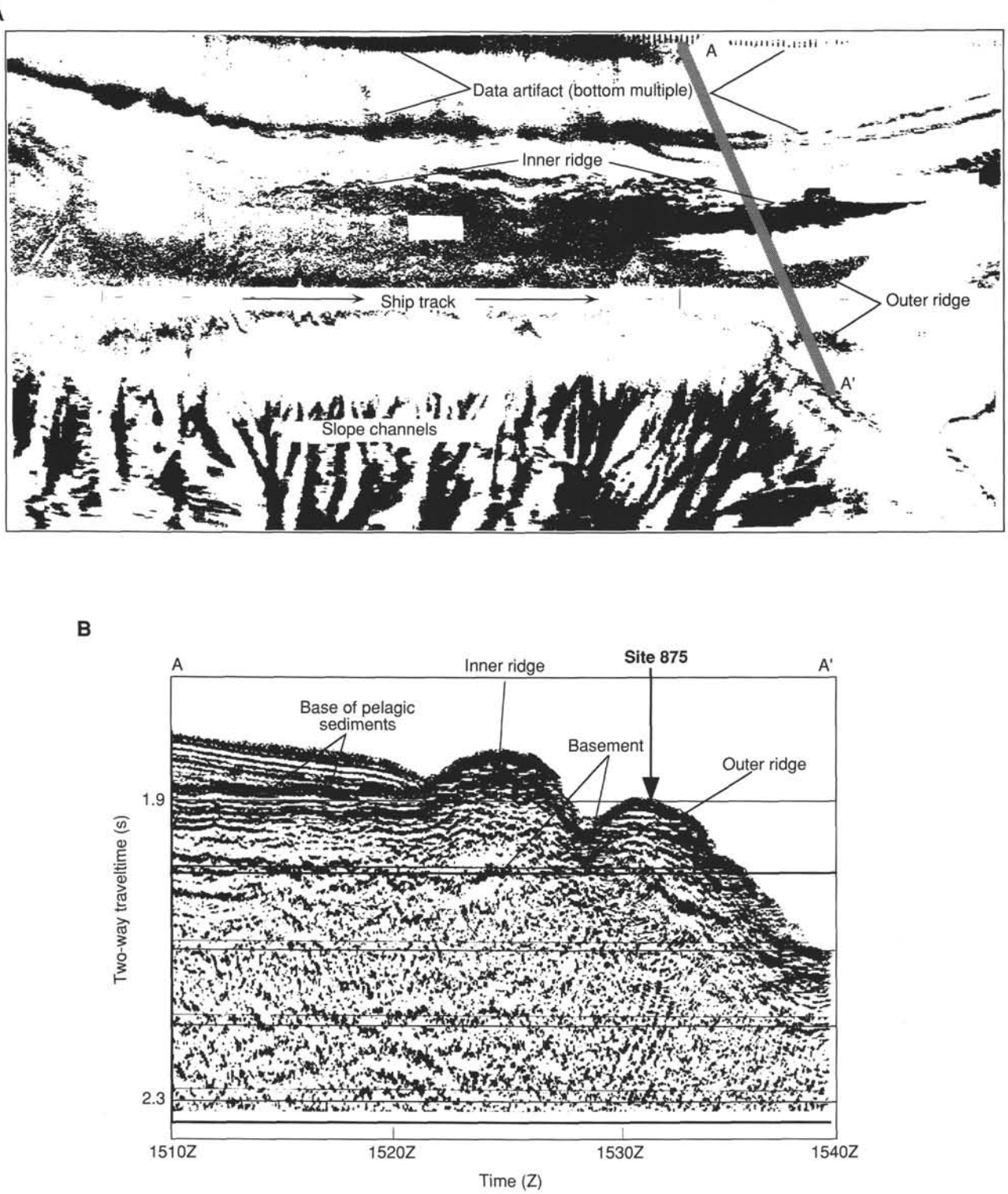

Figure 3. **A.** Side-scan image across the northeast flank of Wodejebato Guyot showing the inner and outer ridges. The shelf formed by the volcanic lobe extending away from the edifice appears at the right-hand side of the figure. The outer ridge disappears near the edge of this shelf, slightly to the left of the line marking Profile A–A′. High-backscatter channels disrupt the flank of the guyot, suggesting that erosion has removed the outer ridge along areas away from a more stable shelf. **B.** A portion of the migrated six-channel seismic profile collected during Cruise MW9009. This line crosses the ridges obliquely, so it does not show the true width of these features. The strong reflector underlying the ridges marks the base of the carbonate sediments. The location of Site 875 has been projected onto this profile.

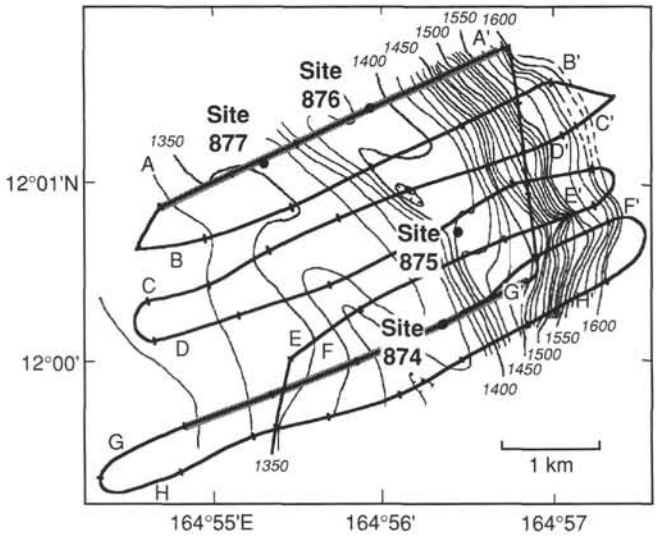

Figure 4. Hand-contoured bathymetry map across the perimeter ridges. Ship tracks show the 3.5-kHz survey implemented during Leg 144. Profiles A–A′ through H–H′ from the 3.5-kHz echo sounder are shown in Figure 5. Thick gray lines designate the location of single channel seismic Profiles A–A′ and G–G′, shown in Figure 6. Contour intervals in 10-m increments.

fragments of red algae (corallinaceans). Red algae associated with other encrusters (especially bryozoans and worms) may form thin encrustations (0.3–1 mm in average thickness) over large skeletal pieces and rhodoliths 1.0–1.5 cm in diameter (e.g., Interval 144-874A-1R-1, 120–133 cm). Larger foraminifers (especially orbitoids) are common and sometimes fragmented. Coral (encrusting and branching forms of *Hexacorallia* and *Octocorallia*), stromatoporoid fragments, and molluscan molds (bivalves, gastropods) also occur; a few fragments of calcareous sponges (chaetetids) are present. Large skeletal fragments typically have millimeter-sized borings. Reworked fragments of black manganese microconcretions occur locally (e.g., Core 144-874B-2R); a few of these concretions are 0.75 mm in diameter and have internal cavities filled with calcite cement. Brown-stained (phosphate?) grains are also present in the same beds. The grainstone and rudstone of Subunit IIA are strongly cemented; multiple generations of banded cements occur throughout, but no consistent pattern was recognized. Locally, cements are conveniently color coded: (1) white to very pale brown isopachous equant calcite; (2) cloudy, translucent, gray isopachous calcite; (3) milky white or yellow spar; (4) clear bladed calcite; and (5) gray, translucent, coarse-crystalline calcite. Porosity ranges from 2% to 20% and is mostly moldic (especially in caprinid shells) with few solution-enlarged interparticle pores. Moldic pores and irregular solution cavities are partially filled with banded (white, very pale brown to rusty orange) isopachous crusts of calcite cements and geopetal "internal sediment" consisting of a very pale brown fine-grained skeletal grainstone that is distinctly different from the host rock.

Intervals 144-874A-1R-1, 92–104 cm, and -1R-2, 51–136 cm, consist of boundstone that contains numerous layers of encrusting stromatoporoids and corals that are apparently interlayered with, or enclose, initially unconsolidated sediment. In addition, extensive red algal encrustations of radiolitid rudists are present, some of which appear to be in growth position (e.g., Intervals 144-874B-1R-1, 66–75 cm, and -1R-1, 95–104 cm). Other framework components include globular stromatoporoids, chaetetids, encrusting worms, and foraminifers. Red algal (corallinaceans) clumps reach at least 40 mm in height. The matrix is skeletal grainstone or generally well-sorted packstone (locally), of medium-sand size (0.25–0.50 mm). Identifiable grains include rudist fragments including both radiolitids and caprinids, benthic foraminifers (miliolids, larger foraminifers), and encrusting foraminifers and worms; there are also many unidentified molds.

Subunits IIA and IIB are distinguished by a clear change in sedimentary texture (see below). The contact was not recovered.

Subunit IIB

Interval: Section 144-874B-2R-2 through Core 144-874B-4R
Depths: 11.1–38.1 mbsf
Age: Maastrichtian

Subunit IIB consists of 27 m of very pale brown (10YR 7/3) to white (10YR 8/2) foraminifer rudist packstone (locally grainstone) and light gray (10YR 7/2) to pinkish gray (5YR 6/2) gastropod wackestone to mudstone. The contact between the packstone and wackestone is generally sharp and scalloped. The average carbonate content in Subunit IIB is 96.5%, and the total organic carbon content is 0.15% (see "Organic Geochemistry" section, this chapter). Recovery in the interval from 11.1 to 38.1 mbsf averaged 19% (see "Operations" section, this chapter).

Major components of the skeletal packstone and grainstone of Subunit IIB are benthic foraminifers (larger foraminifers, miliolids) and rudist fragments, which include both radiolitids and caprinids. Radiolitid clusters occur in Interval 144-874B-3R-3, 0–18 cm (Fig 15). Molds of other bivalves and gastropods are common, as are red algae (corallinaceans). Fragments of calcareous sponges (chaetetids) are rare. Black grains of manganese and brown phosphate grains occur in trace abundances; lithoclasts are rare. Allochems are mostly <500 mm (fine-sand size), although some layers are predominantly medium to coarse grained. Some burrows are present. Porosity ranges from 5% to 20% and is moldic (leached bivalve fragments locally including rudists and gastropods), interparticle, and vuggy (solution-enlarged molds). Packstone are conspicuously "chalky," probably a result of extensive dissolution. Thin-bladed calcite cement crusts line the moldic pores.

Geopetal pockets of yellowish, reddish, or rusty brown internal sediment occur sporadically, especially in centimeter-sized cavities, some of which are dissolved rudist fragments (Figs. 16–17). The average calcium carbonate content in these internal fills is 60%–62%.

Gastropod wackestone and mudstone display laminae that are commonly cut irregularly because of burrowing (common millimeter-sized tubes), loading, and/or fluid escape (Fig. 18). Components include small gastropods, thin-shelled bivalves and benthic foraminifers (miliolids), and at least one mold of dasycladacean algae. Moldic porosity is 5%–10% after these grains.

Subunit IIC

Interval: Cores 144-874B-5R through -9R
Depths: 38.1–80 mbsf
Age: Maastrichtian

The top of Subunit IIC is defined at 38.1 mbsf (top of Core 144-874B-5R) and coincides with uranium and resistivity peaks recorded by downhole logging (see "Downhole Measurements and Seismic Stratigraphy" section, this chapter).

Subunit IIC is comprised of 41.9 m of white (10YR 8/1 to 10YR 8/2) to very pale brown (10YR 8/3) algal-rudist grainstone and rudstone, few packstone layers and, algal-coral boundstone, although the existence of a true framework is difficult to ascertain in cores. Two pieces of skeletal packstone and wackestone recovered at the top of Interval 144-874B-6R-1, 0–7 cm, are drilling pebbles that were probably reworked from the overlying subunit. In Subunit IIC, the average carbonate content is 96.15% and total organic carbon content is 0.15% (see "Organic Geochemistry" section, this chapter). The

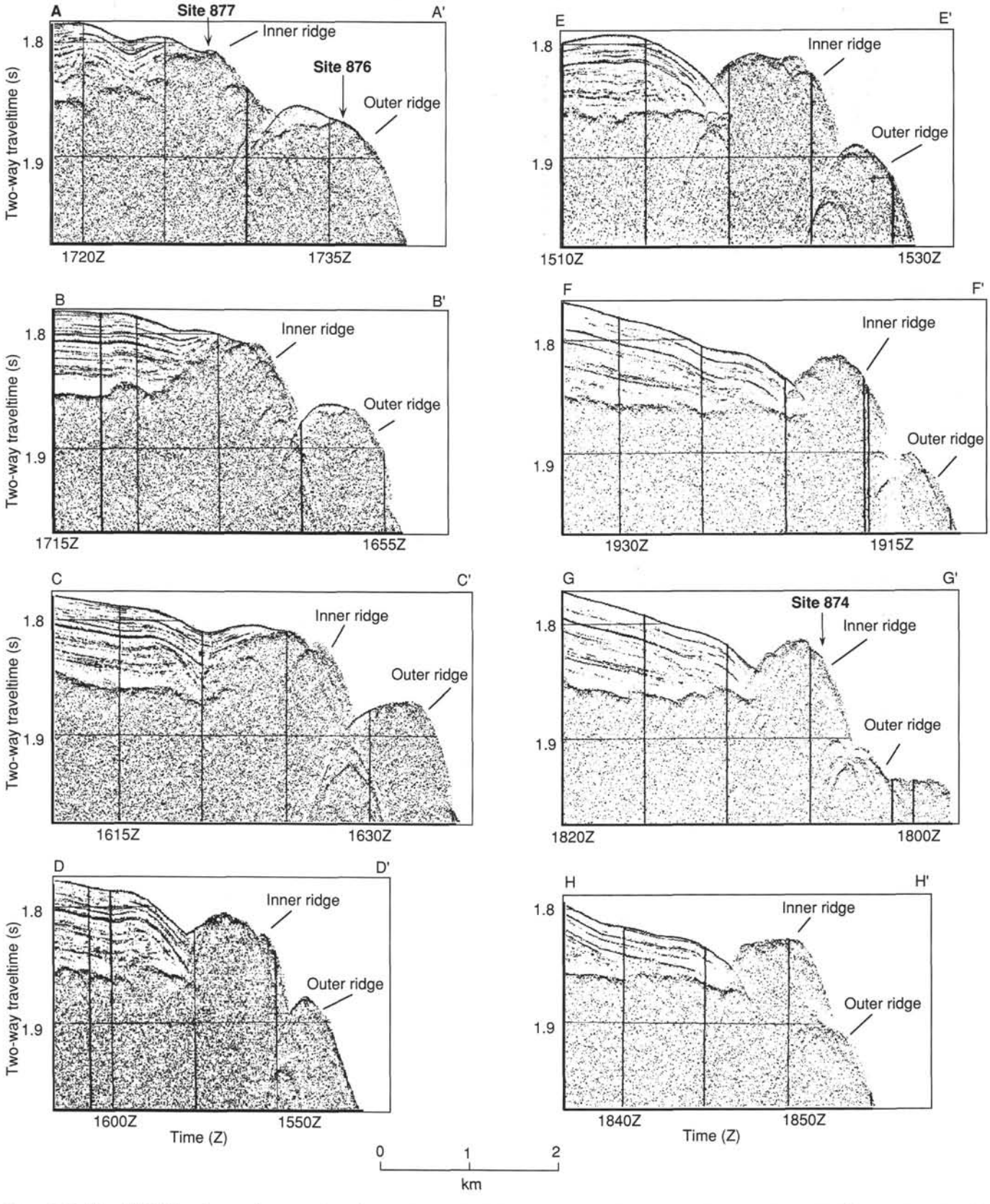

Figure 5. Profiles of 3.5-kHz echo sounder across the perimeter ridges of Wodejebato Guyot. Profiles are arranged from northwest (A–A′) to southeast (H–H′). The location of Site 874 is shown on Profile G–G′; those of Sites 876 and 877 are shown in Profile A–A′; and that of Site 875 in Figure 3.

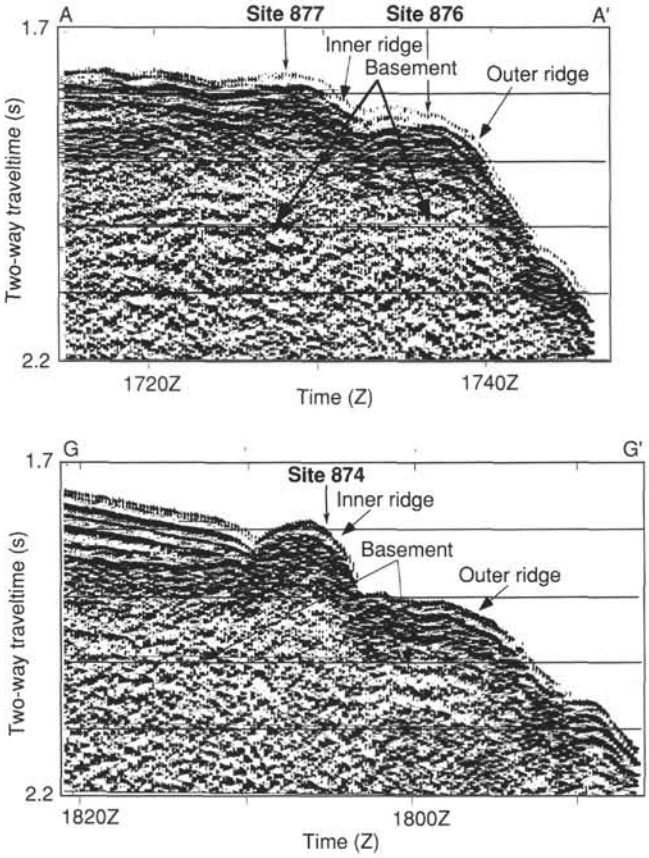

Figure 6. Single-channel seismic Profiles A–A′ and G–G′ across the locations of Sites 874, 876, and 877 on Wodejebato Guyot. A packet of strong reflectors overlying a more acoustically massive unit composes the inner ridge. The reflector interpreted as basement is faintly visible in these profiles.

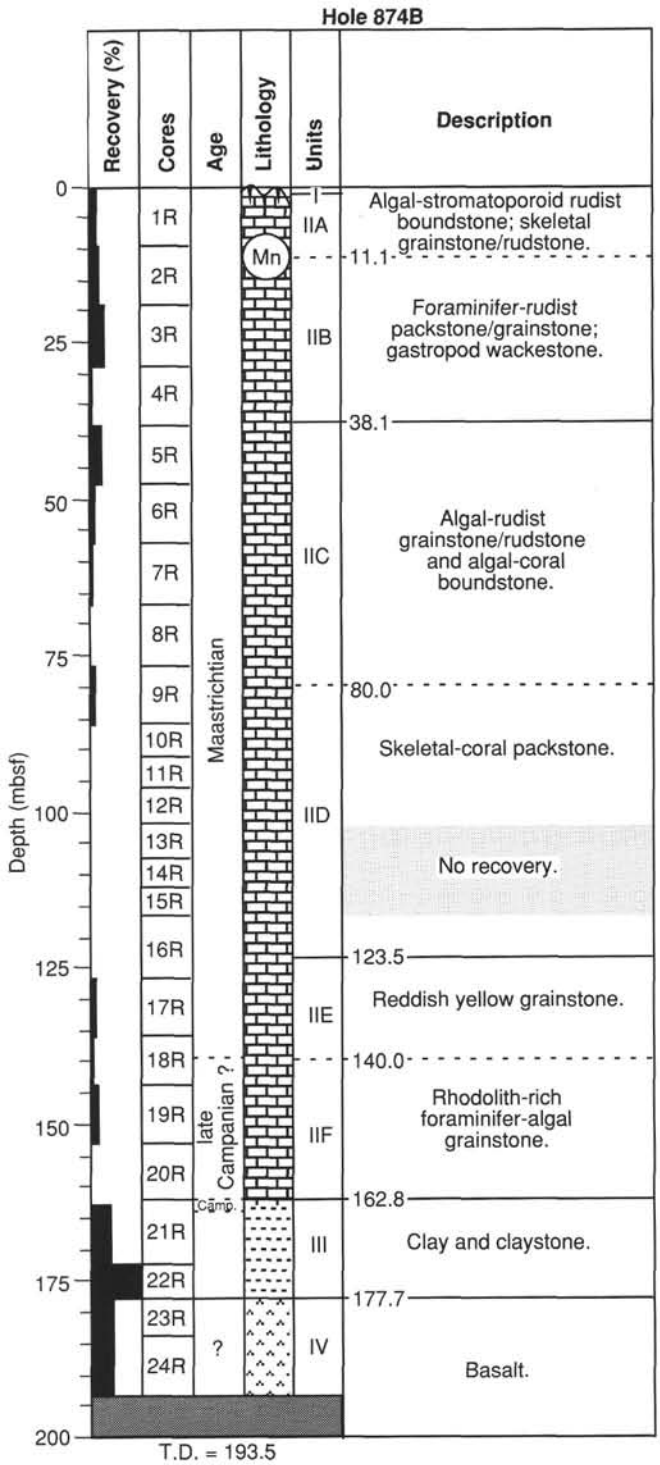

Figure 7. Lithostratigraphic summary of Hole 874B. Hole 874A recovered only 1.74 m; the base of Unit I in Hole 874A is at 0.1 mbsf. Lithologic Unit I = manganese crust and manganese-phosphate-coated limestone conglomerate.

overall recovery for this subunit averaged 12.4% (see "Operations" section, this chapter).

The algal-rudist grainstone and rudstone of Subunit IIC are generally poorly sorted (medium- to very-coarse sand size); some beds are seemingly graded. Grains are well rounded; the major components are rudists (radiolitids and caprinids; Fig. 19) and red algae (corallinaceans). Rudists are generally fragmented, except for the small radiolitids (1 cm in diameter) that apparently are in life position and were recovered in small clusters of a few individuals (Interval 144-874B-5R-1, 32–44 cm). Red algae form encrustations over some large skeletal pieces and form rhodoliths that range in size from 0.5 to 2 cm in diameter (Interval 144-874B-9R-1, 49–73 cm). Coral fragments, gastropods (a few millimeters to 1 cm long), peloids, and small bivalves are common; benthic foraminifers and echinoderm fragments are few. Pink to pinkish white, centimeter-sized lithoclasts of micrite occur locally. Some burrows are filled with coarse-grained skeletal debris. Scattered black specks correspond to manganese-coated grains. The porosity of the grainstone and rudstone facies is typically 20% and is moldic to vuggy with solution-enlarged interparticle pores. Centimeter-sized solution cavities occur in Interval 144-874B-6R-1, 16–58 cm; these cavities are filled by reddish to rusty brown "internal sediment."

The algal-coral boundstone of Subunit IIC includes coral colonies, predominantly tabular, encrusted by red algae (crusts of corallinaceans and rare squamariaceans up to 1 cm thick), encrusting worms and foraminifers; these algal crusts typically contain borings. A few clusters of radiolitids are also present in these beds. The matrix is made of moderately to poorly sorted grainstone or packstone with fragments of corals, red algae, echinoids, calcareous sponges (chaetetids) and benthic foraminifers (especially orbitoids). Cavities, a few millimeters thick, are lined with crusts of isopachous calcite cement that are stained reddish yellow (5YR 7/6).

Core recovery indicates that beds of grainstone and boundstone may alternate in Subunit IIC. Formation MicroScanner (FMS) imagery reveals a series of intervals (each several meters thick) charac-

Table 3. Lithostratigraphic summary, Hole 874B.

Unit/subunit	Depth (mbsf)	Age	Cores	Thickness (m)	Lithology
Unit I	0.0–0.11	late Paleocene, early and middle Eocene	144-874B-1R-1, 0–11 cm	0.11	Mn crust and Mn-phosphate-coated limestone conglomerate
Unit II	0.11–162.82	Maastrichtian	144-874B-1R-1, 11 cm, to -21R-1, 2 cm	162.71	Platform carbonates
Subunit IIA	0.11–11.1	Maastrichtian	144-874B-1R-1, 11 cm, to 2R-1, 140 cm	11.00	Skeletal grainstone, rudstone, and boundstone
Subunit IIB	11.1–38.1	Maastrichtian	144-874B-2R-2 to -4R	27.00	Skeletal packstone, wackestone, and mudstone
Subunit IIC	38.1–80	Maastrichtian	144-874B-5R to -9R	41.90	Skeletal grainstone, rudstone, and boundstone
Subunit IID	80–123.5	Maastrichtian	144-874B-10R to -16R	43.50	Skeletal packstone and grainstone
Subunit IIE	123.5–140	Maastrichtian	144-874B-16R to -18R	16.50	Skeletal grainstone
Subunit IIF	140–162.82	Maastrichtian	144-874B-18R to -21R-1, 2 cm	22.82	Skeletal grainstone and packstone
Unit III	162.82–177.7	Campanian to ?	144-874B-21R-1, 2 cm, to -22R	14.83	Clays and claystones
	162.82–163.21	Campanian	144-874B-21R-1, 2–41 cm	0.39	Black clays
	163.21–164.1	?	144-874B-21R-1, 41–125 cm	0.84	Gray clays
	164.1–177.7	?	144-874B-21R-1, 125 cm	13.60	Red clays and claystones
Unit IV	177.7–193.5	?	144-874B-23R to -24R	15.80	Basalts

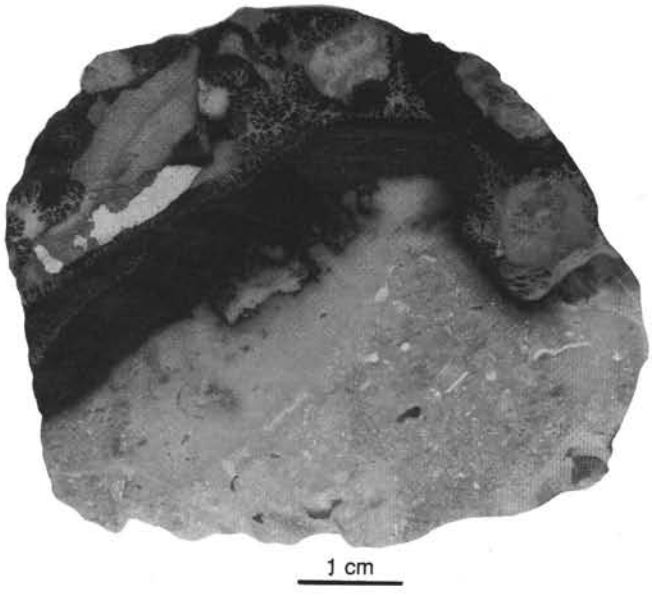

Figure 8. Close-up photograph of manganese crust and manganese-coated limestone conglomerate (Interval 144-874A-1R-1, 7–13 cm).

terized by a progressive upward increase in resistivity. We interpret these resistivity trends as gradational changes from porous grainstone and rudstone to more cemented boundstone, (see "Downhole Measurements and Seismic Stratigraphy" section, this chapter).

A sharp change in resistivity in the FMS imagery and a relative increase in uranium concentration occurs at a depth of 80 mbsf (see "Downhole Measurements and Seismic Stratigraphy" section, this chapter). Recovery of Core 144-874B-9R was 13%; therefore, we assume that the contact between Subunits IIC and IID was not recovered. We place the boundary at 80 mbsf based on the FMS record.

Subunit IID

Interval: Cores 144-874B-10R through -16R
Depths: 80–123.5 mbsf
Age: Maastrichtian

The first of the skeletal packstones that characterize Subunit IID were recovered at the top of Core 144-874B-10R at a depth of 86.2 mbsf. Only 30 cm of drilling pebbles and rollers were recovered in the interval from 86.2 to 101.7 mbsf. These pieces consist of white

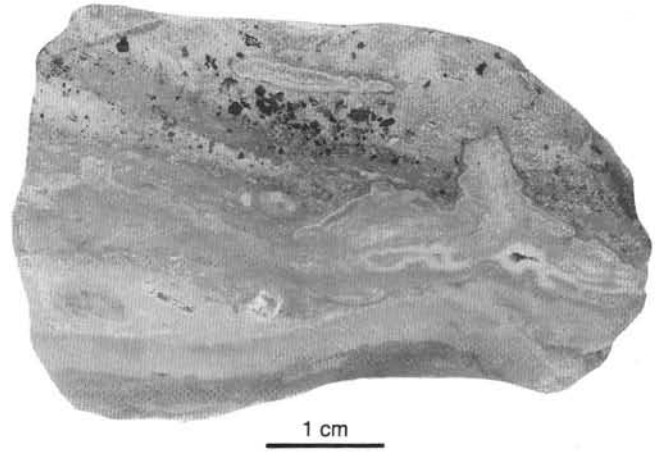

Figure 9. Close-up photograph of cavities platform limestone infilled by pelagic limestone (Interval 144-874B-1R-1, 46–50 cm).

(10YR 8/2), well-sorted, fine-grained skeletal packstone and grainstone with benthic foraminifers (especially orbitoids), fragments of corals, red algae, rudists (radiolitids), and calcareous sponges (chaetetids). Porosity is mostly intergranular to vuggy; intraskeletal voids are generally lined by isopachous crusts of calcite. In Subunit IID, the average carbonate content is 97.3%, and the total organic carbon content is 0.15% (see "Organic Geochemistry" section, this chapter). The average recovery was very low in Subunit IID; 1.3% in the interval from 86.2 to 101.7 mbsf, and 0% in the interval from 101.7 to 116.8 mbsf (see "Operations" section, this chapter).

Characteristics of FMS imagery vary little between 80 and 123.5 mbsf (see "Downhole Measurements and Seismic Stratigraphy" section, this chapter). Therefore, we assume the lithology throughout is similar to 30 cm of limestone recovered from this interval. The recovery in Core 144-874B-16R was only 4.6%, but the contact between Subunits IID and IIE was recovered. A major increase in uranium and thorium concentrations and a high resistivity peak in the FMS imagery occurs at 123.5 mbsf (see "Downhole Measurements and Seismic Stratigraphy" section, this chapter). Based on these logging results, we place the boundary between Subunits IID and IIE at 123.5 mbsf.

Subunit IIE

Interval: Cores 144-874B-16R through -18R
Depths: 123.5–140 mbsf
Age: Maastrichtian

Table 4. Components, porosities, and cements recognized in thin section samples from Lithologic Unit II (platform carbonates), Hole 874B.

Constituent	Subunit IIA	Subunit IIB	Subunit IIC	Subunit IID	Subunit IIE	Subunit IIF
Red algae	A	A	A	A	A	A
Green algae	R	R	F			R
Planktonic foraminifers	R					
Benthic foraminifers	A	C	A	A	A	A
Echinoderm fragments	A	M	A	A	A	A
Corals	C	R	F	R	R	F
Bivalves	F	M	A	A	A	C
Rudists	A	C	M	R	R	A
Gastropods	C	F	M			F
Ostracods	R	R				
Bryozoans						F
Calcispherulids						F
Calcisponges	F					F
Peloids	A	M	C	R		R
Lithoclasts						R

Notes: A = abundant, C = common, M = many, F = few, and R = rare.

Subunit IIE consists of 16.5 m of white (10YR 8/2), pink (7.5YR 8/4), yellow (10YR 7/8), and reddish yellow (5YR 7/8) skeletal grainstone. The average calcium carbonate content in this subunit is 91.15%, and the total organic carbon content is 0.35% (see "Organic Geochemistry" section, this chapter). The average recovery in the interval from 123.5 to 140 mbsf was 7.3% (see "Operations" section, this chapter).

Grainstones of Subunit IIE are poorly lithified, medium to coarse grained, and generally well sorted. They include fragments of red algae, rudists (radiolitids), casts of small bivalve shells, and common larger foraminifers (orbitoids and *Sulcoperculina*). Irregular, white, platy fragments may be spalled pieces of rhodoliths. Intense leaching of the original grains resulted in highly moldic, interparticle, and vuggy porosity, ranging from 30% to 40%; intergranular cement is sparse. A small scour at the base of the coarse-grained grainstone, and vague oblique laminations of 10° inclination were noted in Interval 144-874B-17R-1, 36–44 cm; low-angle cross lamination was noted in Interval 144-874B-17R-1, 47–53 cm. A few burrows are present in Interval 144-874B-17R-1, 36–44 cm; the walls of these burrows are stained by iron oxides. Because recovery in Core 144-874B-18R was only 7.6%, it is unlikely that the contact between Subunits IIE and IIF was recovered. A peak in natural gamma intensity occurred at 140 mbsf. At this depth, the FMS imagery shows several thin beds with slightly higher resistivity that may be horizons of partial cementation (see "Downhole Measurements and Seismic Stratigraphy" section, this chapter). Based on the logging results, we place the boundary between Subunits IIE and IIF at 140 mbsf.

Subunit IIF

Interval: Core 144-874B-18R through Section 144-874B-21R-1, 2 cm
Depths: 140–162.82 mbsf
Age: late Campanian?

Subunit IIF is composed of 22.8 m of white (10YR 8/2) to very pale brown (10YR 8/3), yellow-stained (10YR 7/6 to 10YR 7/8), foraminifer algal grainstone and packstone; these two lithologies are interlayered. The average calcium carbonate content in Subunit IIF is 97.7%, and the average total organic carbon content is 0.19%. Recovery in the interval from 140 to 162.82 mbsf averaged 10.5% (see "Operations" section, this chapter).

The grainstone and packstone of Subunit IIF are poorly cemented and poorly sorted. They include abundant fragments of red algae (corallinaceans and squamariaceans) and rudists (radiolitids and rare caprinids); benthic foraminifers (orbitoids and miliolids) are common. Corals (large fragments and colonies) and 1.0- to 1.5-cm rhodoliths are locally common. Few fragments of green algae (dasycladaceans), gastropods, and echinoderms are present. Burrows, 20 mm long, occur sporadically. Porosity ranges from 10% to 15% in the packstone and as high as 20%–30% in the grainstone; it is moldic, intergranular, and vuggy. Bladed calcite cements occur in molds; they are locally stained yellow.

Unit III

Interval: Section 144-874B-21R-1, 2 cm, to Core 144-874B-22R
Depths: 162.82–177.7 mbsf
Age: Campanian to ?

Unit III consists of 14.88 m of clay and claystone. The boundary between Units II and III was recovered at Section 144-874B-21R-1, 2 cm (depth, 162.82 mbsf). This boundary is also visible in the FMS imagery and the geochemical logs, which indicate a sharp downward decrease in calcium content that corresponds to a sharp downhole increase in iron and silica enrichment between 162 and 163 mbsf (see "Downhole Measurements and Seismic Stratigraphy" section, this chapter).

In Interval 144-874B-21R-1, 2–41 cm, the clay of Unit III is black (12.5Y 2/0). Section 144-874B-21R-1, 41 cm, contains 4-mm-thick lamina with abundant larger foraminifers. The average calcium carbonate content is 0.3% in the black clay. The total organic carbon content is 5.23%, with preserved kerogen-type woody material (see "Organic Geochemistry" section, this chapter). The dark clay contains nannofossils that are Campanian in age (see "Biostratigraphy" section, this chapter).

In Interval 144-874B-21R-1, 41–125 cm, the clay is gray (2.5Y 5/0) and contains abundant, very small crystals of pyrite. The gray clay of Unit III is mostly homogeneous, but the texture of highly altered basalt is locally visible (Interval 144-877A-21R-1, 110–125 cm) as laths of altered plagioclase and remanent vesicles infilled by white patches of zeolites. The average calcium carbonate content is 0.48% in the gray clay, and the total organic carbon content is 3.74%, with preserved kerogen-type woody material. The sulfur content averages 37.27% in the gray clay (see "Organic Geochemistry" section, this chapter).

From Section 144-874B-21R-1, 125 cm, through Core 144-874B-22R, Unit III consists of dusky red (10R 3/1 to 10R 3/4) to dark red (10R 3/6) mottled clay and claystone. The texture of highly altered basalt is locally visible as laths of altered plagioclase and vesicles infilled by white patches of zeolites; veins of zeolites 1- to 3-mm-thick also occur. The degree of alteration decreases downwards. In Interval 144-874B-22R-3, 85–127 cm, the clay includes 20% competent fragments, up to 3 cm in diameter, which retain a basaltic fabric. The average calcium carbonate content of the red clay and claystone of Unit III is 0.2%; the total organic carbon content is 0.13% (see "Organic Geochemistry" section, this chapter).

Unit IV

Interval: Cores 144-874B-23R to -24R
Depths: 177.7–193.5 mbsf
Age: indeterminate

Unit IV consists of altered ankaramitic basalt that is discussed in the "Igneous Petrology" section, this chapter.

Preliminary Interpretation of Depositional History

The depositional history of Site 874 on Wodejebato Guyot began with the end of volcanism before or during late Campanian time. The dusky red to gray clay and claystone, which form the bulk of Unit III, are a subaerial weathering profile of the basalt as shown by the preservation of vesicular texture, including remanent laths of plagioclase and vesicles infilled by white patches of zeolites. The contact

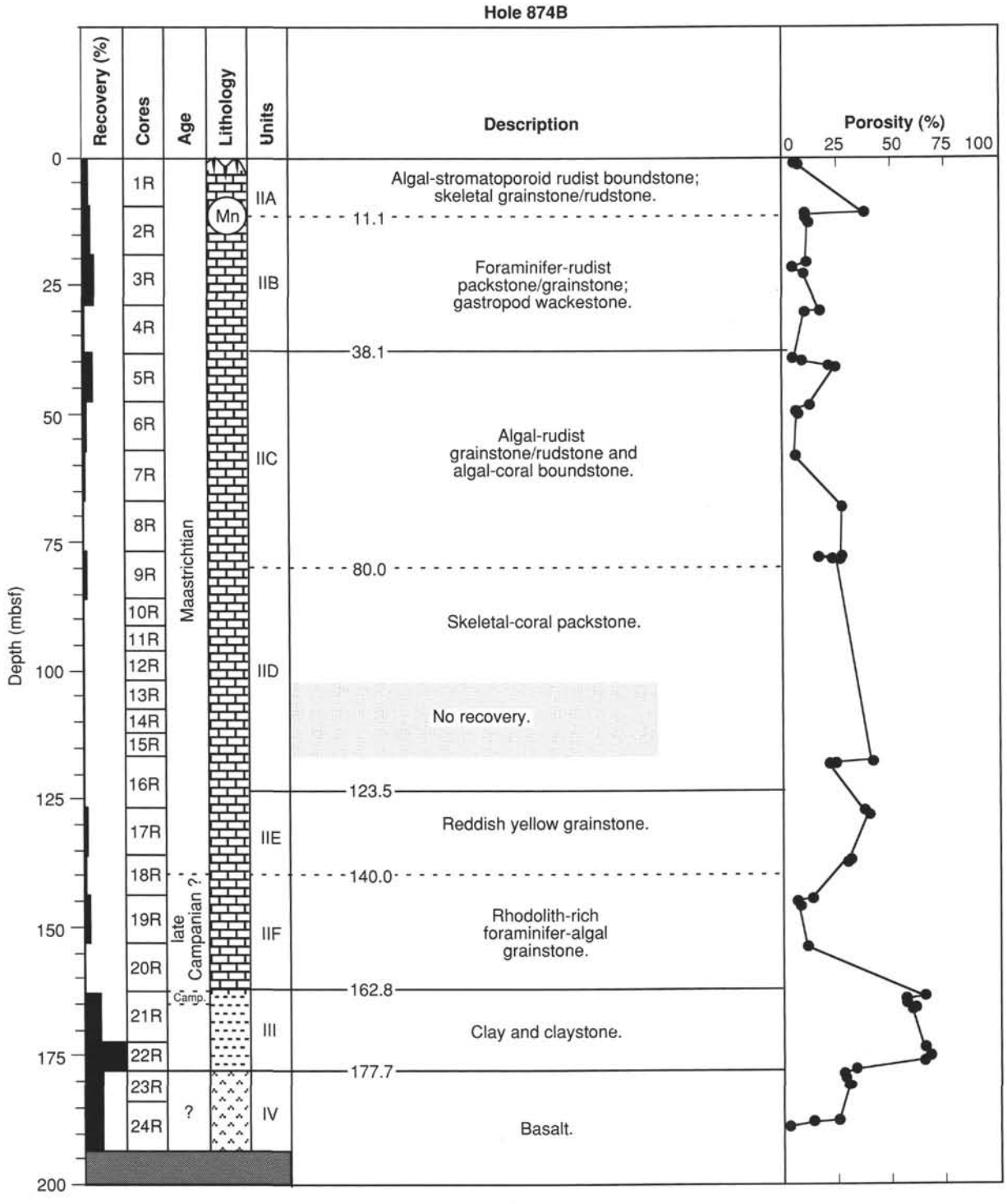

Figure 10. Correlation of the relationships between the lithostratigraphy and porosity data measured in Hole 874B.

between the basalt and the clay is gradational and the degree of alteration decreases downwards; competent fragments occur, which retain the texture of the basalt (e.g., Interval 144-874B-22R-3, 85–127 cm).

The first marine deposit was recovered at Section 144-874B-21R-1, 41 cm, with a 4-mm-thick lamina of large benthic foraminifer sand. The deepest limestone recovered from above the clay (Section 144-874B-21R-1, 2 cm) is grainstone with fauna and flora (larger foraminifers, coral fragments, and red algae) typical of a shallow-water environment with open-marine circulation. The partial preservation of the clay, and the lack of any clay reworking at the base of the platform carbonates of Unit II, are consistent with rapid burial in a low-energy environment.

The platform carbonate sequence (Unit II) documents the submergence of a volcanic island, followed by the development and demise of a Maastrichtian carbonate platform. Subunit IIF consists of grainstone and packstone with a diversified fauna and flora that were deposited in a shallow-marine environment with moderate- to high-energy conditions. The abundance of rhodoliths is a common feature

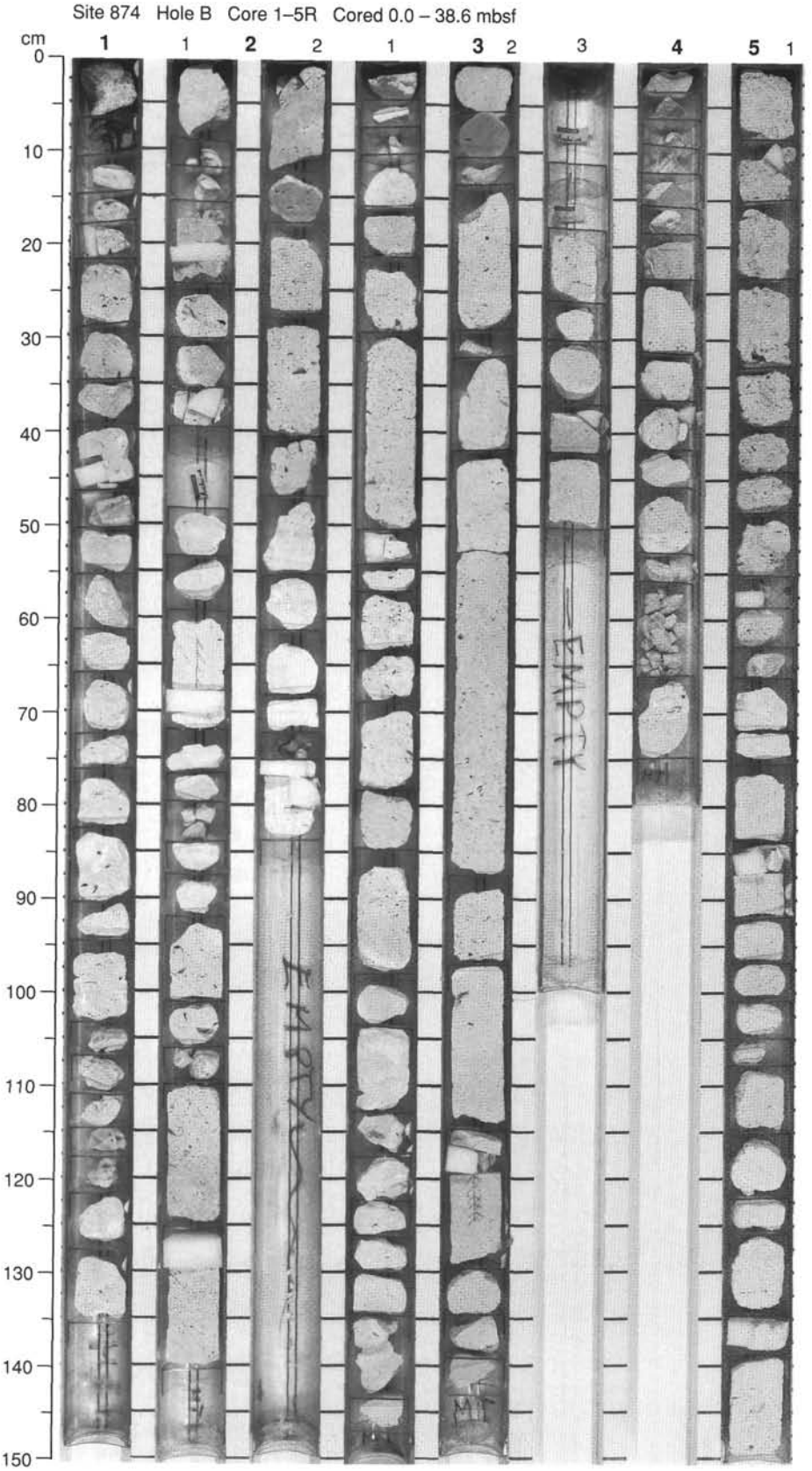

Figure 11. Composite photograph of Unit II from Hole 874B, including Core 144-874B-1R to Section 144-874B-5R-1.

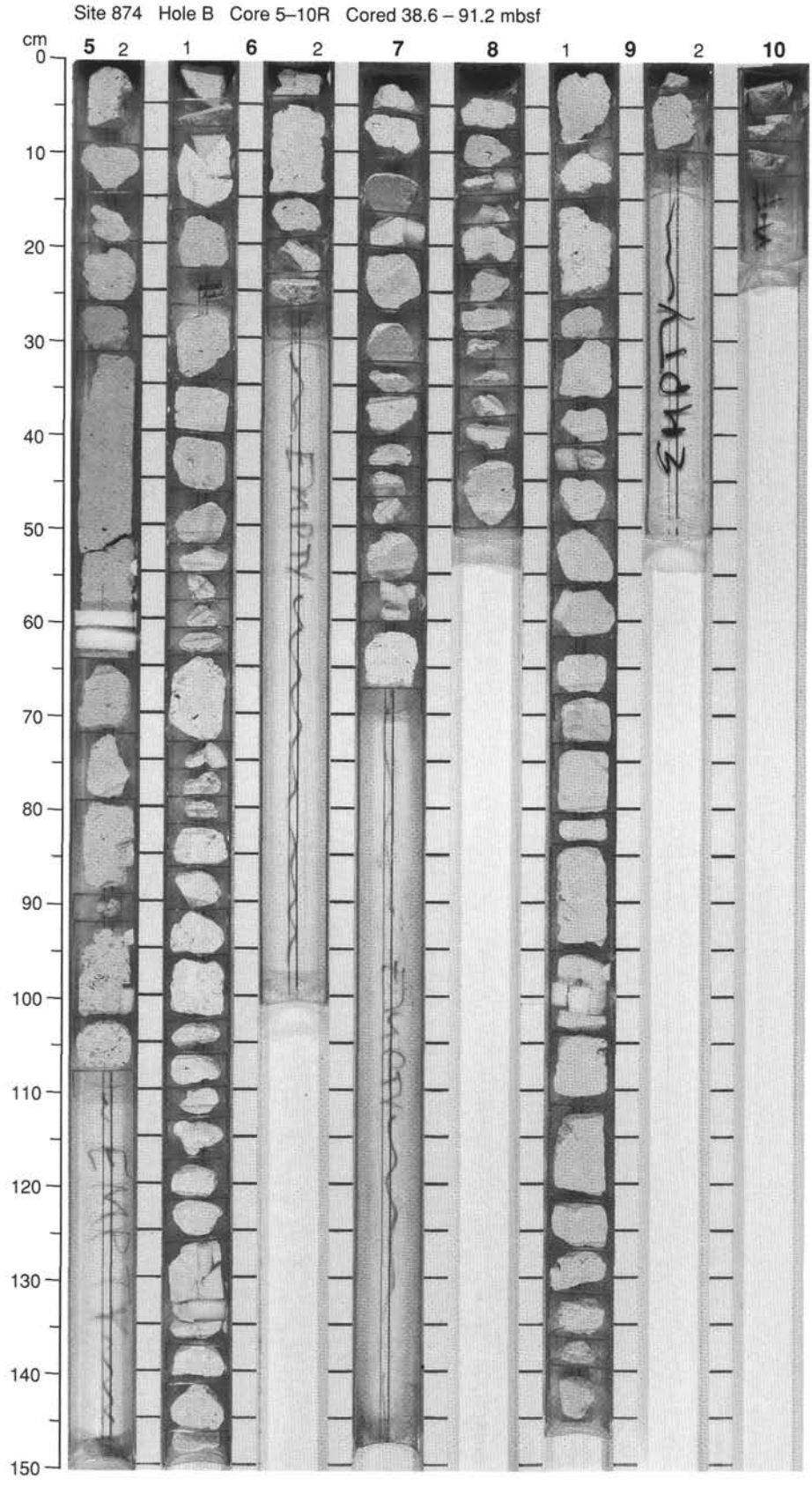

Figure 12. Composite photograph of Unit II from Hole 874B, including Section 144-874B-5R-2 to Core 144-874B-10R.

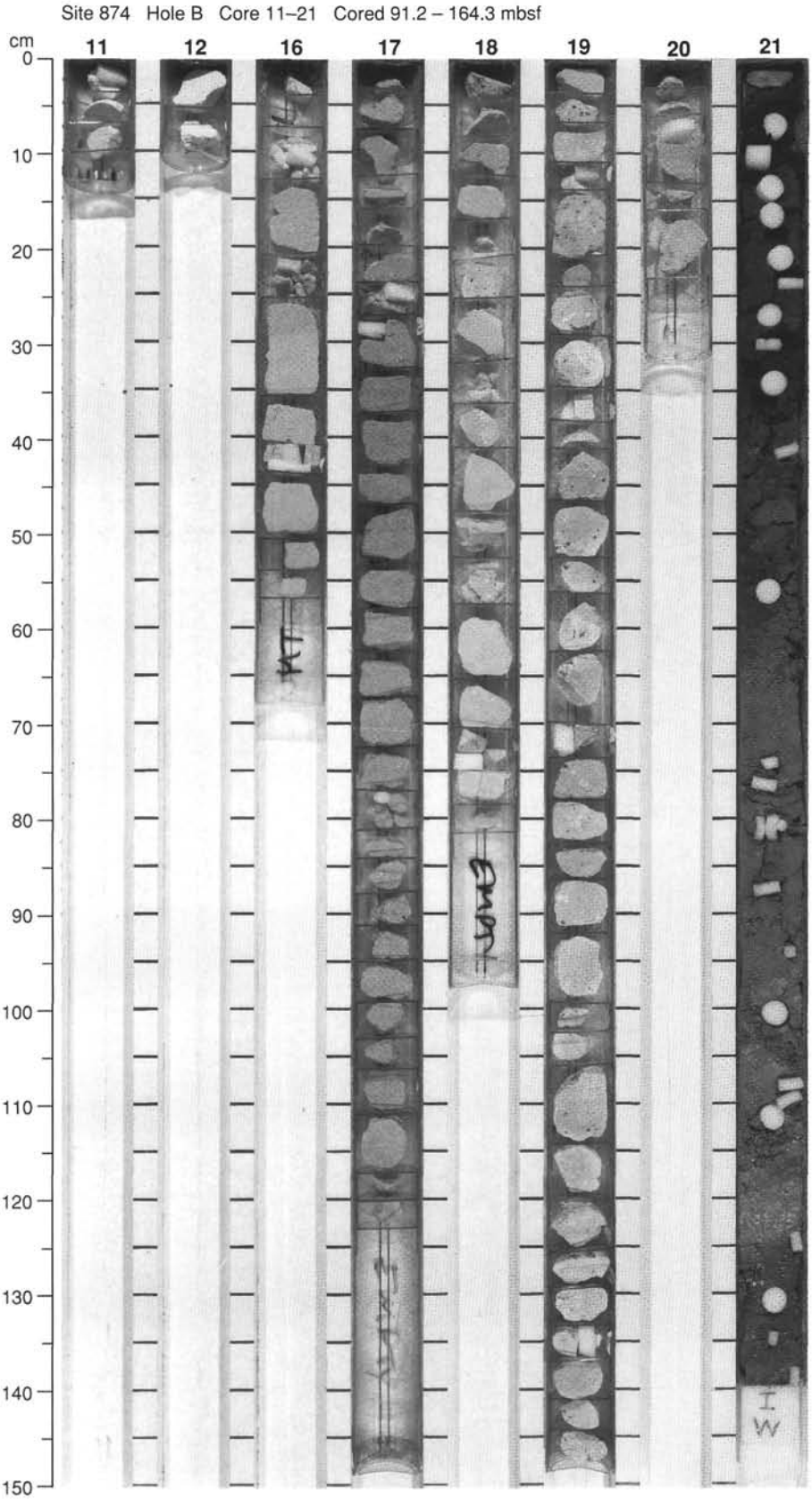

Figure 13. Composite photograph of Unit II from Hole 874B, including Core 144-874B-11R to Interval 144-874B-21R-1, 1–2 cm. Interval 144-874B-21R-1, 3–140 cm, belongs to Unit III.

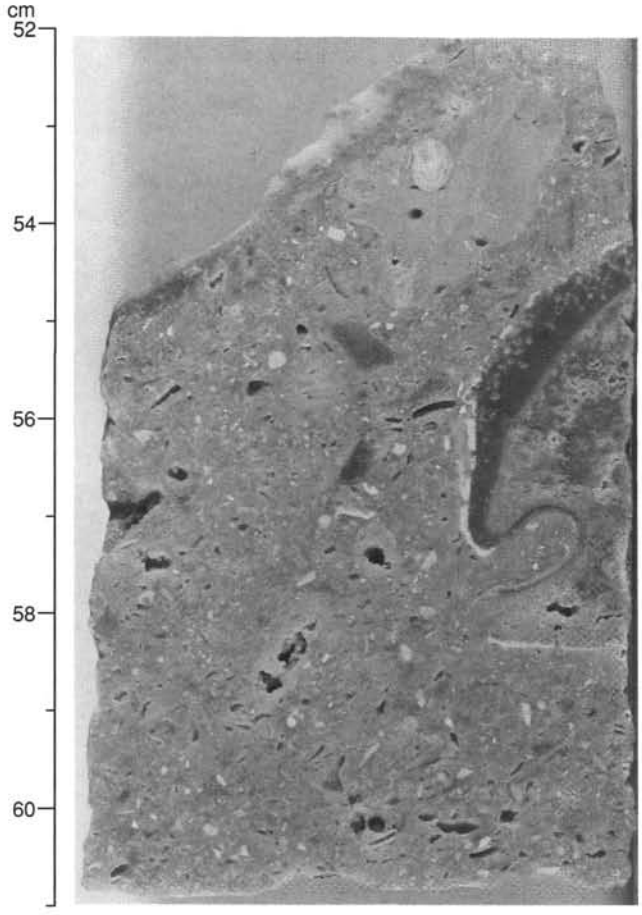

Figure 14. Close-up photograph of rudist limestones (Interval 144-874A-1R-1, 52–61 cm).

in the initial steps of development of Late Cretaceous isolated carbonate platforms (Camoin et al., 1988) and Cenozoic atolls (Collot, Greene, Stokking, et al., 1992). Rhodoliths were also reported in the Paleocene-Eocene shallow-water carbonates of Limalok Guyot at Site 871 (see "Lithostratigraphy" section, "Site 871" chapter, this volume).

Subunit IIE consists of skeletal grainstone, deposited in a shallow-marine environment, which display a similar composition to that of Subunit IIF. Sedimentary structures found in the grainstone (vague oblique lamination of 10° inclination; low-angle cross lamination) are clues that indicate moderate- to high-energy conditions. Their characteristic yellow to reddish yellow color is probably caused by the concentration of iron oxides, which is seemingly related to postdepositional alteration.

Relative to Subunit IIE, Subunit IID consists of more packstone, suggesting a slight decrease in wave energy. Changes in the relative abundance of organisms are also recorded; benthic foraminifers (especially orbitoids) increase in abundance coeval with a decrease in the abundance of red algae and rudists (radiolitids).

Subunit IIC marks the return to more agitated environments marked by the prevalence of poorly sorted, algal-rudist grainstone/rudstone. The occurrence of algal coral boundstone represents the first evidence of organic frameworks at the edge of the guyot. The structure of the boundstone, dominated by tabular coral colonies and encrusting red algae suggests a "domination stage" of reef evolution (Walker and Alberstadt, 1975); a few clusters of radiolitids are also present in these beds. Core recovery and FMS imagery suggest that grainstone and boundstone are interbedded and form cycles several meters thick, probably reflecting minor fluctuations in environmental conditions (i.e., hydrodynamic conditions) and/or in the distribution of bioconstructions.

The deposition of Subunit IIB marks a distinct change in sedimentation to the deposition of fine- to medium-grained foraminifer rudist packstone (locally grainstone) and laminated, burrowed gastropod wackestone and mudstone. The contact between these two lithologies within the subunit is generally sharp and scalloped. These lithologies are consistent with deposition in a shallow lagoon periodically affected by storms, changes in current patterns or short-term relative sea-level fluctuations. The wackestone includes small gastropods and benthic foraminifers suggesting temporary restricted conditions. The packstone commonly displays a chalky appearance related to extensive dissolution processes.

Subunit IIA consists of poorly sorted, medium- to coarse-grained skeletal rudist (mostly caprinids) grainstone and rudstone with several intervals of boundstone made by stromatoporoids, corals, and rudists heavily encrusted by red algae. The deposition of Subunit IIA marks the return to more agitated shallow-marine environments with the formation of bioclastic sand shoals and the growth of organic frameworks. This is the second episode of "reef" development recovered at this site.

The diagenetic features of the upper half of the platform carbonate sequence (Subunits IIA, IIB and IIC) suggest a complex postdepositional history. These diagenetic features include strong cementation, dissolution of skeletal fragments, and formation of large solution cavities. These cavities are filled by reddish to brownish "internal sediments." The oldest pelagic sediments recovered at this site are probably Maastrichtian in age and fill cavities in the Maastrichtian platform carbonates; this indicates drowning during possibly late Maastrichtian time.

Manganese oxide encrusted the platform carbonates following submergence in late Maastrichtian time. During late Paleocene and middle Eocene time, pelagic sediments were deposited over Wodejebato Guyot. These late Paleocene and middle Eocene pelagic sediments were reworked along with some of the underlying platform carbonates to form a limestone conglomerate coated by manganese and phosphate.

BIOSTRATIGRAPHY

Introduction

Site 874 was drilled to investigate the nature of the "inner perimeter ridge" of Wodejebato Guyot. A platform limestone sequence, 162.5 m thick, is topped by a complex series of manganese encrustations. Age dating of various generations of manganese crust and late-stage pelagic cavity fillings in the skeletal limestones was accomplished using planktonic foraminifers and calcareous nannofossils. The platform limestones yielded a similar sequence of age-diagnostic larger benthic foraminifers and distinct biofacies as were found at other sites on the guyot (Sites 873, 875, 876, and 877). The limestones overlie dark clay and volcanic rocks; the dark clay was dated using calcareous nannofossils.

Two holes were drilled at Site 874, but only a single core was recovered from Hole 874A. This core consists of 1.5 m of platform limestone; a few fragments are derived from a well-developed phosphatic manganese-encrusted limestone (Interval 144-874A-1R-1, 7–13 cm). The crust includes a conglomeratic layer containing reworked pebbles of lithologies that are similar to the underlying limestones. Hole 874B was drilled to a total depth of 193.5 mbsf; the upper 162.5 m were limestones (Lithologic Unit II). Manganese encrusted the upper surface of this unit and the conglomerate found in Interval 144-874B-1R-1, 7–12 cm (Lithologic Unit I). Beneath the limestones lie about 15 m of dark-colored clay and claystone (Lithologic Unit III), which in turn overlie volcanics (Lithologic Unit IV). The biostratigraphy of Holes 874A and 874B are combined in Figure 20. The detailed investigations of the different lithologies with each fossil group are summarized in turn below.

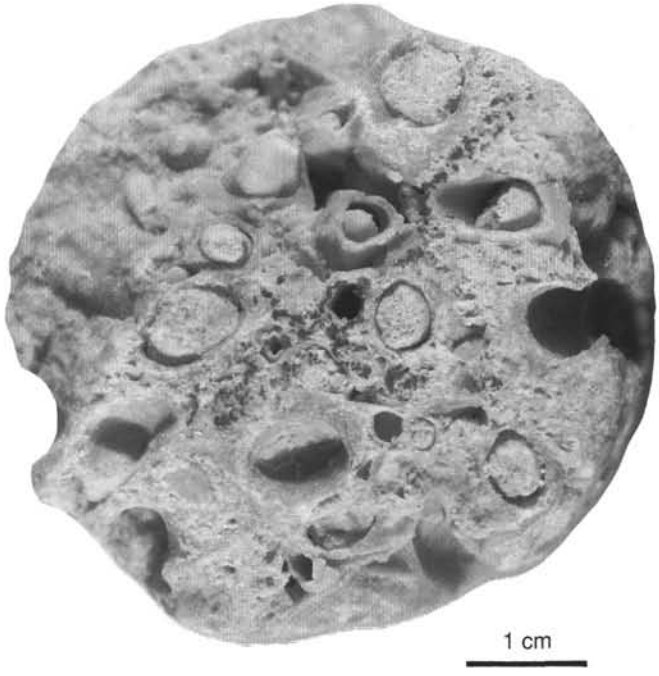

Figure 15. Close-up photograph of a rudist cluster (Interval 144-874B-3R-3, 7–13 cm).

Calcareous Nannofossils

Phosphatic Manganese Crust

Sample 144-874A-1R-1, 7–13 cm, consists of several generations of manganese crusts, enclosing platform carbonate clasts and planktonic foraminifer limestone. The pelagic limestone yields three nannofossil assemblages of distinct ages. The majority of the upper part of this sample (approximately Interval 144-874A-1R-1, 0–2 cm) contains *Discoaster bifax, D. saipanensis, D. barbadiensis, D. strictus, Dictyococcites bisectus, Cribrocentrum reticulata,* and *Reticulofenestra umbilica*, indicating Subzone CP14a of late middle Eocene age. Preservation is generally excellent, with many *R. umbilica* retaining their delicate central nets. However, some of the Subzone CP14a material in this interval has been invaded by manganese dendrites.

A 5-mm-thick rectangular block of pelagic limestone with an apparent dip of approximately 30° also occurs within Interval 144-874A-1R-1, 0–2 cm. This block contains *Fasciculithus tympaniformis* (s.s.), *F. schwabii, F. bobii, F. alanii, Discoaster mohleri, Neochiastozygus protenus, Toweius eminens*, and *Sphenolithus primus*. This association of species is diagnostic for Zone CP8 of late Paleocene age. The fine fraction of the block (<25 µm) is dominated by carbonate debris, with nannofossils comprising <5% of the matrix. The coarse fraction is composed largely of laminated carbonate debris with some foraminifers and one echinoderm fragment. The laminations parallel the borders of the block and maintain the distinct apparent dip of approximately 30°. The perimeter of the block is coated in manganese, although little of this has invaded the block's interior. The block is surrounded, on the three sides visible in the thin section, by Subzone CP14a pelagic limestone and/or manganese. This age relationship and the anomalous dip indicate that the block was broken and redeposited before the late middle Eocene.

Small stringers of pelagic limestone in Interval 144-874A-1R-1, 3–4 cm, contain *Discoaster lodoensis, D. barbadiensis, D. septemradiatus, D. kuepperi, Reticulofenestra dictyoda,* and *Campylosphaera dela,* indicating Zone CP11 (late early Eocene) and Subzone CP12a (early middle Eocene). Preservation within the thin section samples appears very good, with little overgrowth of the discoasters.

Figure 16. Close-up photograph of cavities partially filled by "internal sediments" (Interval 144-874B-2R-1, 40–47 cm).

Cavity Infillings in Limestones

Sample 144-874B-1R-1, 47–50 cm, consists of platform carbonate with a pelagic limestone void filling. Calcareous nannofossils in the pelagic limestone include *Discoaster barbadiensis, D. lodoensis, Chiasmolithus eograndis, C. solitus, C. grandis,* and *Micrantholithus inaequalis*. This assemblage indicates Zone CP10 or the lower portion of Zone CP11. The age of this assemblage is early Eocene.

Sample 144-874B-3R-1, 114–118 cm, consists of platform carbonate with at least two generations of void filling. In the older of the two fillings, which also contains possibly Maastrichtian planktonic foraminifers, calcareous nannofossils are severely recrystallized and therefore unidentifiable. The smaller (approximately 2 mm in diameter) and younger void filling contains an abundant, well-preserved assemblage including *Ericsonia robusta, Chiasmolithus danicus, Cruciplacolithus tenuis, Cruciplacolithus primus, Prinsius martinii, Sphenolithus primus,* and small (1–2 µm) taxa of the Prinsiaceae tentatively identified as *Prinsius tenuiculum* and *P. dimorphus*. This assemblage suggests assignment to Zones CP2–CP3 of early to early late Paleocene age.

Dark Clay

Sample 144-874B-21R-1, 40–41 cm, consists of black clay with large benthic foraminifers and rock fragments. Rare, well-preserved calcareous nannofossils include several Late Cretaceous taxa such as

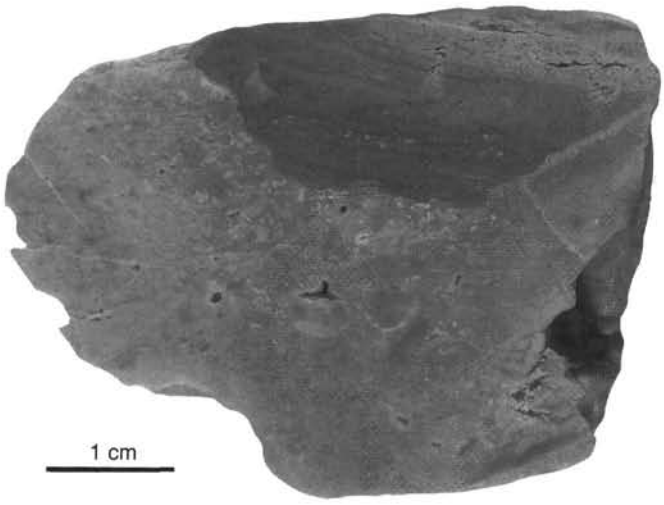

Figure 17. Close-up photograph of a cavity partly infilled with "internal sediment" (Interval 144-874B-3R-1, 113–117 cm).

Watznaueria barnesae, Cribrosphaerella ehrenbergii, Eiffellithus turriseiffelii, and *Prediscosphaera cretacea* (s.s.). The occurrence of *Prediscosphaera honjoi, Eiffellithus eximius, Quadrum gothicum,* and *Nannoconus multicadus* suggests a Campanian age.

Planktonic Foraminifers

Phosphatic Manganese Crust

Like the calcareous nannofossils (see above), the planktonic foraminifers occurring in the crust demonstrate that this manganese-encrusted interval only a few centimeters thick has had a long and complex geological history. Planktonic foraminifers from the outer portion of the crust are the best preserved and most abundant. They belong to Zone P13 of late middle Eocene age, which was identified on the presence of *Orbulinoides beckmanni,* large globigerinathekids, *Turborotalia cerroazulensis, T. pomeroli, Globigerinatheka index, Morozovella lehneri, M. crassata, Acarinina rohri,* and *Truncorotaloides topilensis.*

Older planktonic foraminifer faunas survive in small, lightly phosphatized enclaves within a few more heavily phosphatized patches. These were attributed either to Zone P8 of early Eocene age or to Zone P4 of the late Paleocene. The assemblage identifying Zone P8 includes *Morozovella aragonensis, M. gracilis, M. crassata, "Globigerinatheka" senni, Acarinina pseudotopilensis,* and *Pseudohastigerina danvillensis* in the absence of the hantkeninids, turborotaliids, and the larger globigerinathekids. The Zone P4 assemblage includes rare *Morozovella aequa* and *M. occlusa.* The Paleocene and lower Eocene forms are all poorly preserved because of the phosphatization.

Cavity Infillings in Limestones

Planktonic foraminifers occur within pelagic sediments infilling cavities in the platform limestone. A rich planktonic assemblage of Zone P8 of early Eocene age was recovered in Sample 144-874B-1R-1, 47–50 cm, the highest occurrence within the carbonate sequence. The species identified are *Morozovella aragonensis, M. quetra, Acarinina pentacamerata, A. primitiva, A. pseudotopilensis,* and *"Globigerinatheka" senni.* A pelagic sediment infilling of another cavity occurs in Sample 144-874B-3R-1, 114–118 cm, about 20 m beneath the top of platform limestone. Two assemblages are present, one of Maastrichtian age with *Archaeoglobigerina* sp., *Globigerinelloides messinae, Hedbergella holmdelensis, H. monmouthensis, Heterohelix globulosa,* and *Globotruncanella* sp. associated with numerous fish remains; and a second one, very poorly preserved as the result of strong phosphatization, of probable late Paleocene age.

Figure 18. Close-up photograph of micritic limestones with bored laminae from Subunit IIB (Interval 144-874B-2R-2, 48–57 cm).

Benthic Foraminifers and Other Shallow-water Fossils

The 162.8-m-thick sequence of platform limestone (Lithologic Unit II) recovered in Hole 874B (Core 144-874B-1R to Sample 144-874B-21R-1, 22 cm) and Hole 874A (Core 144-874A-1R) yielded abundant larger foraminifers associated with common to frequent rudist bivalves (especially in the upper half of the unit), coralline algae, echinoderm fragments, and common corals (see Fig. 21). The distribution of the microfaunas and associated faunas from the platform carbonates of Hole 874B was studied using observations of the core surface, thin section samples, and specimens isolated from the saw cuttings of each section of the split core.

As was the case for the platform limestones at Site 873 (see "Biostratigraphy" section, "Site 873" chapter), many taxa present, especially the larger foraminifers, are restricted to the Campanian-Maastrichtian. A single questionable occurrence of *Omphalocyclus* in Sample 144-874B-5R-2, 60–64 cm, would, if confirmed, indicate a Maastrichtian age for the sample.

The interval from Samples 144-874B-19R-1, 11–13 cm, to -20R-1, 16–22 cm, contains different genera and species of the orbitoid groups (*Vaughanina* and *Pseudorbitoides*), as is a different species of *Asterorbis* than occurs in the sequence above. This assemblage is similar to that seen near the base of the limestone sequences at Sites 875, 876,

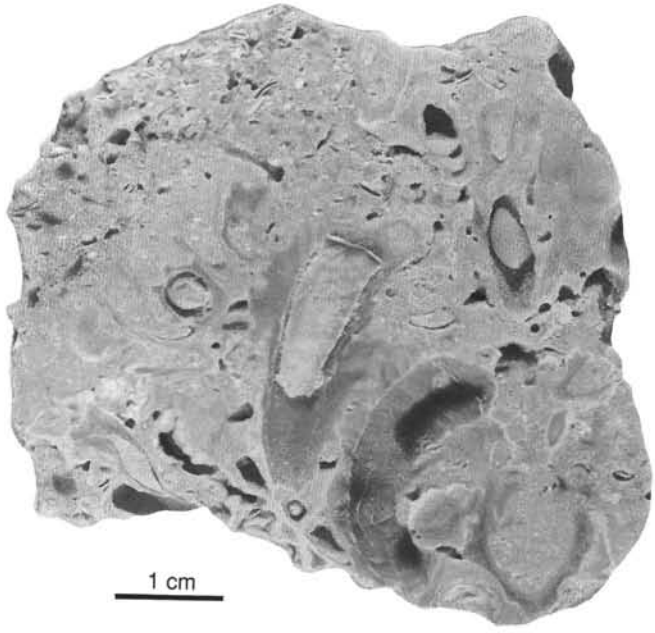

Figure 19. Close-up photograph of rudists (Interval 144-874B-5R-1, 33–39 cm).

and 877. According to the dating of a similar fauna found at Site 462 in the Nauru Basin (Premoli Silva and Brusa, 1981), this assemblage may be late Campanian in age. This assignment would accord well with the Campanian age determined from nannofossils for the underlying black clay in Sample 144-874B-21R-1, 40–41 cm (see above).

Paleoenvironment of Carbonate Platform Sediments

The distribution of larger foraminifers and other fossil groups in Hole 874B varies with facies throughout the limestone sequence. However, the assemblages are noticeably more continuous than those seen at Site 873 (which was centrally located on the guyot). The data presented in Figure 21 are arranged such that the open-marine indicators appear to the left and those indicative of more restricted environments appear to the right. The general environmental trends through the limestones may be deduced from this chart. However, this chart should be considered as preliminary.

Assemblage I (Intervals 144-874B-1R-1, 18–22 cm, to -1R-1, 40–47 cm) is characterized by abundant larger foraminifers *Sulcoperculina* and common *Pseudocyclamminea* with rudists and coralline algae, in the total absence of any species, which would indicate restricted marine conditions. This assemblage is taken to represent fully marine conditions in a carbonate platform environment.

Assemblage II (Intervals 144-874B-2R-1, 19–21 cm, to 144-874B-6R-2, 1–3 cm), as shown in Figure 21, contains typically abundant rudist fragments, corallinacean algae, corals, and the larger foraminifers *Asterorbis* and *Sulcoperculina.* Other important components are gastropods, ostracodes, and echinoderms, which increase in abundance downward. The discorbids, small rotaliids, and miliolids occur sporadically and are generally less abundant. The occurrence of ammonites in Sample 144-874B-6R-2, 1–3 cm, at the bottom of the interval, is remarkable. Assemblage II is taken to represent a carbonate platform environment in which a range of conditions from fairly restricted to fully marine prevailed on occasion. Two specific samples in particular (Samples 144-874B-2R-2, 76–79 cm, and -6R-1, 8–10 cm), which are shaded as gray bands on Figure 21, represent two examples of transient maxima of more restricted marine conditions at this site. They are depleted of echinoderm fragments, corals, rudist bivalves, and those benthic foraminifers typical of open-marine conditions (the orbitoids and *Sulcoperculina*). On the other hand, these samples are rich in gastropods, ostracodes, and certain other benthic foraminifer taxa (particularly the discorbids), which are known to prefer more restricted environments. Sample 144-874B-6R-1, 127–130 cm, also contains a few charophyte oogonia, which indicate proximity to a freshwater or brackish environment.

Observation of the cores corresponding to Assemblage II shows that beds containing restricted faunas increase in frequency upward, but they are also thinner toward the top of the unit. Below Core 144-874B-6R, the assemblages are remarkably poor in coral and rudist fragments. Moreover, gastropods, ostracodes, and smaller benthic foraminifers (except for sparse miliolids) are almost absent. However, the interval from Core 144-874B-7R to Sample 144-874B-20R- 1, 16–22 cm, yields two discrete assemblages on the basis mainly of different larger foraminifers.

Assemblage III (Intervals 144-874B-7R-1, 55–58 cm, to -18R-1, 70–78 cm) is characterized consistently by abundant *Sulcoperculina, Asterorbis,* echinoderms, and less consistent corallinacean algae. Corals, rudists, and miliolids may also occur in some layers. It is worth mentioning that in the upper part of this interval corallinaceans are poorly represented. This low-diversity assemblage represents normal marine conditions.

A remarkable feature of Assemblage IV (Intervals 144-874B-19R-1, 11–13 cm, to -20R-1, 16–22 cm) is the occurrence of different genera and species within the orbitoid group, which also increase slightly in abundance in comparison with the younger faunas. *Pseudorbitoides, Vaughanina*, and different species among the asterorbids characterize this assemblage. Preservation also changed drastically with a pervasive micritization of the foraminifer tests. The high diversity suggests deposition in a fully marine environment.

Palynology

Two samples from Hole 874B were analyzed for palynology: Sample 144-874B-2R-1, 19–21 cm, is from the platform limestone and Sample 144-874B-21R-1, 13–15 cm, is from the soil horizon overlying the basalt. Each sample was digested in 20% HCl, washed, and sieved at 20 µm.

Sample 144-874B-2R-1, 19–21 cm, a fine-grained limestone, was found to be devoid of organic matter except for rare foraminifer linings and rare fragments of highly degraded material. Dark brown to almost opaque flakes of manganese? are fairly common.

Sample 144-874B-21R-1, 13–15 cm, is a black, carbonaceous mud from the upper part of the soil profile. The residue is dominated by woody and cuticular fragments. Smooth trilete fern spores referable to *Leiotriletes* are the dominant palynomorph (over 20 specimens seen), although their numbers are greatly diluted by woody tissues. Also recorded were several multicellate fungal spores, two foraminifer linings, and a single smooth monolete fern spore referable to *Laevigatosporites*. Some pyrite replacement was seen on the woody fragments.

The dominance of fern spores in Sample 144-874B-21R-1, 13–15 cm, suggests that ferns were largely responsible for the organic accumulation in this horizon. Ferns are often the pioneers of ecologically disturbed habitats, and their presence indicates moist conditions. The sediment was evidently deposited in a marginal marine setting, thus accounting for the presence of rare foraminifer linings.

Summary and Discussion

The dark clay that overlies the weathered volcanics at Site 874 was deposited in a marine environment, as inferred from the included calcareous nannofossils and occasional foraminifer linings. However, these clays also contain a high proportion of woody tissue that is likely to have been derived from ferns flourishing on nearby land. The nannofossils indicate a Campanian age.

The thick limestone sequence above the clay is mostly mid- to late Maastrichtian in age, although it is quite possible that the earliest benthic foraminifer assemblage (Assemblage IV) is late Campanian,

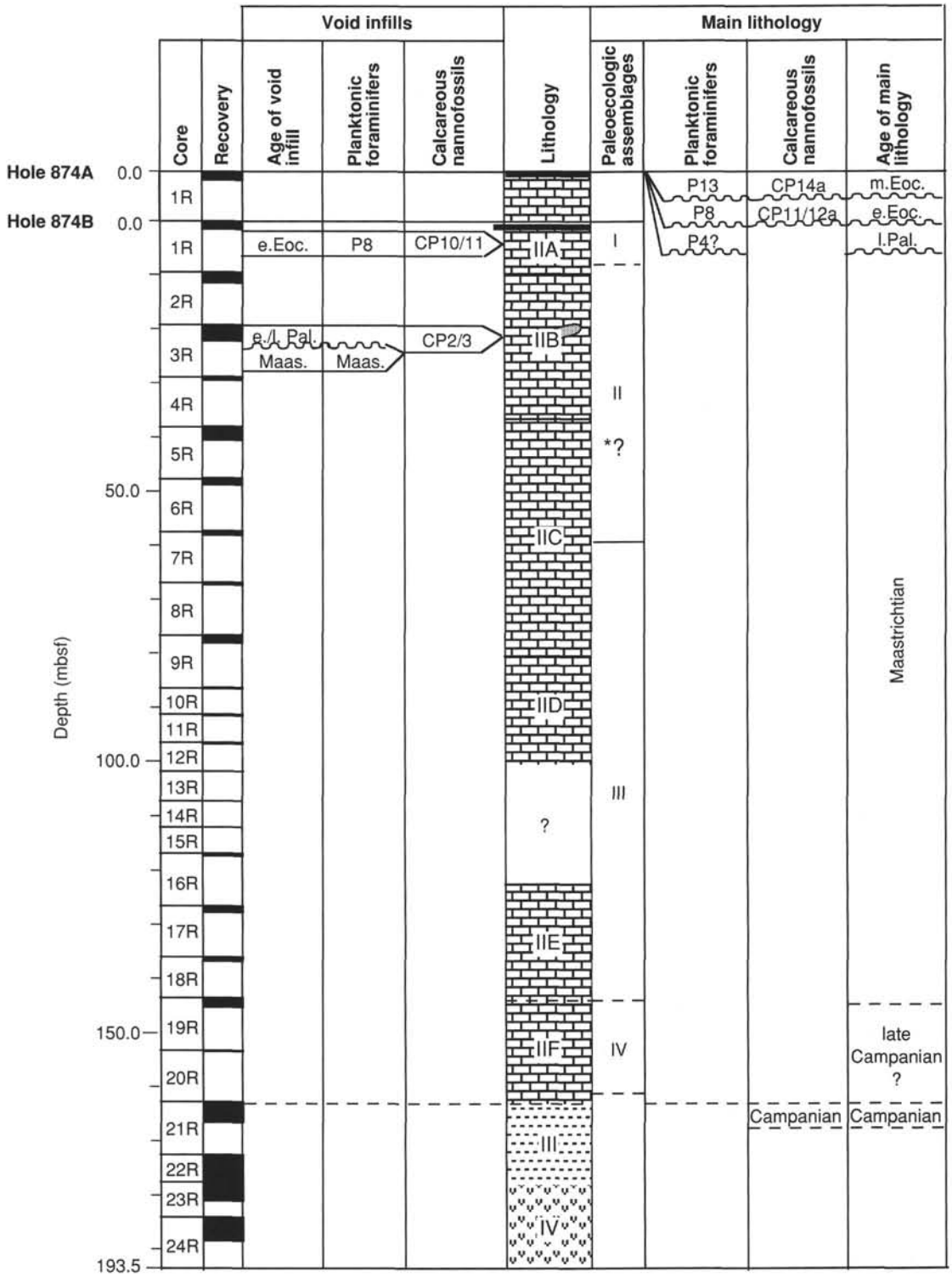

Figure 20. Biostratigraphy of Site 874. All age determinations refer to Hole 874B, except the planktonic foraminifer and nannofossil ages of the surficial manganese crusts, which are from Hole 874A. The asterisk denotes a questionable occurrence of the larger benthic foraminifer *Omphalocyclus,* which is restricted to the Maastrichtian. The Maastrichtian age of the limestones to Core 144-874B-18R is inferred from correlations of the benthic foraminifer assemblages with other sites on Wodejebato Guyot.

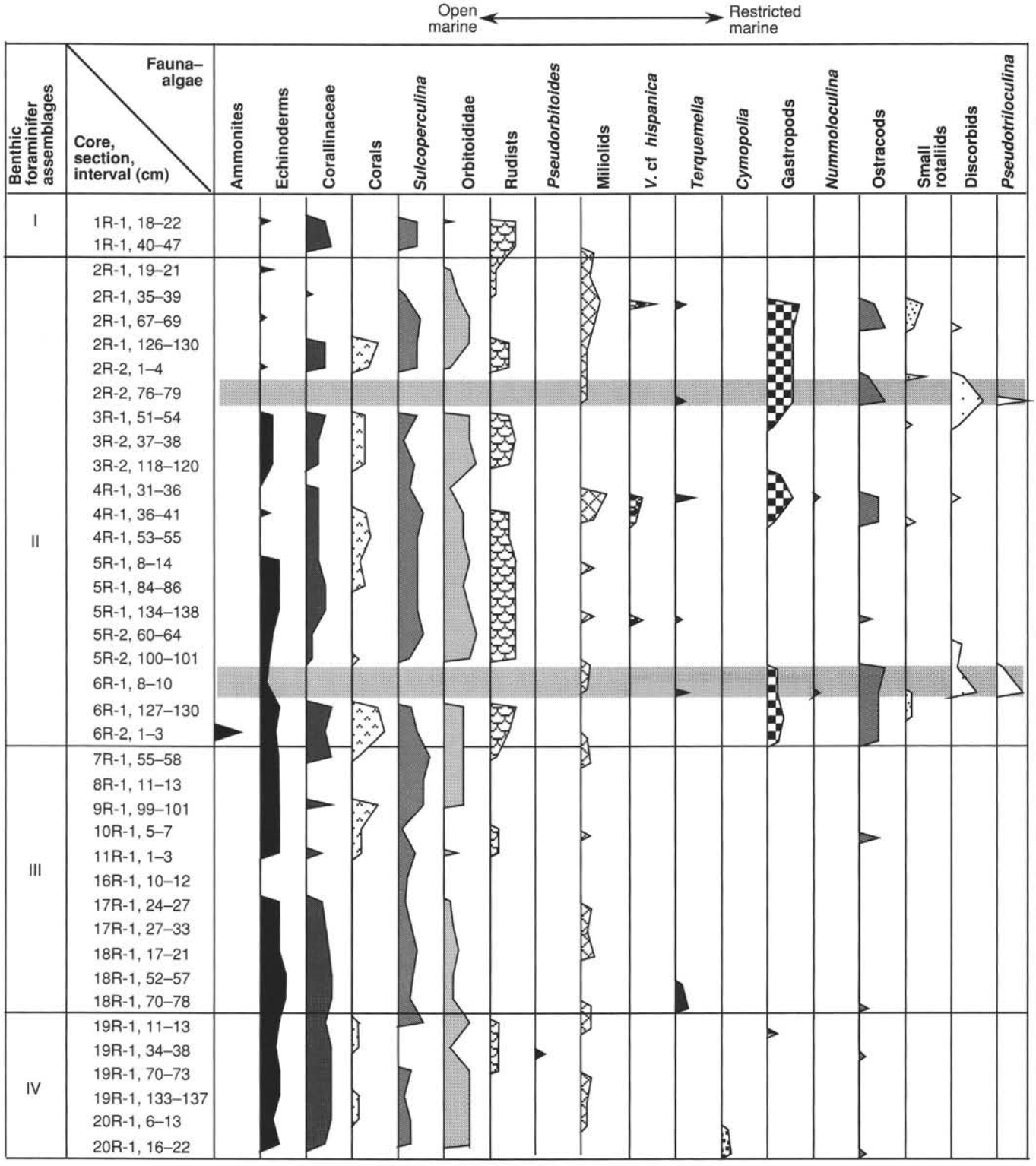

Figure 21. Preliminary summary of the distribution and relative abundance of foraminifers, algae, and other groups from Hole 874B, arranged according to their paleoecologic affinities. The darker shading refers to the most restricted facies.

by comparison with DSDP Site 462 in the Nauru Basin. Assemblage IV is the first of four different paleoecologic assemblages occurring throughout the limestones. The second, Assemblage III, indicates an open-marine environment in the absence of reef buildups. The third, Assemblage II, includes the development of a bioherm. Environmental conditions on the platform, however, varied widely, from fully marine to very marginal marine. The uppermost assemblage, Assemblage I, represents a carbonate platform with no occurrence of restricted faunas.

The carbonate platform was drowned before the end of the Cretaceous, as is evidenced by the occurrence of Maastrichtian planktonic foraminifers in pelagic sediment that infills a cavity in the platform

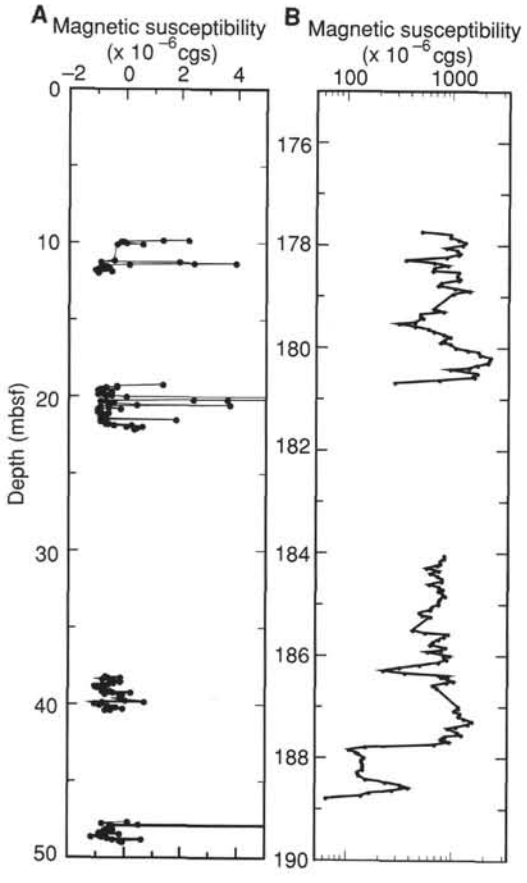

Figure 22. Magnetic susceptibility variations for (**A**) limestone and (**B**) claystone and basalt from Hole 874B. Note change in depth scale.

limestones. Also occurring in cavities are pelagic sediments of early late Paleocene and early Eocene age, as dated by calcareous nannofossils and planktonic foraminifers.

From the late Paleocene to the middle Eocene, a manganese-phosphate crust developed on the surface of the limestones; pelagic sediment of various ages was incorporated in this crust. A conglomeratic layer near the top of the crust was found to contain a block of late Paleocene age, which indicates a time of erosion and redeposition during the middle Eocene. No sediments are preserved from the middle Eocene to the present at this site.

PALEOMAGNETISM

Initial magnetic susceptibility was measured at 5-cm intervals for selected cores with relatively long continuous pieces from Hole 874B (Cores 144-874B-2R, -3R, -5R, -6R, -17R, and -21R through -24R). The susceptibility of the limestone is generally low or negative (Fig. 22A). Although clays overlying volcanic basement were recovered from Hole 874B, the data are unavailable for comparison with the clay interval at Site 873 because of measurements obtained using the wrong range on the Bartington magnetic susceptibility meter (Fig. 22B). Susceptibility values for the basalt in Hole 874B (176.7–193.5 mbsf) are about 10^{-3} cgs. Lower values are associated with smaller pieces and/or a higher degree of alteration (e.g., the lowest part of the section).

Measurements of natural remanent magnetization (NRM) and the remanence after 15-mT alternating field (AF) demagnetization were made at a spacing of 3 cm on several pieces of the limestone in Cores 144-874B-2R through -17R with the pass-through cryogenic magnetometer. This was done because the magnetic moment of a 10-cm^3 minicore of the limestone was too weak to measure. We were unable to determine a magnetostratigraphy; however, the higher sensitivity of shore-based magnetometers should be sufficient to determine the characteristic magnetization of the limestone samples.

Table 5. Results of demagnetization of discrete samples from Hole 874B.

Core section interval (cm)	Lithology	Inclination (degrees)
144-874B-		
23M-3, 40–42	Basalt	*–19.4
24M-1, 18–20	Basalt	+16.5
24M-3, 91–93	Basalt	+23.1
24M-4, 17–19	Basalt	+9.6

*May be inverted (was core catcher on deck).

Four discrete samples of basalt and volcaniclastic materials were stepwise demagnetized with the Schonstedt AF demagnetizer and measured with the pass-through cryogenic magnetometer (Table 5). Examples of the demagnetization behavior of samples from Hole 874B are shown in Figures 23–24. The characteristic remanence directions have positive inclinations except for Sample 144-874B-23R-3, 40–42 cm. The short length of this piece, and its recovered position in the core catcher, suggests that the orientation may be suspect. The range of the inclination of all the samples is from 9.6° to 23.1°, which is slightly lower than that of samples at Site 873 at Wodejebato Guyot (17°–27°). These data may be tentatively interpreted as representing a reversed polarity magnetization acquired at a low southern paleolatitude (about 9°S).

INORGANIC GEOCHEMISTRY

Interstitial Waters

Interstitial waters were taken from two core samples in Hole 874B and analyzed according to the methods outlined in the "Explanatory

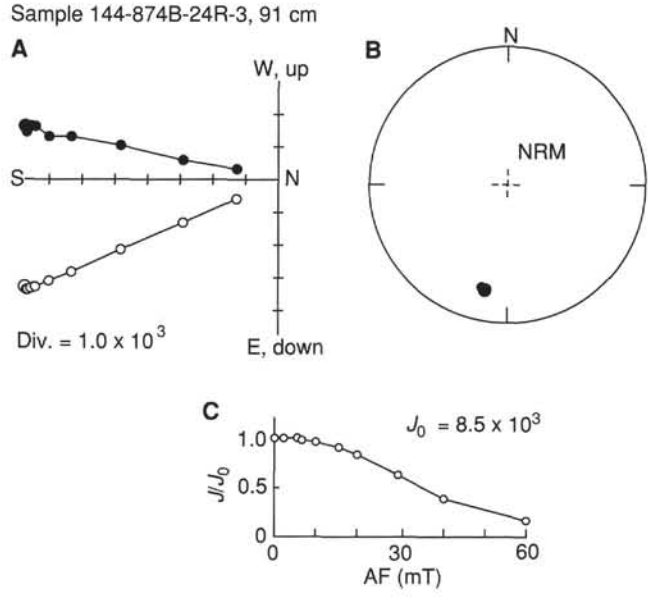

Figure 23. Alternating-field (AF) demagnetization results for basalt Sample 144-874B-24R-3, 91 cm. Demagnetization fields are 0, 2.5, 5, 10, 15, 20, 29, 40, and 60 mT. **A.** Orthogonal vector plot of the progressive AF demagnetization. Closed circles represent horizontal components of the magnetization, and open circles represent vertical components. **B.** Stereonet plot of vector endpoints after progressive demagnetization. **C.** Variation of intensity after progressive AF demagnetization.

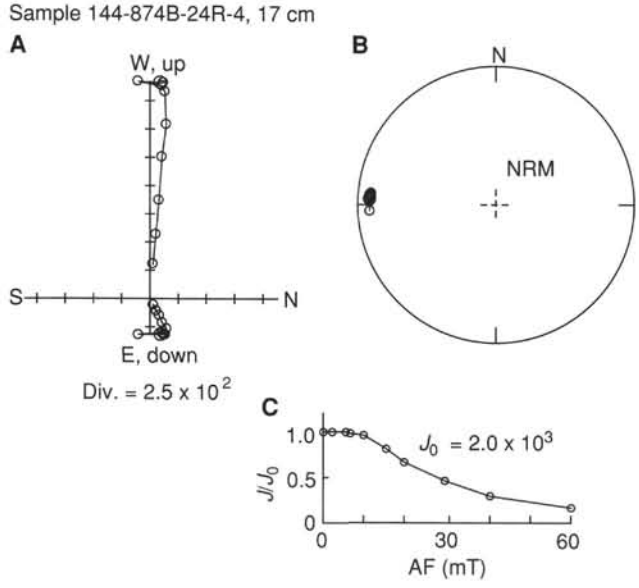

Figure 24. Alternating-field (AF) demagnetization results for basalt Sample 144-874B-24R-4, 17 cm. Demagnetization fields are 0, 2.5, 5, 10, 15, 20, 29, 40, and 60 mT. Other plot conventions are identical to Figure 23.

Notes" chapter (this volume). Both of these samples came from clays. No interstitial water samples were taken from the overlying or underlying units. Shipboard interstitial water data from Site 874 are presented in Table 6.

Salinity and Chlorinity

The salinity and chlorinity of the pore-water samples from Hole 874B are indicative of normal seawater (Table 6).

Alkalinity, pH, Calcium, Magnesium, Sodium, Potassium, Rubidium, Strontium, and Lithium

The pH and alkalinity values and measured sodium and rubidium concentrations are in the range of normal seawater. Calcium, magnesium, potassium, strontium, and lithium concentrations are consistent with chemical exchange between pore water and clay. Pore waters are moderately enriched with respect to seawater in calcium, potassium, strontium, and lithium whereas they are depleted in magnesium (Table 6).

Silica

Silica concentrations of the interstitial water samples from Hole 874B are elevated with respect to seawater (239 and 278 μM).

Sulfate and Ammonium

Sulfate and ammonium concentrations in the interstitial water samples from Hole 874B are indicative of normal seawater (Table 6).

Fluoride

Fluoride concentrations in interstitial water samples from Hole 874B are enriched with respect to normal seawater by 12 μM (Table 6).

Lithologic Data

Eight limestone samples from Hole 874B were analyzed according to the methods outlined in the "Explanatory Notes" chapter (this volume). Shipboard rock-sample data from Site 874 are presented in Table 7. Data are expressed as molar ratios to calcium for both minor and trace elements: $(Mg/Ca \cdot 10^2)$, $(Sr/Ca \cdot 10^3)$, $(F/Ca \cdot 10^3)$, $(PO_4/Ca \cdot 10^3)$, $(Fe/Ca \cdot 10^3)$, and $(Mn/Ca \cdot 10^4)$.

Magnesium, Strontium, Fluoride, and Phosphate

Magnesium/calcium and strontium/calcium ratios in rock samples from Hole 874B range from 1.82 to 2.93 and 0.21 to 0.48, respectively, and are consistent with the alteration of metastable aragonite and high magnesian calcite to more stable low magnesian calcite (3 mM Mg) (Fig. 25). Fluoride/calcium and phosphate/calcium ratios in rock samples from Hole 874B range from 0.65 to 4.84 and 0.56 to 8.31, respectively, and are indicative of the presence of some form of fluorapatite (Fig. 25).

Iron and Manganese

Iron/calcium and manganese/calcium ratios range from 0.17 to 0.41, and 0.21 to 16.0, respectively (Fig. 25).

Summary

Site 874 data are consistent with (1) chemical exchange between clays and their interstitial waters, (2) alteration of metastable aragonite and high magnesian calcite to more stable low magnesian calcite in limestones, and (3) the probable presence of some form of fluorapatite in limestones. Calcites associated with hiatal surfaces appear enriched in a phosphate rich phase.

ORGANIC GEOCHEMISTRY

Introduction

Site 874 was drilled on the inner perimeter ridge of Wodejebato Guyot. The type of rocks encountered at the site included (from top to bottom): manganese crust (Lithologic Unit I; see "Lithostratigraphy" section, this chapter), platform limestone (Unit II), clay and claystone (Unit III), and basalt (Unit IV). The clay and claystone of Lithologic Unit III have been divided into three informal subunits in this chapter: black clay with a thin shell bed at the bottom (Interval 144-874B-21R-1, 0–44 cm), bluish gray clay with relict structures of weathered basalt (Interval 144-874B-21R-1, 44–125 cm), and red clay with relict structures of weathered basalt (Sections 144-874B-21R-1, 125 cm, to -22R-4, 72 cm). The boundary between the gray and the red clay was defined from color alone.

The analytical program for Hole 874B included safety monitoring for hydrocarbon gases and chemical analyses of limestone and clay. Forty-seven samples were analyzed for inorganic carbon (IC), total organic carbon (TOC), nitrogen (N), and total sulfur (TS). Moreover, three samples from the clay were analyzed for organic matter type by pyrolysis. The procedures used for the analytical program are described in the "Organic Geochemistry" section, "Explanatory Notes" chapter (this volume).

Volatile Hydrocarbons

The shipboard safety and pollution monitoring program requires measurements of light hydrocarbon gases (C_1 to C_3) in cores immediately after retrieval onto the core deck. At Site 874, two headspace gas samples were obtained from the black and the red clay (Lithologic Unit III). The results of the analyses are given in Table 8. Very low concentrations of light hydrocarbon gases were detected. Methane concentration varied from 2.2 to 3.8 ppm, the highest value found in the black clay at the top of Section 144-874B-21R-1. This interval also contained small but measurable amounts of ethane and propane. The methane concentrations were slightly higher than the background

Table 6. Surface seawater and interstitial water geochemical data, Hole 874B.

Core, section, interval (cm)	Depth (mbsf)	pH	Alkanity (mM)	Salinity (g/kg)	Cl^- (mM)	Mg^{2+} (mM)	Ca^{2+} (mM)	SO_4^{2-} (mM)	NH_4^+ (μM)	SiO_2 (μM)	K^+ (μM)	Rb (μM)	Sr^{2+} (μM)	Na^+ (mM)	F (μM)	Li (μM)
Surface seawater	0	—	—	35.0	561	54.03	10.45	28.8	23	3	10.00	1.40	91	477	72	26
144-874B-																
21R-1, 140–150	164.20	7.59	2.95	36.0	562	50.91	13.49	29.1	116	239	10.74	1.20	116	478	85	45
22R-2, 140–150	175.30	7.60	2.58	35.5	565	50.69	14.19	29.4	114	278	11.35	1.57	122	488	84	45

Table 7. Lithologic geochemical data, Hole 874B.

Core, section, interval (cm)	Depth (mbsf)	Mg/Ca (· 10^2)	Sr/Ca (· 10^3)	F/Ca (· 10^3)	SiO_2/Ca (· 10^3)	PO_4/Ca (· 10^3)	Fe/C (· 10^3)	Mn/Ca (· 10^4)
144-874B-								
1R-1, 27–31	0.27	2.93	0.48	1.95	NA	3.06	0.410	2.07
1R-1, 43–47	0.43	1.95	0.30	4.84	NA	8.31	0.280	15.61
1R-1, 80–87	0.80	2.01	0.21	0.65	NA	0.78	0.230	0.33
1R-1, 92–100	0.92	2.80	0.51	1.11	NA	0.75	0.170	0.37
1R-1, 100–104	1.00	2.11	0.38	0.75	NA	0.73	0.245	0.21
2R-1, 27–31	9.97	2.06	0.36	0.48	NA	0.56	0.170	0.33
2R-1, 27–31	9.97	1.82	0.37	1.93	NA	2.85	0.230	0.34
2R-1, 27–31	9.97	2.12	0.37	1.59	NA	2.39	0.220	0.21

Note: NA = not applicable.

Table 8. Results of headspace gas analyses, Hole 874B.

Sample identification	Methane (ppm)	Ethane (ppm)	Propane (ppm)	Lithology
144-874B-				
21R-1, 0–5 cm	3.8	0.9	0.7	Black claystone
21R-2, 0–5 cm	2.2	None	None	Red claystone
Laboratory background	2.2	None	None	
Core deck background	1.8	None	None	
Sea air background	1.8	None	None	

Notes: Tr = trace, and None = no gas detected.

in the laboratory and on the core deck, which was found to be 2.2 and 1.8 ppm, respectively. The most likely source of the elevated methane concentration in the black clay was bacterial degradation of organic matter (TOC from 5% to 10%; see paragraph on organic carbon). The very low light gas concentration in the red clay can be ascribed to low concentration of organic carbon (TOC below 0.1%). Light hydrocarbon gases were not considered a safety hazard at this site.

Carbonate Carbon

Inorganic carbon (IC) content was measured in 47 samples from Holes 874B with the Coulometrics carbon dioxide coulometer and reported as weight% calcium carbonate. Sampling was performed in a way to obtain representative material with regard to both lithotypes and depth. Thirty-two microsamples from the limestone (approximately 100 mg each) were collected by hand drilling with a standard 5-mm drill bit. Fifteen samples of the clay underlying the limestone were collected directly on the split core. No sampling was done in the basalt. Results of the inorganic carbon analyses are given in Tables 9–10. Calcium carbonate data are shown in Figure 26.

Carbonate content was high in all samples from the platform limestone in Cores 144-874B-1R through -20R (Lithologic Unit II, average $CaCO_3$ = 95.0%), but showed greater variation than in limestone samples from Sites 871, 872 and 873. Grainstone samples had significantly lower carbonate values (average $CaCO_3$ = 93.6%, N = 14) than boundstones (average $CaCO_3$ = 98.8%, N = 5), whereas the other lithotypes (wackestone, packstone, and rudstone) had carbonate values between these two types. No significant changes were seen with depth. Two samples with <80% calcium carbonate were a phosphatized packstone (Sample 144-874B-1R-1, 19–23 cm, $CaCO_3$ = 77%) and a void-filling mudstone (Sample 144-874B-3R-1, 114–118 cm, $CaCO_3$ = 65%).

The boundary between Lithologic Units II and III is marked by a sharp decline in carbonate content. The $CaCO_3$ values drop from 97% in the packstone and grainstone from Core 144-874B-20R to >1% in the clay from Core 144-874B-21R. A similar drop was observed in the calcium value in the geochemical log between 162 and 164 mbsf (see "Downhole Measurements and Seismic Stratigraphy" section, this chapter). The highest carbonate values in Lithologic Unit III (up to 0.8% $CaCO_3$) were found close to the bottom of the black clay. At this level (Interval 144-874B-21R-1, 42–44 cm) a horizon rich in calcareous benthic microfossils and shell fragments was observed in the split core section (not sampled for chemical analysis). The gray clay below the shell horizon contained very little carbonate (average $CaCO_3$ = 0.4%), whereas the red clay was virtually carbonate free.

Organic Carbon and Total Sulfur

The content of total carbon (TC), nitrogen (N), and total sulfur (TS) was determined using the Carlo Erba Model NA1500 elemental analyzer. Total organic carbon (TOC) values were calculated from the difference between TC and IC. Detection limits for TOC, N, and TS are 0.2%, 0.02%, and 0.02%, respectively. Analyses were performed on the 47 samples used for carbonate carbon determinations. The results of the TOC, N, and TS analyses are given in Tables 9–10 and in Figures 26–28.

Very low TOC values were found in the shallow-water limestone from Lithologic Unit II (average TOC = 0.2%). In the same unit, nitrogen and sulfur concentrations were below detection limit. The boundary between the limestone in Unit II and the clay in Unit III was marked by a drastic increase in organic carbon and sulfur (Fig. 27) and a parallel but smaller increase in nitrogen. The black clay subunit had very high concentrations of organic carbon (average TOC = 5.3%) and extremely high concentrations of sulfur (average TS = 16.3%, corresponding to 30.5% pyrite). Large amounts of pyrite were observed in the core, mostly in the form of framboidal to euhedral pyrite crystals one tenth of a millimeter to a millimeter in size. Some of the sulfur probably also occurred as organic-bound sulfur, but no attempt were made to determine the distribution of sulfur between pyrite and organic matter. No other sulfur-bearing minerals were identified. Although sulfur content was relatively constant in the black clay, two upward-increasing cycles were evident in organic carbon content of this subunit (Fig. 27).

The bluish gray clay subunit below the black clay had low to very low concentrations of organic matter (average TOC = 0.9%), whereas sulfur remained high in the upper part and dropped to lower concentrations in the lower part of the clay (average TS = 7.8%). Pyrite was observed as euhedral crystals less than a millimeter in size, often concentrated in thin, horizontal zones. The boundary between the greenish gray and red clay subunits was easily recognizable from the sulfur content, which dropped from 3.1% to 0.0% within a 10-cm interval. The red clay contained neither organic carbon nor sulfur. Nitrogen was only identified in the black clay (average N = 0.05%), where it showed strong correlation to the amount of organic carbon (Fig. 28).

The TS/TOC ratios were high throughout the black clay and reached values from 10 to 70 at the base of the black clay and the top

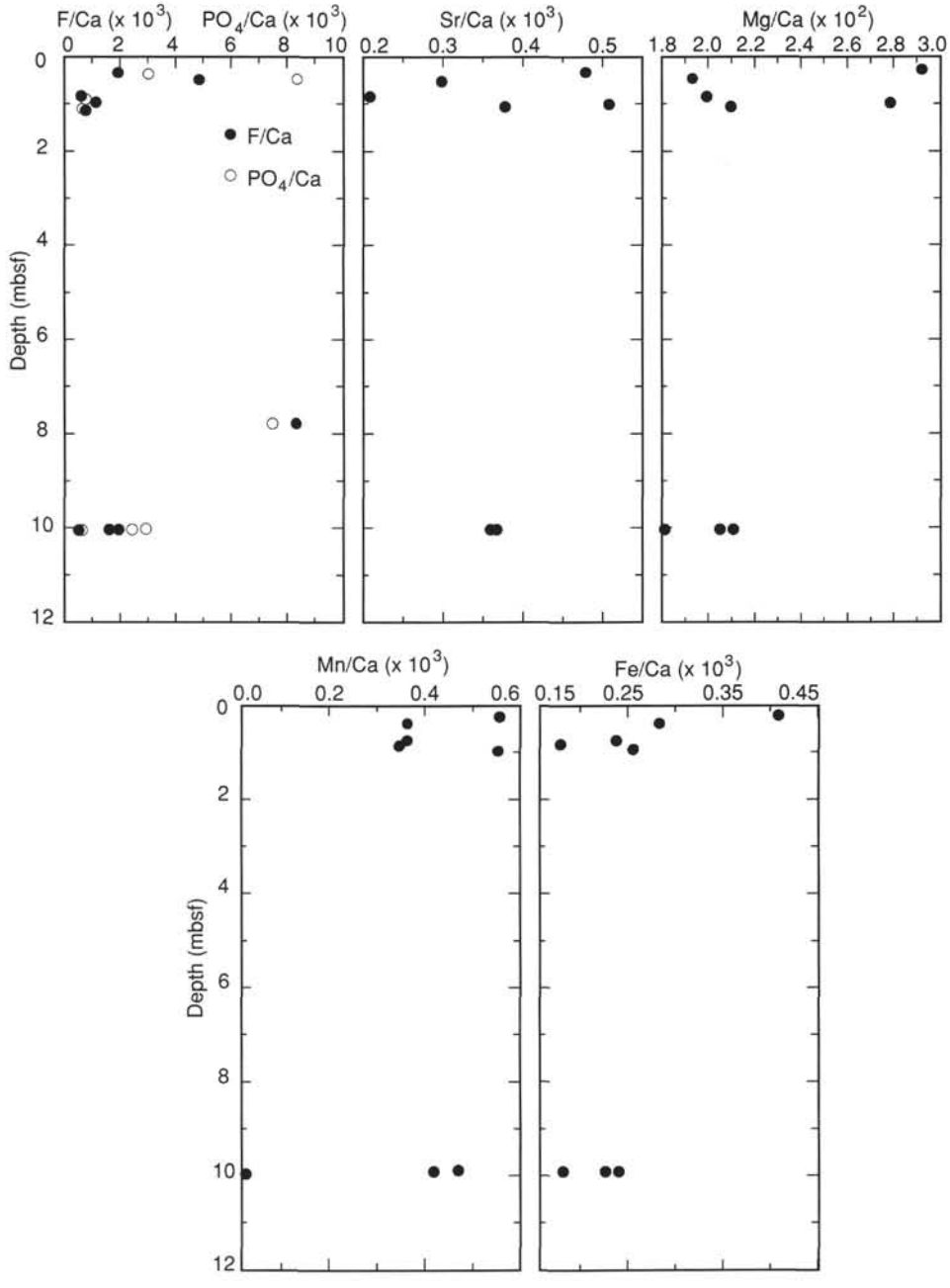

Figure 25. Elemental abundances of rock samples vs. depth in Hole 874B. Abundances are expressed as a molar ratio with respect to calcium.

of the bluish gray clay. The N/TOC ratios, on the other hand, were very low throughout the whole clay unit and never reached values higher than 0.01.

Organic Matter Type and Thermal Maturation Level

Shipboard geochemical characterization of organic matter is normally performed by Rock-Eval (RE) and pyrolysis gas chromatographic (Py-GC) analysis. Only samples containing more than 1% organic matter are considered suitable for these types of analyses. During the time spent at Site 874, the Rock-Eval instrument suffered an irreparable breakdown, and organic matter characterization was confined to the Geofina instrument. This instrument provided reliable pyrolysis data (S_1, S_2, and T_{max}) for Site 874 but failed to produce GC analyses.

Three samples from the black clay in Hole 874B (Samples 144-874B-21R-1, 13–14 cm, -21R-1, 19–20 cm, and -21R-1, 23–24 cm) were analyzed by the Geofina pyrolysis instrument. Results are reported in Table 11 and in Figure 29. Organic matter from the black clay contained very small amounts of free or pyrolyzable hydrocarbons and belonged to the type III ("woody" or vitrinitic) kerogen. The T_{max} and PI values showed the organic matter in Hole 874B to be immature with regard to thermal modification. Optical inspection demonstrated mainly woody material (see "Biostratigraphy" section, this chapter).

Interpretation of Organic Facies and Depositional Environments

Three major depositional environments are represented in Hole 874B: (1) shallow-water, open marine (represented by the platform

Table 9. Results of geochemical analyses, Hole 874B.

Core, section, interval (cm)	Depth (mbsf)	IC (wt%)	$CaCO_3$ (wt%)	TC (wt%)	TOC (wt%)	N (wt%)	TS (wt%)	Lithology
144-874B-								
1R-1, 19–23	0.19	11.88	98.96	12.13	0.25	0.01	0	Phosphatic packstone
1R-1, 47–50	0.47	9.27	77.22	9.82	0.55	0.01	0.02	Phosphatic packstone
1R-1, 92–99	0.92	11.87	98.88	11.97	0.10	0	0.01	Rudist boundstone
1R-1, 128–136	1.28	11.86	98.79	11.99	0.13	0	0	Rudist boundstone
2R-1, 30–34	10.00	11.75	97.88	12.00	0.25	0.01	0	Grainstone
2R-1, 124–134	10.94	11.83	98.54	11.68	0	0	0	Grainstone
2R-2, 48–56	11.59	11.09	92.38	11.17	0.08	0	0.01	Packstone
3R-1, 22–30	19.42	11.66	97.13	11.87	0.21	0	0	Packstone
3R-1, 114–118	20.34	7.85	65.39	8.00	0.15	0	0.15	Grainstone
3R-2, 115–128	21.82	11.88	98.96	12.03	0.15	0	0	Grainstone
3R-3, 18–26	22.28	11.55	96.21	11.72	0.17	0	0	Wackestone
4R-1, 23–30	28.93	11.76	97.96	11.92	0.16	0.01	0	Wackestone
5R-1, 33–38	38.43	11.85	98.71	11.98	0.13	0.01	0	Rudist grainstone
5R-1, 115–121	39.25	11.85	98.71	11.86	0.01	0	0	Rudist grainstone
5R-2, 51–54	40.11	11.73	97.71	12.01	0.28	0	0	Rudist grainstone
6R-1, 7–16	47.67	11.69	97.38	8.29	0	0.02	0	Wackestone
6R-1, 96–103	48.56	11.88	98.96	11.88	0	0	0	Rudist rudstone
6R-2, 4–14	49.14	11.77	98.04	11.95	0.18	0	0	Boundstone
7R-1, 19–26	57.39	11.78	98.13	11.78	0	0	0	Coral framestone
8R-1, 42–49	67.32	11.74	97.79	11.83	0.09	0	0	Coral boundstone
9R-1, 30–37	76.90	10.60	88.30	11.07	0.47	0	0	Grainstone
9R-1, 68–73	77.28	11.30	94.13	11.63	0.33	0	0	Algal rudstone
9R-2, 3–9	78.11	10.79	89.88	10.97	0.18	0	0	Grainstone
10R-1, 0–4	86.20	11.50	95.80	11.70	0.20	0	0	Packstone
11R-1, 4–7	91.24	11.73	97.71	11.98	0.25	0	0	Coral packstone
12R-1, 0–5	96.20	11.82	98.46	11.82	0	0	0	Packstone
16R-1, 20–25	117.00	11.74	97.79	11.68	0	0	0	Grainstone
17R-1, 32–37	126.72	10.14	84.47	10.84	0.70	0	0	Grainstone
18R-1, 25–31	136.25	11.80	98.29	11.99	0.19	0.01	0	Grainstone
19R-1, 24–28	143.74	11.69	97.38	11.96	0.27	0	0	Grainstone
19R-1, 121–126	144.71	11.64	96.96	11.75	0.11	0	0	Packstone
20R-1, 6–13	153.16	11.76	97.96	11.95	0.19	0	0	Grainstone
21R-1, 0–5	162.82	0.03	0.20	9.26	9.23	0.09	16.16	Pyritic black clay
21R-1, 13–14	162.93	0.02	0.17	5.06	5.04	0.06	17.13	Pyritic black clay
21R-1, 19–20	162.99	0.03	0.25	2.77	2.74	0.03	17.07	Pyritic black clay
21R-1, 23–24	163.03	0.03	0.25	8.67	8.64	0.07	16.05	Pyritic black clay
21R-1, 35–36	163.15	0.07	0.58	4.80	4.73	0.05	17.87	Pyritic black clay
21R-1, 44–45	163.24	0.10	0.83	1.22	1.12	0	13.77	Pyritic black clay
21R-1, 74–75	163.54	0.03	0.72	0.72	0.69	0	16.55	Pyritic gray clay
21R-1, 93–94	163.73	0.03	0.25	0.09	0.06	0	3.81	Pyritic gray clay
21R-1, 112–113	163.92	0.03	0.25	1.90	1.87	0	3.14	Pyritic gray clay
21R-1, 125–126	164.05	0.03	0.25	0.03	0	0	0.01	Red clay
21R-1, 135–136	164.15	0.03	0.25	0.10	0.07	0	0	Red clay
21R-1, 140–150	164.20	0.01	0.08	0	0	0	0	Red clay
21R-2, 32–33	164.62	0.01	0.07	ND	ND	ND	ND	Red clay
21R-2, 134–135	165.64	0.01	0.08	1.45	1.44	0.01	0.57	Red clay
22R-2, 140–150	175.30	0.01	0.08	0.05	0.03	0	0.01	Red clay

Notes: IC = inorganic carbon, $CaCO_3$ = carbonate carbon calculated as calcium carbonate, TC = total carbon, TOC = total organic carbon, N = nitrogen, TS = total sulfur, and ND = no determination. All numbers are in weight percent.

limestone in Lithologic Unit II); (2) shallow-water, restricted marine (represented by the black clay in Unit III); and (3) terrestrial (represented by the bluish gray and red clay in Unit III). The thin layer, rich in calcareous marine shells at the base of the black clay in Unit III (Interval 144-874B-21R-1, 40–42 cm), probably formed as a lag deposit during the transition from terrestrial to marine conditions at this site.

In the first environment, preservation of organic matter was extremely poor. The TOC values below 0.3% in all but three samples and the TS values below detection limit indicate deposition under oxic conditions with very low preservation potential for organic matter. Most of the organic matter probably was of marine origin.

In the second environment, preservation of organic matter of terrestrial origin was highly favorable. The very high content of pyritic sulfur in the black clay must be a result of intense bacterial sulfate reduction under subaquatic, anoxic conditions. The sulfate source most probably was seawater, which replenished the reservoir of sulfate ions and at the same time kept salinity within biologically acceptable limits. Organic matter necessary for the sulfate reduction was provided by influx from terrestrial sources and from local growth of algae and bacteria. The reaction products of sulfate reduction are hydrogen sulfide, bicarbonate, and refractive organic matter. If the amount of reactive iron is sufficient, hydrogen sulfide will precipitate as pyrite. In the present case, production of hydrogen sulfide in the black clay far exceeded the amount of reactive iron, and downward diffusion of hydrogen sulfide into the underlying weathering profile led to the reduction of ferric iron (probably occurring as red hematitic iron pigmentation) and the subsequent precipitation of pyrite. The boundary between bluish gray and red clay most probably represents the reduction front.

The high TS/TOC ratios in the black clay reflects a level of sulfate reduction, which is much higher than can be explained from the amount of organic matter found in the clay today. Probably most of the original organic matter was decomposed by the sulfate-reducing bacteria leaving only the woody fraction of organic matter, which is refractive to bacterial activity. The very low N/TOC values of the organic matter indicate strong alteration and thus support this interpretation.

The good preservation of pyrite-rich clay directly below platform deposited under oxic conditions presents a problem. The FMS log for this interval does not identify any thick clay sequence on top of the black clay (see "Downhole Measurements and Seismic Stratigraphy" section, this chapter). On the contrary, the black clay seems to be overlain by a strongly cemented limestone. It is thus possible that a carbonate sequence was deposited directly on top of the sulfide-rich mud, and that bicarbonate released by sulfate reduction led to rapid cementation of the carbonate and formation of an impermeable seal above the clay. Carbon isotope studies of the limestone recovered in Section 144-874B-20R-1 may provide further information into this problem.

Table 10. Averages of geochemical results, Hole 874B.

Lithologic units	$CaCO_3$ (wt%)	TOC (wt%)	N (wt%)	TS (wt%)	General lithology
II					Limestone
Average	95.00	0.19	0	0.01	
SD	7.20	0.16	0	0.03	
N	32	32	32	32	
III-1					Pyritic black clay
Average	0.38	5.25	0.05	16.34	
SD	0.27	3.20	0.03	1.43	
N	6	6	6	6	
III-2					Gray clay
Average	0.41	0.87	0	7.83	
SD	0.27	0.92	0	7.56	
N	3	3	3	3	
III-3					Red clay
Average	0.15	0.31	0	0.12	
SD	0.09	0.63	0	0.25	
N	5	5	5	5	

Notes: Subunits in Unit III are informal and are only used in this chapter. SD = standard deviation, and *N* = number of samples.

Conclusions

The following conclusions can be made regarding the organic geochemistry at Site 874:

1. No volatile hydrocarbons were encountered at this site.
2. The platform limestone (Lithologic Unit II) had calcium carbonate contents from 95% to 98%. Only very low concentrations of organic matter were encountered. The unit was deposited under oxic conditions.
3. The black clay at the top of Lithologic Unit III was very rich in organic carbon and pyritic sulfur. The clay was deposited under strongly sulfate-reducing conditions probably in direct contact with seawater.
4. The organic matter in the black clay, as found today, had a composition corresponding to a type III (woody) kerogen of terrestrial origin.
5. The high sulfur content of the gray clay and weathered basalt below the black clay reflects downward diffusion of reducing hydrogen-sulfide-rich fluids. The boundary between the gray and red clay represents the reduction front.
6. Organic matter at this site is thermally immature with regard to hydrocarbon formation.

IGNEOUS PETROLOGY

Introduction

Site 874 was drilled on the inner perimeter ridge near the northern edge of Wodejebato Guyot. Basalt recovered in Hole 874B is overlain by 14.9 m of clay and claystone (Lithologic Unit III). The upper portion (Sections 144-874B-21R-1, 2 cm, through -22R-2, 77 cm) of the claystone has relict texture of a vesicular, plagioclase phyric basalt, similar to the basalt recovered in Hole 875C. The lower portion of the claystone (Sections 144-874B-22R-2, 77 cm, through -22R-3, 150 cm) has relict texture resembling the underlying basalt. The claystone unit is clearly a thick, in-situ, subaerial weathering profile through basaltic flows.

The basalt in Lithologic Unit IV was reached at 177.7 mbsf in Hole 874B (Section 144-874B-22R-4, 0 cm); 16.5 m of basalt were drilled, but only 7.76 m were recovered (47% recovery).

Hole 874B

The basaltic lava samples recovered in Hole 874B appear to be from a single ankaramite flow (Unit 1). They are, as shown in Figures 30–31, highly porphyritic, containing 25% fractured, subhedral olivine grains, 1–8 mm in diameter; 15% rounded clinopyroxene grains, 1–14 mm in diameter; and 5%–10%, prismatic to anhedral plagioclase grains, 0.2–3 mm in diameter. Olivine is completely pseudomorphed by iddingsite and green clay near the top of the unit (e.g., Fig. 30 and thin-section Sample 144-874B-23R-3, 40–42 cm). Deeper in the hole, progressively more fresh olivine is present (e.g., thin-section Sample 144-874B-24R-4, 112–113 cm, where only minor clay alteration has occurred). Clinopyroxene is unaltered throughout the unit except for minor clay development along fractures (Figs. 30–31). Optically continuous, skeletal quench overgrowths occur along the edges of most clinopyroxene phenocrysts. Large plagioclase phenocrysts have been completely altered to clay minerals in the upper portion of the unit; in the lower portion of the unit (e.g., thin-section Sample 144-874B-24R-4, 17–19 cm), however, the plagioclase is quite fresh. Often the phenocrysts occur as glomerocrysts. Single large clinopyroxene grains occasionally enclose several smaller olivines. Some clinopyroxene grains show evidence for having reacted with the melt; they consist of small regions of contrasting color, either pleochroic in pale browns or clear. Often, clinopyroxene grains of this type are irregularly embayed by (altered) glass along their edges. These observations strongly suggest that many of the primary phenocrysts are xenocrysts transported by the host magma from a cumulate wehrlite or gabbro.

The matrix is microcrystalline with a variable, intersertal to pilotaxitic, texture. Primary minerals include 25%–40% pink titanaugite grains, 0.02–0.1 mm in diameter; 10% titanomagnetite cubes, 0.02 mm in diameter; 5% olivine grains altered to orange, speckled clay, 0.02 mm in diameter; and 40% plagioclase laths, 0.01–0.05 mm in diameter. Plagioclase has been altered to green clay and zeolites in the upper portion of the unit (e.g., thin-section Sample 144-874B-24R-1, 18–20 cm), but it is mostly unweathered in the lower portion of the unit (e.g., thin-section Sample 144-874B-24R-4, 122–113 cm). Green and brown clay is abundant throughout the groundmass. The matrix, viewed as the host lava for the xenocrysts, appears to be an alkali olivine basalt.

A portion of Unit 1 (Sections 144-874B-24R-1, 78 cm, to -24R-2, 78 cm) contains a large vein with an accompanying alteration halo. The vein is subvertical and filled with a soft, dark greenish yellow (10Y 6/6), waxy mineral. The vein is irregularly lined with 1–7 mm of impure sparry calcite. Immediately adjacent to the vein, the basalt matrix is very dark grayish green (10G 3/1). In the first 3 cm out from the vein, olivines are altered to dusky red (10R 3/2) and clinopyroxenes show considerable moderate yellow green (5GY 7/4) clay development along fractures. A band of red (10R 4/6) olivines is present 3–5 cm out from the vein; clinopyroxenes show only slight alteration to clay along fractures, as in other places in the core.

Summary

A single basaltic lava flow recovered in Hole 874B is overlain by a claystone weathering profile (Lithologic Unit III), indicating a low-energy environment during the transition to a marine environment.

The lava flow is a highly phyric ankaramite containing xenocrysts of olivine, clinopyroxene, and plagioclase in a groundmass of alkali olivine basalt, which is much like the basalt samples from other Wodejebato Guyot sites.

PHYSICAL PROPERTIES

Introduction

The objectives of the physical properties measurement program at Site 874 were (1) to measure standard shipboard physical properties and (2) to identify downhole geotechnical units. Standard index properties measurements and Hamilton Frame compressional wave velocities, measured using sample cubes of limestone and basalt, comprised the major part of the shipboard analyses ("Explanatory Notes" section, this volume) at Site 874. Thermal conductivity measurements were only done on part of the clayey material because of a malfunction of the Thermcon needle-probe system.

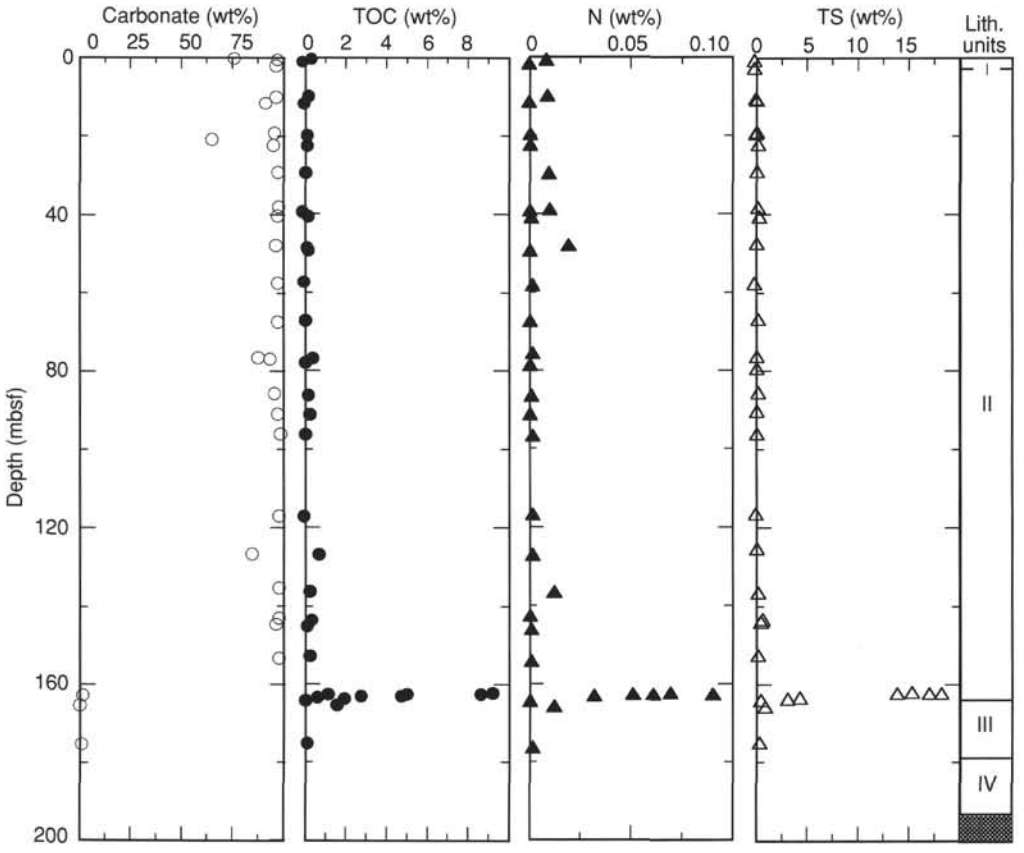

Figure 26. Carbonate (calculated as calcium carbonate), total organic carbon (TOC), nitrogen (N), and total sulfur (TS) contents of sediments in Hole 874B. Also shown are the major lithologic units, as given in the "Lithostratigraphy" section (this chapter).

Sediments recovered at Site 874 consist of Maastrichtian white and very pale brown, skeletal packstone, grainstone and boundstone (0–123 mbsf), reddish yellow grainstone (123–140 mbsf), foraminifer algal grainstone (140–163 mbsf), and saprolitic clays and claystone (163–178 mbsf) derived from the weathering of the underlying basalt. The upper surface of limestone was found to have a thin, burrowed surface, encrusted by manganese oxide.

Index Properties

Index properties measurements were made on 35 limestone, 9 clay, and 6 basalt samples. Wet/dry weights and volumes were used to calculate wet- and dry-bulk density, grain density, porosity, and water content ("Explanatory Notes" section, this volume). The results, corrected for 3.5% salt, are given in Table 12 and Figure 32.

In the limestone, wet- and dry-bulk densities vary from 2.2 to 3.2 g/cm^3 and from 1.8 to 3.1 g/cm^3, respectively. Grain density varies in the limestone from 2.55 to 2.9 g/cm^3. In the clays and claystones, wet- and dry-bulk density values are much lower; grain density in contrast is higher in the clays at more than 3 g/cm^3. These relatively high values are consistent with those for similar saprolitic clays from Sites 871 and Site 873 ("Physical Properties" section, "Site 871" and "Site 873" chapters, this volume). Basalt, when relatively fresh, has more or less identical wet, dry, and grain densities equal to ≈3 g/cm^3. Water content (% dry wt) in the limestone and basalt varies between 1% and ≈20%, higher values of up to 60% are found in the clayey sediments. Porosity rises to a maximum of 30% in the limestone; it is about 63% in the clayey material. The porosity of Site 874 basalts depends primarily on the degree of weathering they have undergone. Therefore, porosities of more than 20% in the basalt are indicators of a high degree of alteration.

The fact that, in some of the samples and especially in the limestones, measured values of wet-bulk and even dry-bulk density are higher than grain density values must be a result of problems with the measurement process. These physically impossible results can be explained in the following ways: (1) the samples showing these results are very dense with only minor porosity and/or the sample volume was too small for accurate pycnometer measurements of dense material; (2) as ODP sampling policy does not allow limestone samples to be crushed after being dried, grain density measurements may be partly in error; and (3) dry volume pycnometer measurements are assumed to be more accurate than wet volume measurements (Shipboard Scientific Party, 1992). Careful shore-based evaluation of the data is needed, therefore. Nevertheless, values for water content and porosity should be quite reasonable.

P-wave Velocity

Hamilton Frame (HF) compressional wave velocity measurements were made in three directions on oriented sample cubes of limestone (nine samples) and basalt (six samples) from Hole 874B. As a result of the highly weathered condition of the basalt, two samples disintegrated during the measurements. The data are given in Table 13. Compressional wave velocities vary in the limestone from 3174 to 5152 m/s, with a mean of 4304 m/s. The highest velocity values are found in the dense, well-cemented limestone with low porosity. Compressional wave velocity values in the basalt range from 2513 to 5667 m/s, with a mean of 3680 m/s (Fig. 33). Again, the highest velocities are found in dense rocks with low

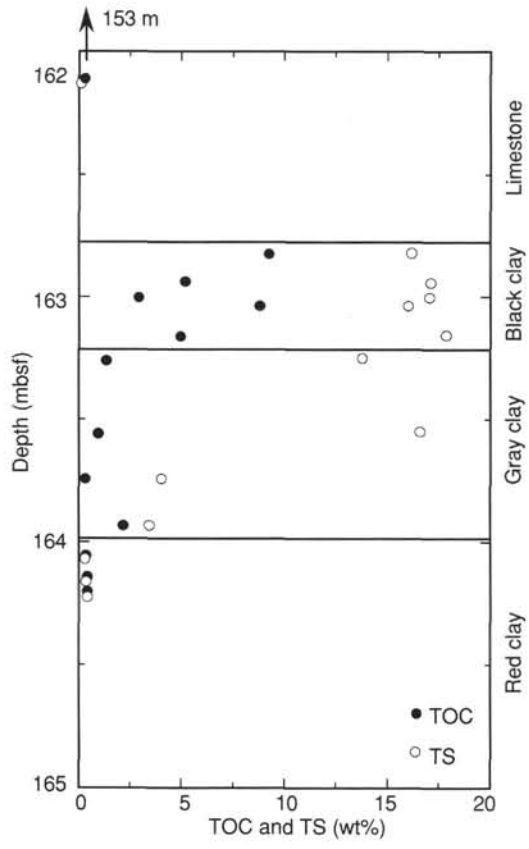

Figure 27. Total sulfur (TS) and total organic carbon (TOC) content for the transition from limestone to clay in Hole 874B.

porosity whereas the lowest velocities are found in highly weathered basalt showing high porosity. The velocity anisotropy index is mostly negative in the limestone, indicating higher vertical than horizontal compressional wave velocity. No consistent trend in compressional wave anisotropy is apparent in the basalt.

Thermal Conductivity

Thermal conductivity was measured on three whole-round sections of clayey material from Core 144-874B-21 before the breakdown of the Thermcon needle-probe device. The results, given in Table 14, are highly variable, ranging from 2.52 W/(m · K) in the first section to 1.07 W/(m · K) in the third section. This variability may be caused by compositional changes in the clay.

Relationship of Physical Properties to Lithology

A comparison between index properties and lithology reveals that a particular range of index property values can be clearly correlated with the limestone, clay, and basalt units at Site 874. The change in lithology from limestone to clay and claystone results in an abrupt increase in water content, porosity, and grain density and a decrease in wet- and dry-bulk density at a depth of 163 mbsf. In the basalt, wet- and dry-bulk density, porosity, and water content are similar to the index properties of the limestone, whereas grain density is more similar to the clay unit. Amid the moderate scatter of the geotechnical data in the limestone unit, index properties cannot be specifically related to lithologic subunits (see "Lithostratigraphy" section, this chapter). A slight increase in porosity and water content below 65 mbsf might be related to a faint change in lithology.

DOWNHOLE MEASUREMENTS AND SEISMIC STRATIGRAPHY

Log Types, Processing, Reliability, and Resolution

Logs were obtained in Hole 874B on the northeast margin of Wodejebato Guyot with the geophysical (two passes), Formation MicroScanner (two passes), and geochemical tool strings. The log measurements extend from the top of the volcanic edifice into the upper portion of the carbonate platform. These logs are valuable for interpreting the sedimentary succession and possible discontinuities in accumulation within the carbonate platform, because core recovery within the 160 m interval of platform carbonates (Cores 144-874B-1R through -20R) averaged only 10%, and was less than 2% for Cores 144-874B-10R through -15R. In particular, the high-resolution FMS coverage of the borehole wall is excellent for imaging the lower carbonate platform succession.

Logging tool strings were lowered to approximately 175 mbsf where a constriction in the borehole prevented further penetration. This is within the clay-rich weathering zone overlying the volcanic edifice. The spacing of tools on the various logging tool strings implies that the lower boundary of logging data from each tool varies (see diagram of tool strings in "Explanatory Notes" chapter, this volume). The varying position of the drill string (35 mbsf for the geophysics tool runs, 40 mbsf for FMS and geochemistry tool runs) changed the upper limit of useful measurements.

The natural gamma tool (NGT) run on each string recorded distinct narrow peaks within the carbonate platform facies at approximately 123 and 140 mbsf (Fig. 34). The locations of these natural gamma events were used to calibrate the wireline depths from the various runs. The geochemistry run recorded natural gamma peaks which were approximately 0.1 m lower than in the geophysics run, and approximately 0.3 m higher than in the FMS run. To calibrate these relative depths to drilled depths in the hole, we used the base of the drill pipe, positioned at 1420 m below rig floor (40 mbsf) during the geochemistry run as the standard to define meters below seafloor (mbsf). The end of the drill pipe is recognized by a sharp increase in iron abundance measured by the geochemical string, with the midpoint of this rise, corresponding to the approximate center of tool resolution, occurring at 1418.6 m in log wireline depth, which is 1.4 m shallower than the drill-pipe depth. Therefore, the conversion from wireline logging depths (meters below rig floor) to mbsf (meters below seafloor according to drilled depth) is: (1) subtraction of 10.9 m (distance from rig floor to mean sea surface); (2) subtraction of 1374.0 m (depth from sea surface to seafloor according to drilling operations); (3) adding 1.4 m to calibrate the geochemical run with the drill pipe; and (4) correction for offsets between different logging runs by adding 0.1 m to the geophysics log measurements and subtracting 0.3 m from the FMS measurements. The daily tide range during the drilling and logging operations was <1 m in this region (Hydrographer of the Navy, 1991), so we did not compute differential tide corrections to the intercalibration of logging and drilling depths.

The caliper log of the borehole diameter can be interpreted in terms of the relative degree of consolidation and cementation of the limestone facies. Hole 874B displays a major "washout" from 85 to 125 mbsf, corresponding to the poor recovery in Cores 144-874B-10R through -16R (Fig. 34). In this interval, the FMS pads are no longer in complete contact with the borehole walls and one or more of the four traces may be incoherent (see "Explanatory Notes" chapter, this volume). The lithodensity tool has incomplete contact against the borehole wall where borehole diameter exceeds 46 cm (18 in.) producing unreliably low values (Fig. 34).

Overview of Resistivity, Density, and Natural Gamma Relationships

In general, resistivity, density, and sonic velocity display similar increases and decreases throughout the logged interval at Hole 874B,

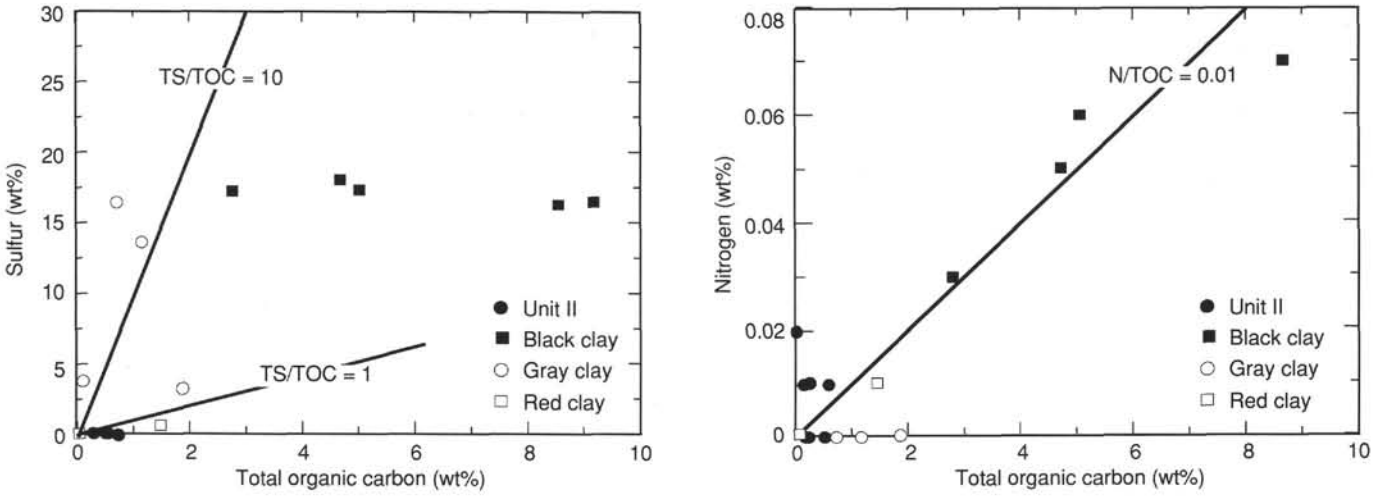

Figure 28. Total sulfur vs. total organic carbon (TS/TOC) and nitrogen vs. total organic carbon (N/TOC), Hole 874B. The black, gray, and red clays are all from Lithologic Unit III.

Table 11. Results of the pyrolysis analyses of organic-rich samples from Hole 874B obtained by means of the Geofina hydrocarbon meter.

Core, section, interval (cm)	TOC (wt%)	S1 (mg/g)	S1/TOC	S2 (mg/g)	HI (mg/g)	PI	T_{max} (°C)	Lithology
144-874B-								
21R-1, 13–14	5.06	0.22	0.04	3.60	71	0.06	409	Black clay
21R-1, 19–20	2.77	0.18	0.06	1.99	72	0.08	409	Black clay
21R-1, 23–24	8.67	0.31	0.04	4.14	48	0.07	409	Black clay

Notes: TOC = total organic carbon, from Table 9; S1 and S2 = mg hydrocarbon/gram of rock; HI = hydrogen index (mg hydrocarbon/gram of organic carbon); PI = production index (free hydrocarbon relative to total hydrocarbon); and T_{max} = maximal S2 pyrolysis temperature (in degrees Celcius). Further explanation of the pyrolysis parameters are given in the "Organic Geochemistry" section, "Explanatory Notes" chapter (this volume).

both in terms of changing average values among facies and as small-scale peaks within each facies (Figs. 34–35). Similar relationships observed in Holes 871C and 873A are interpreted to reflect differences in carbonate depositional facies enhanced by differential porosity, cementation, and hole diameter (see discussion in "Downhole Measurements and Seismic Stratigraphy" section, "Site 871" chapter, this volume). However, these correlations among geophysical parameters are not as clear as those in Holes 871C and 873A, representing lagoonal carbonate facies. The recovered core material suggests that the composition of the limestone also influenced the degree of cementation, with skeletal grainstones being less cemented than micritic mudstone or algal boundstone. This lithologic control appears to be especially important in the lower portion of the carbonate platform. As a result, the corresponding responses of the density tool and especially the resistivity tool are magnified by these changes in facies (Figs. 34–36).

Resistivity measurements were observed to depend on the depth of penetration of the different resistivity sondes, which is largely an artifact of the irregular hole diameter; therefore, we consider the medium-penetration resistivity measurements to provide the more reliable values and detail (see "Explanatory Notes" chapter, this volume). The FMS provides the highest resolution (about 5 mm) mapping of the resistivity variations of the borehole wall, and indicates that many of these short-wavelength features have internal complexity, such as groupings of thin beds or irregular patterns of cementation. However, the FMS record is incomplete in the clay facies and "washed-out" intervals because of the enlarged borehole diameters.

Natural gamma intensity displays several anomalous peaks within the carbonate platform, most of which are caused by uranium concentrations (Figs. 34 and 37). Most of the major peaks do not appear to directly correspond to high-density or high-resistivity peaks; for example, the largest observed uranium concentration (7 ppm) at 140 mbsf has no corresponding feature in either density or resistivity logs. Many of the minor uranium fluctuations in Hole 874B appear to mimic some of the density-resistivity features. This correlation is similar to logs within the carbonate platform of the Great Barrier Reef region, in which uranium mimicked the porosity pattern of the density and resistivity logs (e.g., Shipboard Scientific Party, 1991). However, we suspect that the majority of the major uranium enrichment horizons are associated with hiatuses or condensed sedimentary intervals, or are associated with uranium concentrations at redox interfaces (see discussion in "Downhole Measurements and Seismic Stratigraphy" section, Site 871" chapter, this volume). The relatively higher background uranium level from 140 through 150 mbsf appears to be associated with an abundance of algal rhodoliths (Cores 144-874B-18R and -19R), and may reflect uranium scavenging in the redox microenvironments of the red algal crusts ("thalli").

Sonic Traveltime Computations

An attempt was made to recover the seismic velocity profile from the sonic log by averaging the four traveltimes from each sonic log measurement. Because a variation of this technique yielded anomalously low velocities at previous Leg 144 sites, and the sonic records themselves were very noisy, we switched from the long-spaced to the short-spaced sonic tool at Hole 874B. This latter tool gives the same output signal amplitude, but measures the arrival times and wave forms over shorter pathways than the long-spaced tool. Thus, we hoped to raise the signal-to-noise levels with this instrument, despite giving up the longer pathway averages of the previous tool.

The records look substantially more coherent with the short-spaced tool than with the long-spaced version. For instance, no signal "spikes" of greater than 4 km/s had to be eliminated from these records before averaging. Thus, we did not think it necessary to pick the fastest remaining pathway at each point for averaging into the traveltime/depth curve as we had at the previous holes. We simply averaged all four traveltimes at each measurement point. These average traveltimes were summed (integrated) to obtain two-way traveltime as a function of depth in the hole (mbsf) (Fig. 38). No obvious breaks in slope were present in the resulting traveltime/depth curve, so we can only estimate the average formation velocity over the entire logged interval. This logged interval extends from 34 to 156 mbsf (122 m), where two-way traveltime was measured to increase from 1.88 to 1.975 s (0.095 s). The resulting average formation velocity for this portion of the limestone section is 2.6 km/s.

Only the basement reflection was observed as a coherent subsurface event in the seismic reflection profile, so a corresponding average formation velocity for the entire limestone section can be calculated

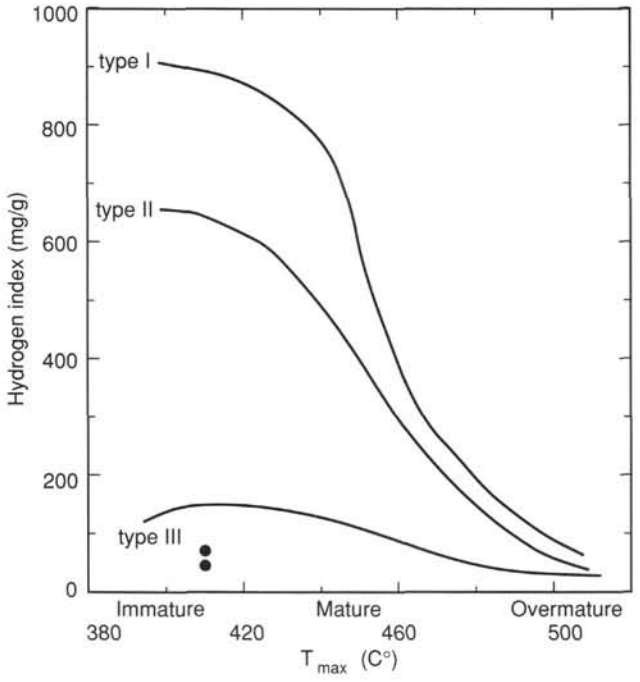

Figure 29. Kerogen typing and thermal maturation for organic matter from Hole 874B. Samples are from Interval 144-874B-21R-1, 13–24 cm. Roman numerals refer to kerogen types: type I is algal, type II is algal/herbaceous, and type III is woody. The samples investigated belong to kerogen type III.

from that record (Fig. 39). The total limestone section occurs between 1.87 and 2.01 s total TWT (0.14-s interval TWT), and between 0 and 172 mbsf in the cored section, assuming that the top of the basalt at 172 m correlates with the basement event on the reflection profile. The resulting average formation velocity is 2.5 km/s, in good agreement with the sonic log analysis and with velocities measured on similar limestone sections at previous sites. Thus, we conclude that both the sonic log and the seismic reflection profile can be used to calculate reasonable formation velocities at Hole 874B.

The basement section was not logged with the sonic tool at Hole 874B, so its average formation velocity cannot be estimated.

Log-facies Comparisons

Lithologic units and subunits defined on the basis of the limited core recovery are generally recognized in the composite logs. A dusting of pelagic foraminifer ooze is on top of the manganese crust of Lithologic Unit I. These surface units were logged only by the geochemical string through the drill pipe, and this data requires post-cruise processing.

The carbonate platform (Lithologic Unit II) extending from Cores 144-874B-1R through -20R (0–162.8 mbsf) can be divided into six main facies or subunits on the basis of the recovered lithologic succession and distinctive characteristics in the logs (see "Lithostratigraphy" section, this chapter). The various logs indicate that these carbonate platform facies display considerable internal lithologic variation, and that the boundaries between facies are often demarcated by natural gamma intensity peaks induced by uranium concentrations. The logging signatures of the different lithologic units can be used to set more precise boundaries between these facies (Fig. 34). The combined FMS resistivity maps of the borehole, coupled with the natural gamma and medium-penetration resistivity signals, provide details of sedimentary structures on the meter to centimeter level. Some of the major features within the carbonate platform succession are summarized for each shipboard-defined lithologic subunit. Lithologic Subunit IIA (algal

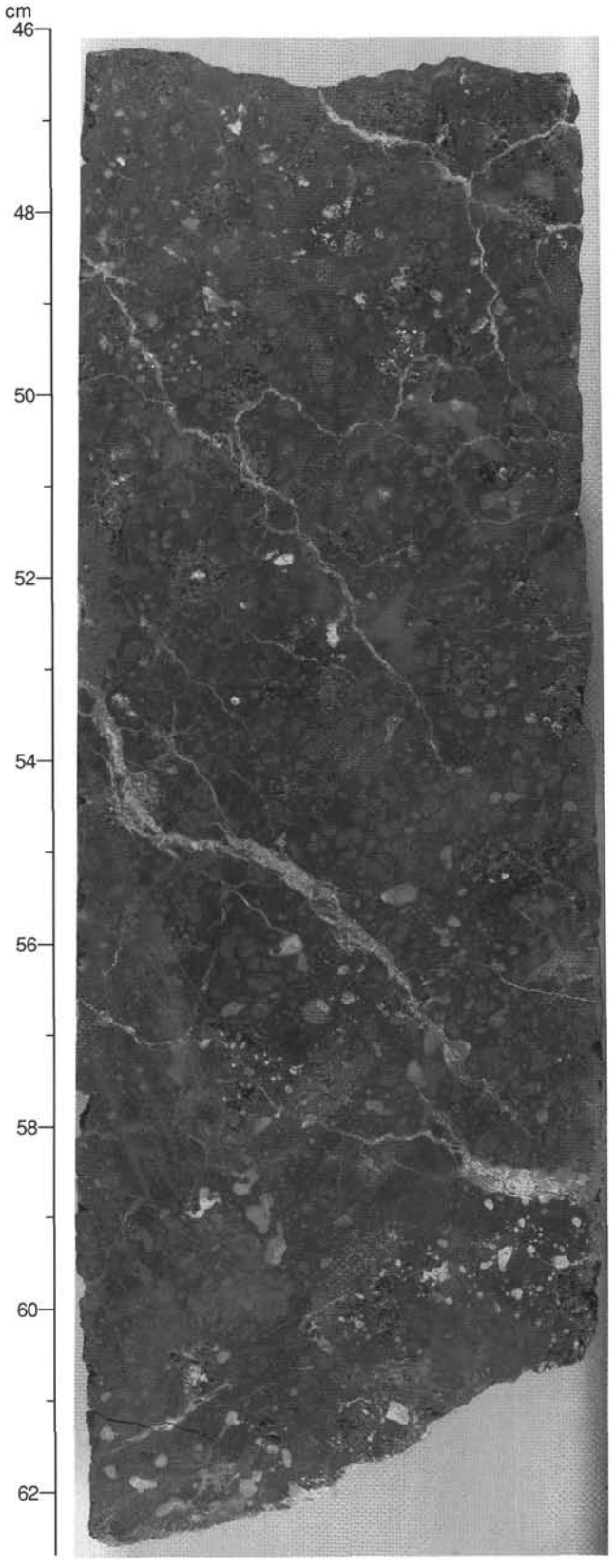

Figure 30. Upper portion of the massive ankaramitic basalt flow in Igneous Unit 1 (Interval 144-874B-23R-1, 46–62 cm) in which calcite veining is common, olivine grains (light grays) are completely pseudomorphed by clay, and clinopyroxene grains (dark, mottled patches) are unaltered except for clay development along fractures.

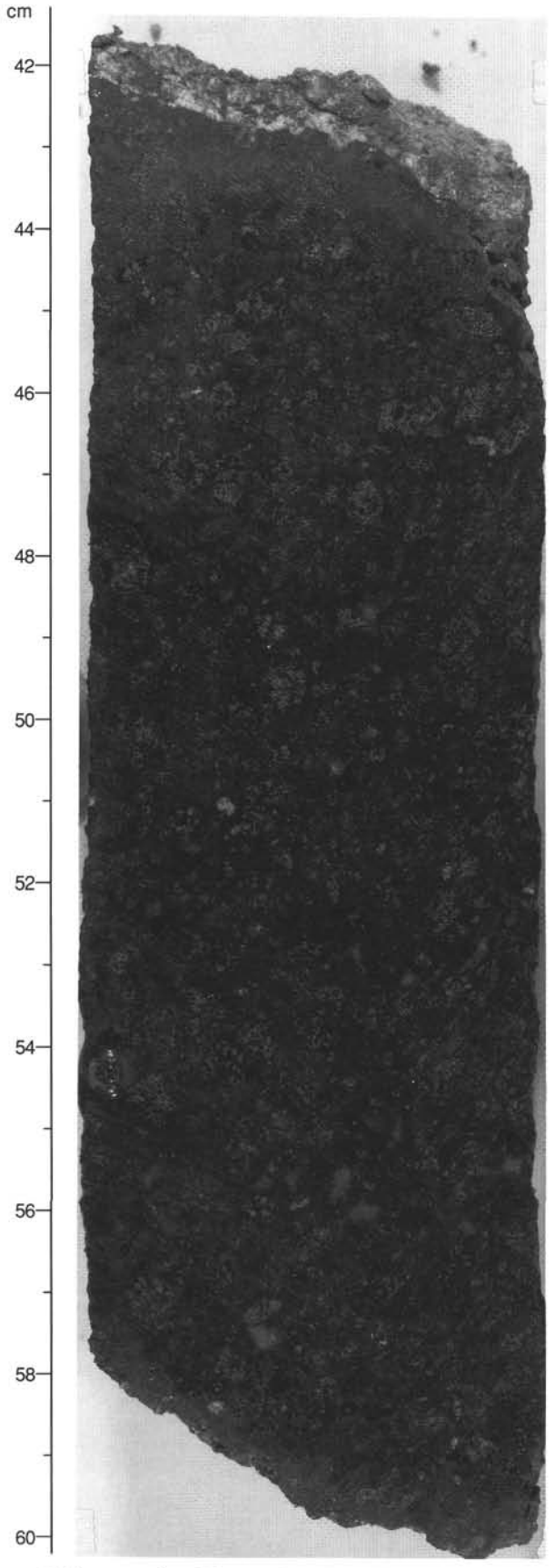

Figure 31. Lower portion of the massive ankaramitic basalt flow in Igneous Unit 1 (Interval 144-874B-24R-1, 41–60 cm), in which much of the olivine is unaltered and clinopyroxene grains are as in Figure 30.

stromatoporoid rudist boundstone and skeletal grainstone/rudstone) and Lithologic Subunit IIB (foraminifer rudist packstone/grainstone and gastropod wackestone) were above the logged interval.

Lithologic Subunit IIC

Nature: algal-rudist grainstone/rudstone and algal-coral boundstone
Interval: lower Core 144-874B-6R through upper -9R
Depths: assigned depth from logs, 38–80 mbsf
Age: Maastrichtian

Lithologic Subunit IIC has very variable lithologies, varying from porous rudstone-grainstone to well-cemented, algal-coral boundstone. This variability in porosity is amplified in the medium-penetration resistivity log, which displays eight distinct sharp peaks within this 45-m interval (35–80 mbsf) (Figs. 34–35). The highest resistivity values are four narrow peaks exceeding 25 Wm, semi-evenly spaced from 35 to 53 mbsf. The lower 25 m of Subunit IIC has more subdued peaks in resistivity. Density and natural gamma intensity through Subunit IIC displays low-amplitude variations with about 1-m wavelengths (Figs. 35 and 37), with density varying between 2.0 and 2.5 g/cm^3. Almost every resistivity peak has a corresponding density increase, but several density peaks do not have a corresponding resistivity increase.

The FMS imagery of these features reveals a series of multimeter-thick cycles, characterized by a progressive upward increase in resistivity, ending in a sharp contact or narrow transition to the low-resistivity base of the next cycle (Fig. 40A). The main six cycles of this type are at 40.1–42.3, 43.9–46.4, 46.4–48.3, 48.3–52.5, 52.5–58.0, 59.9–67.0, and perhaps 69.0–77 mbsf. The resistivity progressions are generally more pronounced in the higher (and thinner) cycles. Within each cycle, the lithology consists of a framework of higher-resistivity material honeycombed by 3- to 10-cm diameter patches of low-resistivity material or cavities.

Core recovery indicates that this cyclic facies consists of interbedded rudstone and boundstone with red algae, coral, and rudists. We interpret the cycles to be a progression from more porous rudstone upward to more cemented algal-rich boundstone, and to represent a series of shallowing-upward sequences. Such meter-scale shallowing-upward cyclicity is characteristic of most carbonate platforms (e.g., reviewed by Tucker and Wright, 1990).

At 42.3–43.8 mbsf, a 1.5-m granular-textured bed of very high resistivity is present (the maximum resistivity observed in Hole 874B). This bed has a sharp lower contact to very low-resistivity material and a sharp upper contact to a 1-m granular-textured bed of lower resistivity. Based upon its granular appearance in the FMS imagery, we interpret this bed as a grainstone, and it may represent a well-cemented skeletal-sand shoal.

The base of Lithologic Subunit IIC is placed at 80 mbsf where a series of features coincide: (1) the low-resistivity base of the lowest beds displaying "boundstone-rudstone texture" characteristic of Subunit IIC in FMS imagery; (2) just above an irregular surface (20-cm "relief") observed on the FMS imagery terminating the high-resistivity upper portion of a bed having "granular texture" characteristic of Lithologic Subunit IID; (3) a minor concentration in uranium (1.5 ppm vs. the "background" of about 0.5 ppm uranium) causing a natural gamma intensity peak of 12 AGI units; and (4) a 1-ppm peak in thorium immediately underlying and overlapping the uranium peak. This combination of sharp irregular contact and elevated uranium levels is suggestive of a hiatus in sedimentation or a condensation horizon.

Lithologic Subunit IID and Unnumbered Subunit

Nature: skeletal coral grainstone, and interval of no recovery
Interval: lower Core 144-874B-9R through -15R
Depths: assigned depth from logs, 80–123 mbsf
Age: Maastrichtian

Table 12. Index properties data, Hole 874B.

Core, section, interval (cm)	Depth (mbsf)	Wet-bulk density (g/cm^3)	Dry-bulk density (g/cm^3)	Grain density (g/cm^3)	Porosity (%)	Water content (% dry wt)	Void ratio
144-874B-							
1R-1, 18–20	0.18	2.77	2.71	2.71	5.3	2.0	0.06
1R-1, 40–42	0.40	2.81	2.74	2.76	6.7	2.5	0.07
2R-1, 19–21	9.89	2.36	1.98	2.89	37.7	19.6	0.61
2R-1, 67–69	10.37	2.53	2.42	2.75	10.6	4.5	0.12
2R-1, 126–128	10.96	2.70	2.59	2.74	10.8	4.3	0.12
2R-2, 76–78	11.87	2.63	2.51	2.81	12.1	4.9	0.14
3R-1, 51–53	19.71	3.21	3.09	2.84	11.1	3.7	0.12
3R-1, 114–116	20.34	2.82	2.78	2.76	4.3	1.6	0.04
3R-2, 118–120	21.85	2.84	2.73	2.70	10.1	3.8	0.11
4R-1, 31–33	29.01	2.55	2.37	2.79	17.7	7.7	0.22
4R-1, 56–58	29.26	2.57	2.47	2.75	10.4	4.3	0.12
5R-1, 55–57	38.65	2.75	2.69	2.68	5.7	2.2	0.06
5R-1, 84–86	38.94	2.82	2.73	2.74	8.9	3.4	0.10
5R-2, 7–9	39.67	2.57	2.35	2.71	20.8	9.0	0.26
5R-2, 60–62	40.20	2.59	2.34	2.79	24.1	10.5	0.32
6R-1, 8–10	47.68	2.91	2.78	2.81	12.6	4.7	0.14
6R-1, 74–76	48.34	2.83	2.77	2.71	5.8	2.2	0.06
6R-1, 134–136	48.94	3.05	2.98	2.76	7.0	2.4	0.08
7R-1, 16–18	57.36	2.85	2.79	2.66	5.4	2.0	0.06
8R-1, 15–17	67.05	2.70	2.42	2.75	27.7	11.7	0.38
9R-1, 41–43	77.01	2.70	2.42	2.78	26.8	11.3	0.37
9R-1, 56–58	77.16	2.76	2.60	2.79	16.0	6.3	0.19
9R-1, 99–101	77.59	2.75	2.51	2.76	23.6	9.7	0.31
9R-1, 99–101	77.59	2.44	2.19	2.77	24.7	11.6	0.33
16R-1, 22–24	117.02	2.46	2.04	2.78	40.7	20.4	0.69
16R-1, 40–42	117.20	2.69	2.45	2.73	23.0	9.6	0.30
16R-1, 40–42	117.20	2.47	2.26	2.74	20.9	9.5	0.26
17R-1, 27–29	126.67	2.25	1.87	2.79	37.2	20.4	0.59
17R-1, 77–79	127.17	2.23	1.82	2.82	39.5	22.2	0.65
18R-1, 17–19	136.17	2.38	2.06	2.77	30.7	15.2	0.44
18R-1, 70–72	136.70	2.36	2.06	2.78	28.8	14.3	0.40
19R-1, 34–36	143.84	2.69	2.55	2.79	13.3	5.3	0.15
19R-1, 70–72	144.20	2.87	2.81	2.75	6.4	2.3	0.07
19R-1, 133–135	144.83	2.89	2.82	2.70	7.1	2.6	0.08
20R-1, 6–8	153.16	2.65	2.53	2.74	11.2	4.5	0.13
21R-1, 30–32	163.10	1.74	1.07	2.84	65.3	62.7	1.88
21R-1, 89–91	163.69	2.03	1.45	3.17	57.3	40.5	1.34
21R-2, 12–14	164.42	2.00	1.41	3.04	57.8	42.1	1.37
21R-2, 92–94	165.22	1.97	1.35	3.10	60.9	46.4	1.56
21R-3, 12–14	165.92	1.93	1.32	3.02	59.6	46.3	1.47
22R-1, 75–77	173.15	1.78	1.11	2.96	65.3	60.4	1.88
22R-2, 95–97	174.85	1.76	1.07	2.87	68.1	65.5	2.14
22R-3, 40–42	175.80	1.97	1.31	3.33	64.6	50.5	1.83
22R-4, 69–71	177.36	2.46	2.11	2.92	33.8	16.4	0.51
23R-1, 50–52	178.20	2.60	2.32	3.05	27.5	12.1	0.38
23R-1, 106–108	178.76	2.60	2.32	3.03	28.0	12.4	0.39
23R-2, 124–126	180.43	2.49	2.18	2.98	30.3	14.3	0.44
24R-3, 13–15	187.07	2.61	2.35	2.98	26.0	11.3	0.35
24R-3, 91–93	187.85	2.76	2.62	2.95	13.7	5.4	0.16
24R-4, 17–19	188.55	3.15	3.12	3.05	2.9	1.0	0.03

Only 20 cm of white skeletal coral grainstone was recovered from the upper portion of this poorly cemented 43-m interval. In addition, the hole diameter exceeded the log caliper's 50-cm limit, so the degree of washout is unknown. As a result, the sustained low medium-penetration resistivity (1.3–2.5 Ωm) and density (averaging 2.4 g/cm^3) measurements by the logging tools are not reliable. The FMS imagery was limited to the contact of only two pads against the widened borehole wall, but it was adequate to characterize the sedimentary structures. The upper 6 m (79.8–86.1 mbsf on the FMS imagery) is a homogeneous moderate-resistivity bed with a granular texture at the subcentimeter scale, which grades upward to a high-resistivity (well-cemented) upper surface. Core recovery indicates that the facies is a grainstone, which is consistent with the granular appearance in the FMS imagery.

The next 11 m (86.1–97.5 mbsf) consists of a relatively high-resistivity matrix with numerous patches of very low resistivity, 10–20 cm in diameter, which may be cavities or poorly cemented material; this interval also has a high-resistivity layer that coincides with a 1.5-ppm peak in uranium at 96 mbsf, which causes a natural gamma intensity spike of 15 AGI units. This is the only significant natural gamma intensity fluctuation within Subunit IID, and it may represent a condensation horizon.

The underlying 25 m (97.5–123 mbsf) appear to have a relatively low resistivity with a granular texture at the subcentimeter scale, according to the two FMS pads in intermittent contact with the borehole wall. The facies contains several irregularly shaped patches (cavities?) of very low resistivity with about 10-cm average diameter. At 111.5–112.5 mbsf, a 1-m-thick interval with higher resistivity is present.

We place the base of Subunit IID at 123 mbsf, where a major increase in uranium and thorium concentration is indicated in the natural gamma log.

Lithologic Subunit IIE

Nature: reddish yellow grainstone
Nature: Cores 144-874B-16R and -17R
Depths: assigned depth from logs, 123–143 mbsf
Age: Maastrichtian

At 122–123 mbsf, a peak in natural gamma intensity of 25 API units is caused by an increase in uranium concentration (2.1 ppm vs. adjacent "background" of approximately 0.4 ppm) and, to a lesser extent, of thorium (1.2 ppm). This feature is just above a minor peak in resistivity and density (3 g/cm^3), although the enlarged borehole makes this density measurement unreliable. Underlying this uranium-rich horizon is a featureless low-resistivity and partially "washed out" facies. The FMS imagery indicates that the high-resistivity peak corresponds to a 10-cm bed at 123.4–123.5 mbsf. Core recovery indicates that this subunit is dominated by grainstones that have orange to yellowish tan staining, which may suggest postburial oxidation. No distinct concentrations of either iron or aluminum associated with the capping uranium peak are present; therefore, a significant "terra rossa" soil horizon is probably not present. It is possible that the uranium peak has partially resulted from diagenetic concentration associated with a redox front between these oxidized grainstones of Subunit IIE and the overlying unrecovered facies of Subunit IID. Therefore, we have tentatively placed the upper boundary of Lithologic Subunit IIE at this horizon at 123 mbsf.

The FMS imagery from the grainstone facies shows a general massive facies with a granular appearance at the subcentimeter scale. The lowest 9 m have scattered high-resistivity "clasts" of 2- to 8-cm diameter, which resemble the signature of red-algal rhodoliths in other subunits. Between 139 and 141 mbsf are several thin layers of slightly higher resistivity, which may be horizons of partial cementation.

Lithologic Subunit IIF

Nature: rhodolith-rich foraminifer algal grainstone
Interval: Core 144-874B-18R through -20R
Depths: assigned depth from logs, 143–163 mbsf
Age: late Campanian?

The upper portion of this algal-rich facies is characterized by elevated resistivity (averaging approximately 4–5 Ωm) and uranium content (averaging approximately 2 ppm) (Figs. 35 and 37). Several peaks in both resistivity and uranium content are superimposed on these average values. The peaks in resistivity are probably associated with beds of lower porosity, possibly corresponding to algal-rich wackestones. The FMS imagery indicates that most of the high-resistivity peaks are from distinct 5- to 10-cm diameter blocks (large red-algal rhodoliths?), rather than continuous beds. The general appearance of this upper algal-rich facies in the FMS imagery is similar to a porous rudstone. Uranium can display relative concentrations in algal carbonate mats on account of their reducing microenvironments, which are conducive to redox scavenging of uranium from seawater (e.g., Serra, 1989). Although this uranium concentration process is usually associated with blue-green algal mats, it may also be applicable to the red algal encrustations and concretions (rhodoliths) within this Subunit IIF. A similar natural gamma (uranium) enrichment is observed in the rhodolith-rich grainstone facies (Lithologic Sub- unit IIE) of Site 871 (see "Downhole Measurements and Seismic Stratigraphy" section, "Site 871" chapter, this volume). Another process that may contribute

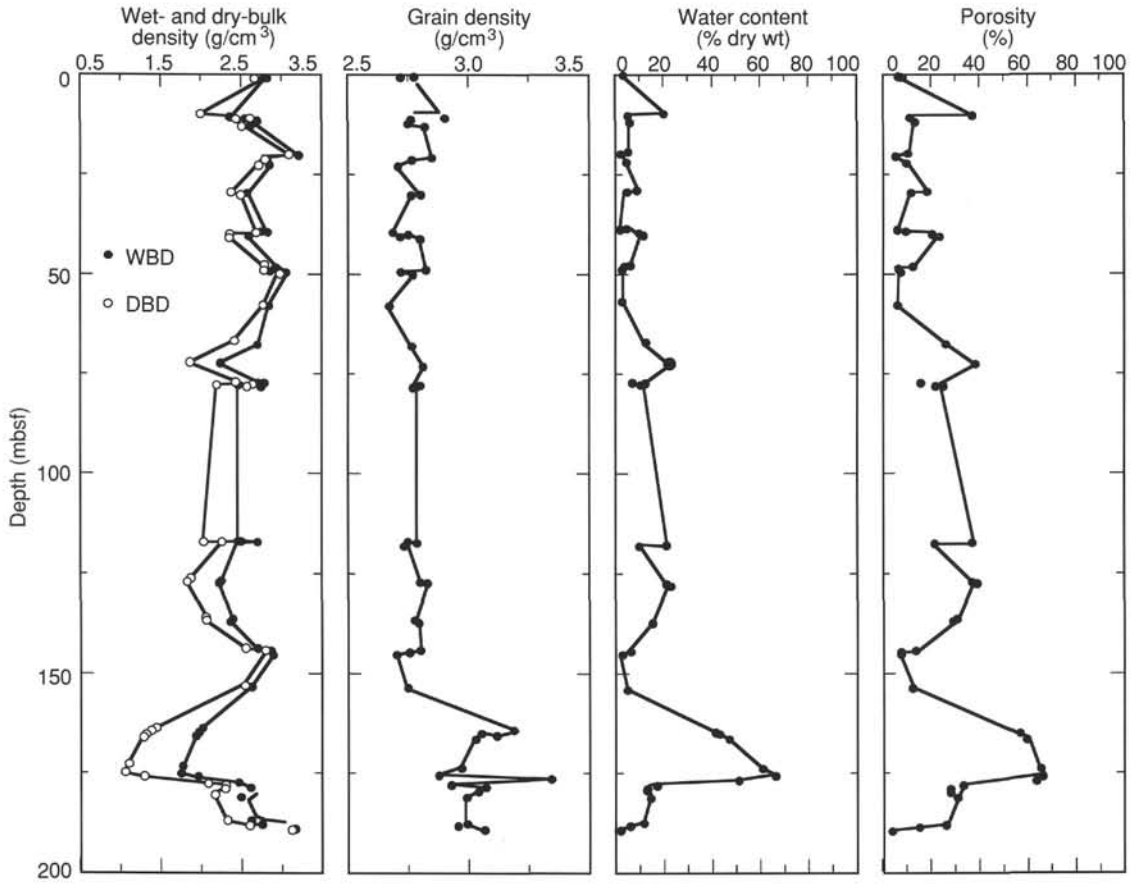

Figure 32. Measurements of index properties (wet- and dry-bulk density, grain density, water content, and porosity) vs. depth, Hole 874B.

to peaks in uranium enrichment in Hole 874B is condensed sedimentation and/or enhanced cementation.

A peak in natural gamma intensity (60 AGI units) caused by anomalous uranium concentrations (over 7 ppm) at 139.5–140.5 mbsf appears to overlie the top of this algal-rich subunit. This horizon is just above the uppermost high-resistivity (10 Ωm) bed at 143 mbsf (143.7 mbsf on the FMS log) (Fig. 40B). We suspect that this uppermost anomalous uranium concentration is partially a diagenetic feature produced by enhanced uranium precipitation at the redox boundary between the algal-rich facies to the overlying oxidized grainstone facies.

The lower facies of Subunit IIF, from 153 to 160 mbsf, has a lower average resistivity than the upper facies and does not contain significant resistivity peaks above the base. Thorium displays two 2-m-thick, 1.5-ppm peaks centered at 154 and 159 mbsf. The lower thorium peak coincides with only significant aluminum concentration measured within the carbonate platform section (Fig. 36). We interpret these thorium peaks to indicate clay-rich beds. Recovery in this interval (Core 144-874-20R) consists of only 20 cm of grainstone to packstone.

The FMS imagery of the interval from 153 through 162.6 mbsf reveals a massive high-resistivity bed that displays a progressive upward decrease in resistivity, indicating an upward increase in porosity. The images have a granular appearance, with scattered 5- to 10-cm diameter spots of low-resistivity material, which may be less cemented pockets or voids.

A sharp lower boundary to the carbonate platform succession is displayed on the FMS imagery at 162.6 mbsf consisting of high-resistivity (well-cemented) lithology overlying very low resistivity (clay) material. Geochemical logs indicate a sharp downward termination of calcium-enriched facies to an iron- and silica-rich facies at between 162 and 163 mbsf. The aluminum-tool did not penetrate to this boundary. The basal bed of the carbonate platform at 161–162.5 mbsf has a higher resistivity (6 Wm) and calcium content than the next higher few meters (Figs. 35–36), which suggests that the base of the carbonate platform facies may have significant diagenetic cementation.

Lithologic Unit III

Nature: brownish red clay
Interval: Cores 144-874B-21R through -22R
Depths: assigned depth from logs and cores, 163–178 mbsf
Age: Campanian or older

Only the upper 7 m of the clay was logged by the gamma spectrometer of the geochemical string and the resistivity tool of the geophysical string. As expected, resistivity values are very low (approximately 1 Ωm). Iron and silicon show relative enrichments from 161 to 165 mbsf and from 166.5 mbsf downward, with an anomalously low iron layer at 165–166.5 mbsf (Fig. 36). The lower iron variation corresponds to the reddish weathering profile on the volcanic edifice (iron- and silica-rich) overlain by an organic-rich clay (iron- and silica-poor because of the leaching of ions?) within Core 144-874B-21R. However, the upper level of iron- and silica-enrichment just below the lowest limestone bed was apparently not recovered.

The FMS imagery of the uppermost 2 m (162.6–164.6 mbsf) of the clay, which displays a grading upward to a lower resistivity, has a slightly higher average resistivity at the base. This interval may correlate with the dark gray clay facies that overlies the reddish clay, or it may indicate a pulse of carbonate influx (storm washover?) followed by temporary resumption of clay-rich sedimentation. A sharp downward contact occurs at 164.6 mbsf to a very low relative

Table 13. Hamilton Frame measurements of compressional wave velocity, Hole 874B.

Core, section, interval (cm)	Depth (mbsf)	Distance (mm)	Axes of measurement	Traveltime (μs)	Corrected traveltime (μs)	Measured velocity (m/s)	Velocity anisotropy index
144-874B-							
2R-1, 67–69	10.37	21.28	a	8.08	5.08	4193.10	
2R-1, 67–69	10.37	21.48	b	8.21	5.21	4126.80	
2R-1, 67–69	10.37	21.41	c	7.87	4.87	4400.82	–0.06
2R-1, 126–128	10.96	20.85	a	7.91	4.91	4250.77	
2R-1, 126–128	10.96	21.77	b	7.89	4.89	4456.50	
2R-1, 126–128	10.96	21.40	c	7.76	4.76	4500.53	–0.03
3R-2, 118–120	21.85	21.08	a	7.39	4.39	4807.30	
3R-2, 118–120	21.85	21.34	b	7.19	4.19	5099.16	
3R-2, 118–120	21.85	21.33	c	7.14	4.14	5152.17	–0.04
5R-1, 84–86	38.94	20.34	a	7.12	4.12	4936.89	
5R-1, 84–86	38.94	21.38	b	7.45	4.45	4809.90	
5R-1, 84–86	38.94	21.45	c	7.26	4.26	5035.21	–0.03
5R-2, 60–62	40.20	22.27	a	8.16	5.16	4320.08	
5R-2, 60–62	40.20	21.45	b	8.31	5.31	4043.36	
5R-2, 60–62	40.20	21.35	c	8.16	5.16	4141.61	0.01
6R-1, 134–136	48.94	21.55	a	7.42	4.42	4875.57	
6R-1, 134–136	48.94	21.36	b	7.40	4.40	4854.55	
6R-1, 134–136	48.94	21.54	c	7.19	4.19	5140.81	–0.06
9R-1, 99–101	77.59	21.21	a	8.64	5.64	3760.64	
9R-1, 99–101	77.59	20.90	b	8.63	5.63	3712.26	
9R-1, 99–101	77.59	21.30	c	8.56	5.56	3830.94	–0.02
16R-1, 40–42	117.20	21.43	a	8.20	5.20	4121.15	
16R-1, 40–42	117.20	21.25	b	8.48	5.48	3877.74	
16R-1, 40–42	117.20	21.46	c	8.50	5.50	3901.82	0.02
18R-1, 70–72	136.70	25.90	a	10.77	7.77	3335.48	
18R-1, 70–72	136.70	21.44	b	9.76	6.76	3173.95	
18R-1, 70–72	136.70	21.51	c	9.41	6.41	3358.31	–0.03
22R-4, 69–71	177.36	22.25	a	9.46	6.46	3446.94	
22R-4, 69–71	177.36	21.42	b	9.74	6.74	3180.40	
22R-4, 69–71	177.36	21.50	c	9.31	6.31	3407.29	–0.03
23R-1, 50–52	178.20	22.51	a	10.56	7.56	2977.51	
23R-1, 50–52	178.20	21.44	b	10.35	7.35	2918.99	
23R-1, 50–52	178.20	21.44	c	10.46	7.46	2874.00	0.03
23R-1, 106–108	178.76	21.57	b	10.78	7.78	2772.49	
23R-1, 106–108	178.76	21.65	c	10.47	7.47	2898.26	–0.04
23R-2, 124–126	180.43	21.45	b	11.40	8.40	2555.09	
23R-2, 124–126	180.43	21.54	c	11.57	8.57	2513.42	0.02
24R-3, 91–93	187.85	23.10	a	8.22	5.22	4429.53	
24R-3, 91–93	187.85	21.53	b	7.81	4.81	4476.09	
24R-3, 91–93	187.85	21.49	c	7.94	4.94	4354.61	0.02
24R-4, 17–19	188.55	21.19	a	7.06	4.06	5225.65	
24R-4, 17–19	188.55	21.82	b	6.85	3.85	5667.53	
24R-4, 17–19	188.55	21.62	c	6.94	3.94	5487.31	–0.01

Notes: a = direction perpendicular to split core plane, b = direction transverse to split core plane, and c = core axis; all axes are orthogonal.

Table 14. Thermal conductivity data, Hole 874B.

Core, section, interval (cm)	Depth (mbsf)	Thermal conductivity (W/[m · K])	Error range (W/[m · K])	Drift (K/min)
144-874B-				
21R-1, 54–54	163.34	2.52	0.004	0.025
21R-2, 50–50	164.80	1.80	0.004	–0.005
21R-3, 16–16	165.96	1.07	0.005	–0.014

resistivity clay that continues to the base of the logged section at 170 mbsf. This lower clay interval contains rare higher resistivity "clasts" of about 5 cm diameter, which could be the result of incompletely weathered volcanic material.

Seismic Stratigraphy Interpretation

Single-channel seismic profiles were obtained on two crossings of Hole 874B using a 200-in.^{3} water gun as a sound source. These data were recorded on a Masscomp computer, refiltered, and displayed; they were found to be inferior, however, to the seismic record collected on a previous survey across the Site 874 location with two 80-in.^{3} water guns shot to a six-channel seismic streamer. These multichannel data were processed up through migration and are displayed in Figure 39. Comparison with the coring results suggests some correlations to the recovered lithologic section and the downhole measurements.

The seafloor at Hole 874B is an erosional surface "hardground" of post-middle Eocene age. This is marked by a hard, opaque seafloor reflector on both the 3.5-kHz and seismic reflection records (Fig. 39). Below this hard reflector is a seismic unit that is almost opaque of about 0.04 s TWT. This probably corresponds to the top 50 m of Hole 874B that was characterized by well-indurated rudstone and grainstone, which was slow to drill, and contains several high-resistivity spikes (Fig. 34). This seismic unit seems to continue south onto the main guyot platform where it becomes less opaque, and therefore easier to recognize, but probably less indurated and more like the underlying sedimentary sequence at Hole 874B.

Below this almost opaque seismic reflection unit is a more homogeneous unit from 1.91 to 2.01 s TWT characterized by discontinuous reflectors throughout the sequence. This probably correlates to the remainder of the sedimentary section down through the weathered clay that rest on basalt starting at 178 mbsf. It is unlikely that the reflector that terminates this sequence at 2.01 s TWT corresponds to the top of the algal rhodolith-rich grainstone unit at about 140 mbsf even though this unit has an apparent increase in bulk density (Fig. 34). This is probably an artifact of poor hole conditions for logging above the 140 mbsf level, and such a correlation would yield an unreasonably low formation velocity for the entire sedimentary section. On the assumption that the reflector in question corresponds to the top of basaltic basement at 178 mbsf, this yields a formation velocity of 2.5 km/s, in agreement with the formation velocities of limestone sections at other guyot drill sites within the Marshall Islands. If this correlation is correct, then no seismic event correlates to the basal limestone sequence of algal rhodolith-rich grainstone (Lithologic Subunit IIF).

No coherent seismic reflectors are present below the basement reflector at 2.01 s TWT, and drilling ended at 193.5 mbsf.

The above correlations and formation velocities are reasonably confident statements of in-situ conditions at Hole 874B. As such, they can be used with regional seismic surveys to construct a seismic stratigraphic map of the entire Wodejebato Guyot platform.

In summary, the logging and seismic stratigraphy section at Site 874 on Wodejebato Guyot may be divided into three main parts:

1. A manganese crust capping the carbonate platform that represents an apparent condensation in sedimentation from the Latest Cretaceous to the present.
2. A 163-m-thick carbonate platform. A rudist-rich grainstone is interbedded with well-cemented algal boundstone and/or wackestone from 80 to 40 mbsf. The next 35 m are poorly consolidated carbonates of grainstone and/or chalkified packstone. A condensed horizon at 123 mbsf is underlain by 20 m of poorly cemented grainstones that overlie, at 143 mbsf, a lower algal-rhodolith-rich facies.
3. A lower basalt with its upper surface weathered into a clay layer. The top of the clay layer is at 163 mbsf.

SUMMARY AND CONCLUSIONS

At Site 874, we recovered only a single basaltic lava flow belonging to the igneous basement (Unit IV). The upper part of this ankaramitic basalt flow has been deeply weathered to form a red-brown claystone. The relict fabric of the ankaramite, including its upper boundary, is well preserved within the lower part of this flow. Also preserved in the claystone is the fabric of an overlying, plagioclase phyric, vesicular basalt flow. Therefore, this lower portion of Unit III is an in-situ weathering profile.

The transition to marine conditions occurred in a low-energy environment and sulfate-reducing conditions. The first marine influx is recorded by a black clay (Unit III) that yielded marine organisms, including calcareous nannofossils of Campanian age, and abundant woody material that may have been derived from vegetation on the exposed volcanic edifice. The absence of reworked clay in the overlying platform limestones may be interpreted as the result of rapid burial, preservation in a low-energy environment, or partial erosion and redeposition elsewhere.

The carbonate succession may have been deposited as early as the late Campanian. These initial platform deposits are grainstone and packstone; they are rich in larger foraminifers, rudists, corals, and red algae (including rhodoliths). These deposits are interpreted to be sand shoals with open-marine circulation and moderate to high energy. After a brief episode of a slight decrease in wave energy, higher energy conditions resumed. The decrease in wave energy is inferred from the absence of rhodoliths, a decrease in abundance of radiolitids, and an increase in abundance of larger foraminifers directly overlying the initial platform deposits. The subsequent increase in energy conditions is indicated by the deposition of poorly sorted algal rudist grainstone/rudstone. A bioherm was developed at this time, as recorded by a Maastrichtian boundstone with encrusting red algae, tabular coral colonies, and a few clusters of radiolitids. This short episode of reef growth was followed by deposition in a shallow lagoon periodically affected by (1) storms, (2) changes in current patterns or short-term sea-level fluctuations, and (3) possible emersion. A return to a more agitated shallow-marine environment is associated with the second and last episode of bioherm development during the Maastrichtian, as documented by an algal-stromatoporoid-coral boundstone.

The first pelagic sediments recorded at Site 874 are Maastrichtian in age and infill cavities within the upper part of the shallow-carbonate sequence. Site 874 drowned before the end of the Cretaceous. The cavities were either produced by an emersion episode preceding the drowning or by submarine dissolution, implying only a single drowning event. The overall lack of pelagic ooze, and the presence of manganese-encrusted, phosphatized lithoclasts of varying origins and ages overlying the cavities containing pelagic infilling, suggest that Site 874 was, and is, a location of prevailing nondeposition.

REFERENCES*

Camoin, G., Bernet-Rollande, M.-C., and Philip, J., 1988. Rudist-coral frameworks associated with submarine volcanism in the Maastrichtian strata from Pachino area (S.E. Sicily). *Sedimentology,* 35:123–138.

Collot, J.-Y., Greene, H.G., Stokking, L.B., et al., 1991. *Proc. ODP, Init. Repts.,* 134: College Station, TX (Ocean Drilling Program).

Hydrographer of the Navy, 1991. *Admiralty Tide Tables* (Vol. 3): *Pacific Ocean and Adjacent Seas:* London (Hydrographer of the Navy).

Premoli Silva, I., and Brusa, C., 1981. Shallow-water skeletal debris and larger foraminifers from Deep Sea Drilling Project Site 462, Nauru Basin, western equatorial Pacific. *In* Larson, R.L., Schlanger, S.O., et al., *Init. Repts. DSDP,* 61: Washington (U.S. Govt. Printing Office), 439–473.

Serra, O., 1989. 6.8 shallow water carbonate environment. *Sedimentary Environments from Wireline Logs* (2nd ed.): Houston, TX (Schlumberger Well Services), 199–211.

Shipboard Scientific Party, 1991. Site 812. *In* Davies, P.J., McKenzie, J.A., Palmer-Julson, A., et al., *Proc. ODP, Init. Repts.,* 133 (Pt. 1): College Station, TX (Ocean Drilling Program), 135–176.

————, 1992. Explanatory notes. *In* Mayer, L., Pisias, N., Janecek, T., et al., *Proc. ODP, Init. Repts.,* 138 (Pt. 1): College Station, TX (Ocean Drilling Program), 13–42.

Tucker, M.E., and Wright, P.V., 1990. *Carbonate Sedimentology:* Oxford (Blackwell Sci. Publ.).

Walker, K.R., and Alberstadt, L.P., 1975. Ecological succession as an aspect of structure in fossil communities. *Paleobiology,* 1:238–257.

*Abbreviations for names of organizations and publication titles in ODP reference lists follow the style given in *Chemical Abstracts Service Source Index* (published by American Chemical Society).

Ms 144IR-107

NOTE: For all sites drilled, core-description forms ("barrel sheets") and core photographs can be found in Section 3, beginning on page 453. Forms containing smear-slide data can be found in Section 4, beginning on page 1017. Thin-section data are given in Section 5, beginning on page 1037. Conventional log, FMS, dipmeter, and geochemical log (element and oxide weight %) data can be found in CD-ROM form (back pocket).

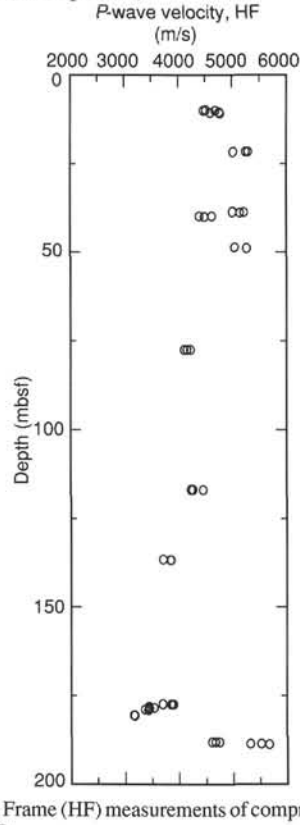

Figure 33. Hamilton Frame (HF) measurements of compressional wave velocity vs. depth, Hole 874B.

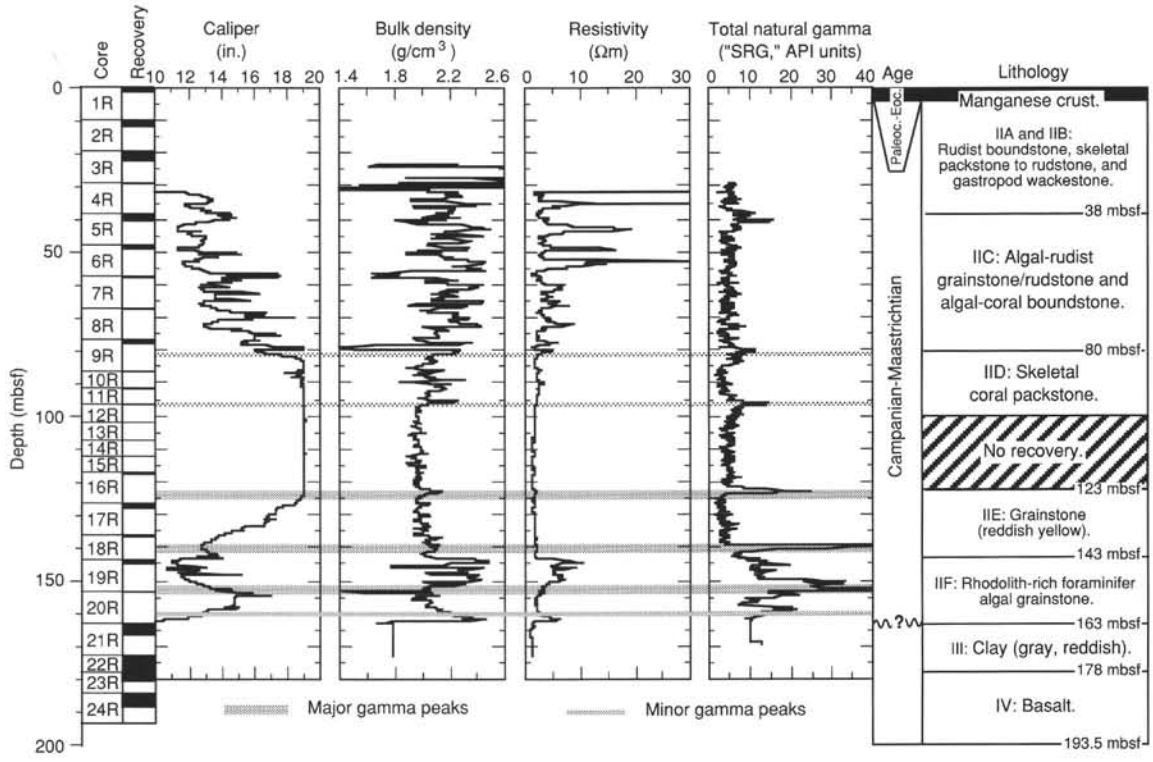

Figure 34. Stratigraphy of Hole 874B from selected geophysical logs compared to cored intervals, lithostratigraphy, and biostratigraphic ages within Hole 874B. Resistivity is from the medium-penetration phasor-induction (IMPH) tool. Total natural gamma measurements are from the Formation MicroScanner run. Caliper, or apparent hole diameter, does not record values greater than 19 in. (48 cm); drill-bit diameter is 9.9 in. (25 cm). Fluctuations in density and resistivity generally coincide within the carbonate platform; therefore, these variations provide a record of relative porosity of different limestone beds. Peaks in natural gamma intensity are marked by shaded lines. In the carbonate platform facies, these peaks in natural gamma intensity are also a result of concentrations of uranium and may be associated with hiatuses in sedimentation or exposure surfaces. In contrast, adjacent to the basal clay facies, the total natural gamma variations are also caused by thorium concentrations in clay-rich zones. The gamma peak at 40 mbsf is an artifact that occurred when the natural gamma tool entered the drill pipe.

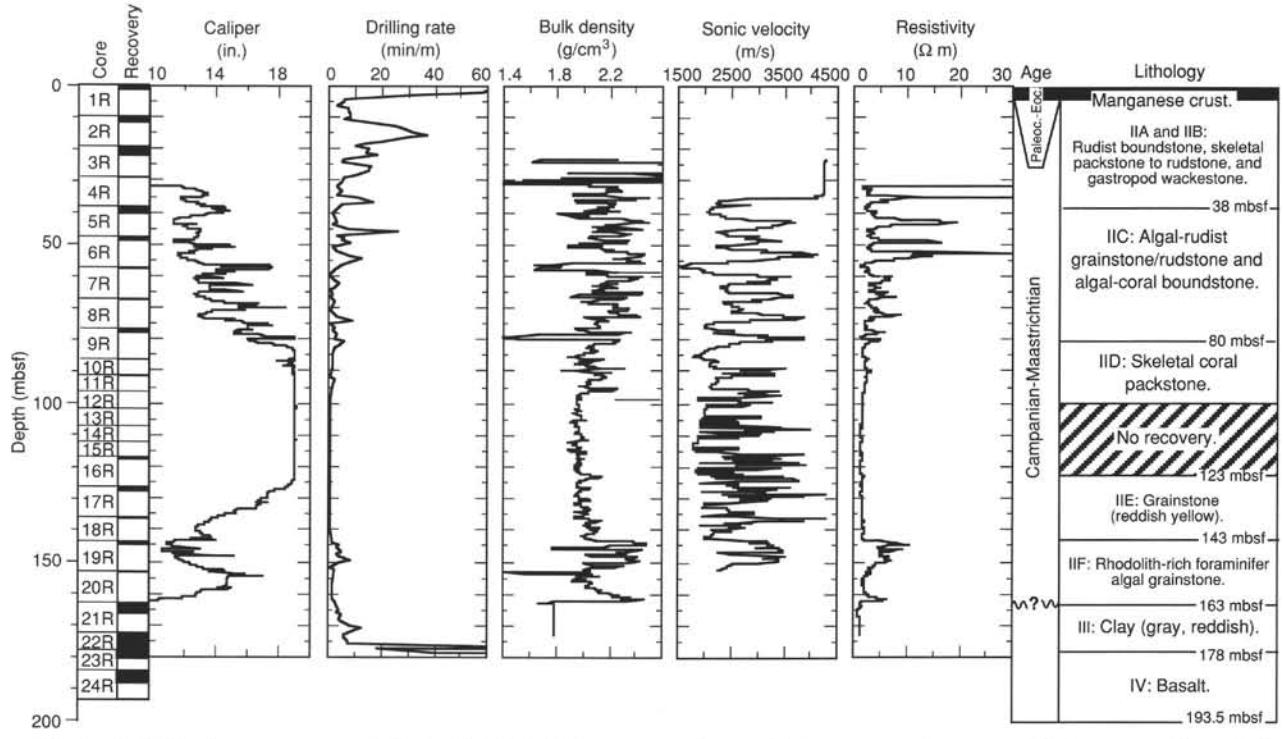

Figure 35. Geophysics logging measurements in Hole 874B. Individual peaks generally correlate among these logs and probably correspond to variations in porosity and cementation within the carbonate platform facies and to intervals of clay enrichment. Drilling or penetration rates were recorded at about 1-m intervals.

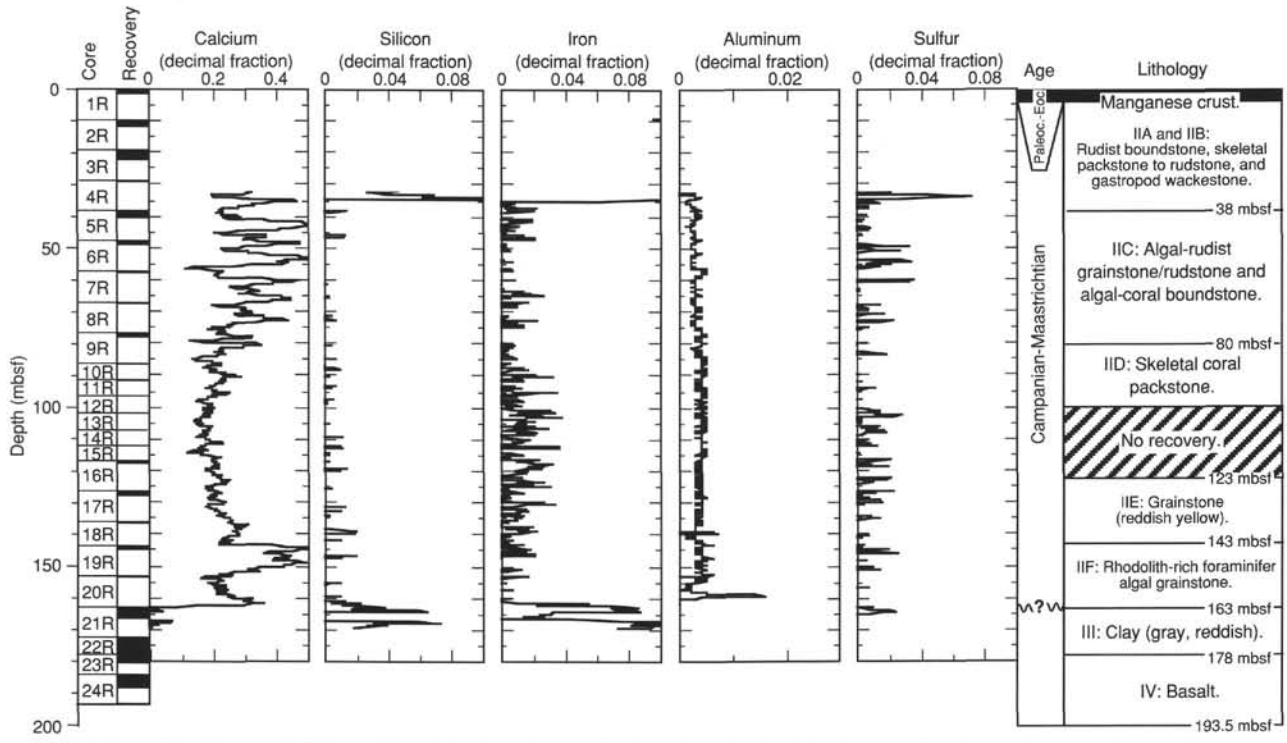

Figure 36. Relative stable elements (calcium, silicon, aluminum, iron, and sulfur) in Hole 874B. Values are given in relative proportions and have not been adjusted for porosity variations. Except for calcium, all other elements are in trace amounts within the shallow-water carbonates. Iron, silica, and aluminum dominate within the clay and volcanic facies in the lower half of the hole, with the highest Al values occurring within a clay-rich interval in the basal carbonate. Anomalous readings above 35 mbsf for these elements are a result of logging through the drill pipe.

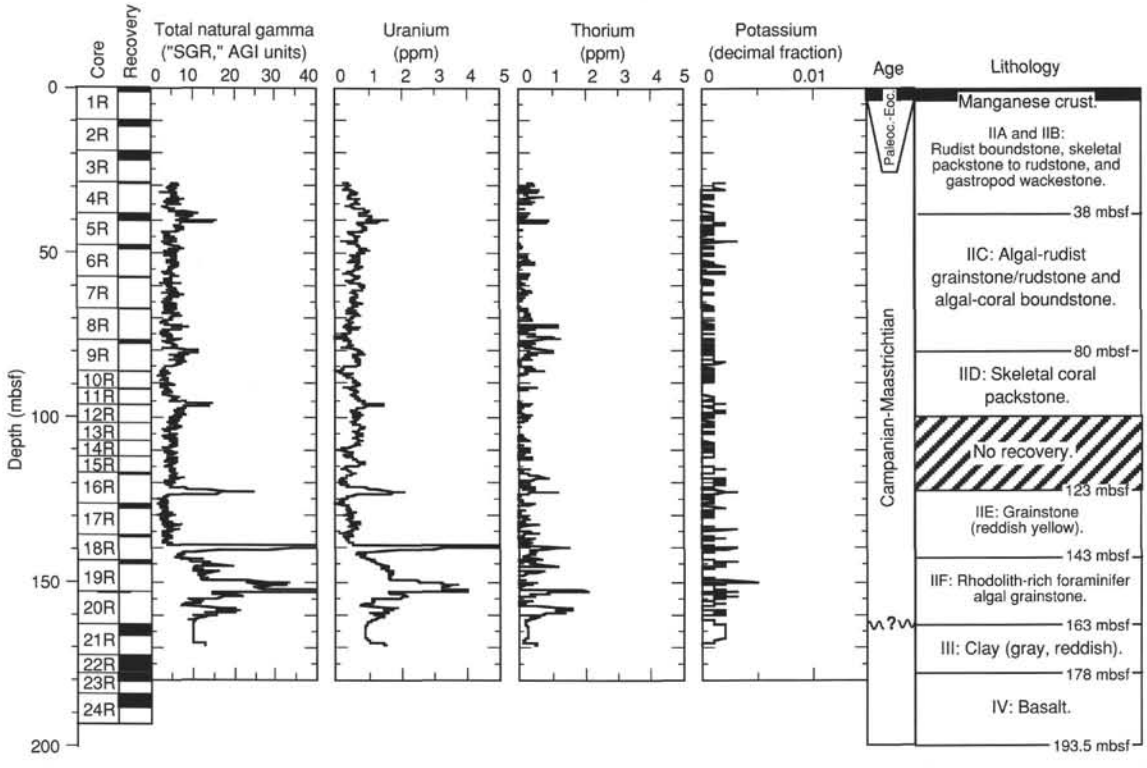

Figure 37. Radioactive element concentrations in Hole 874B, as recorded by the natural gamma tool on the geochemical tool string. Potassium remains near the noise level of the measurements. The gamma peak at 40 mbsf is an artifact that occurred when the natural gamma tool entered the drill pipe.

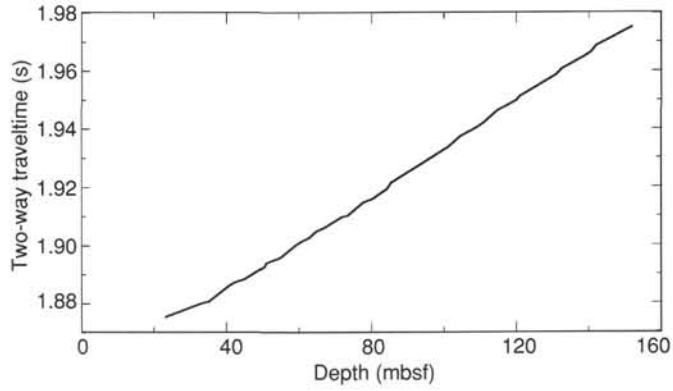

Figure 38. Integrated sonic traveltime vs. depth in the carbonate platform from Hole 874B, based on an average of all four measured sonic transit time values.

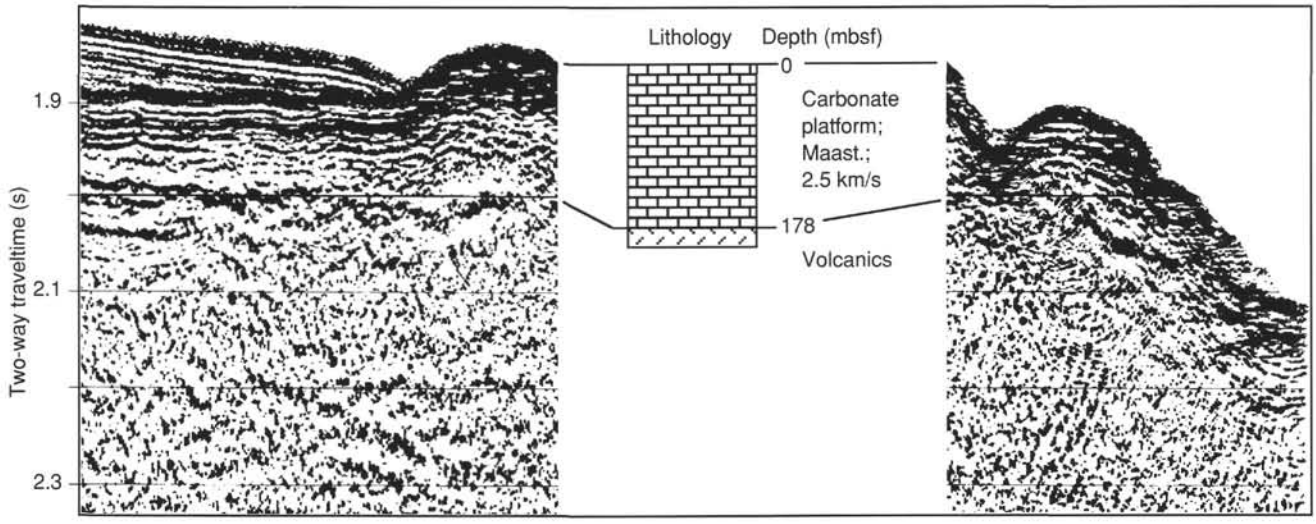

Figure 39. Lithostratigraphic correlations to the seismic stratigraphy sections crossing Sites 874 (left) and 875 (right). Major reflectors correspond to stratigraphic breaks in deposition or to major facies changes. Meter levels of key stratigraphic horizons are based upon the identification of the lithologic units in logs (Hole 874B) or on measurements of drilling rates (Hole 875A).

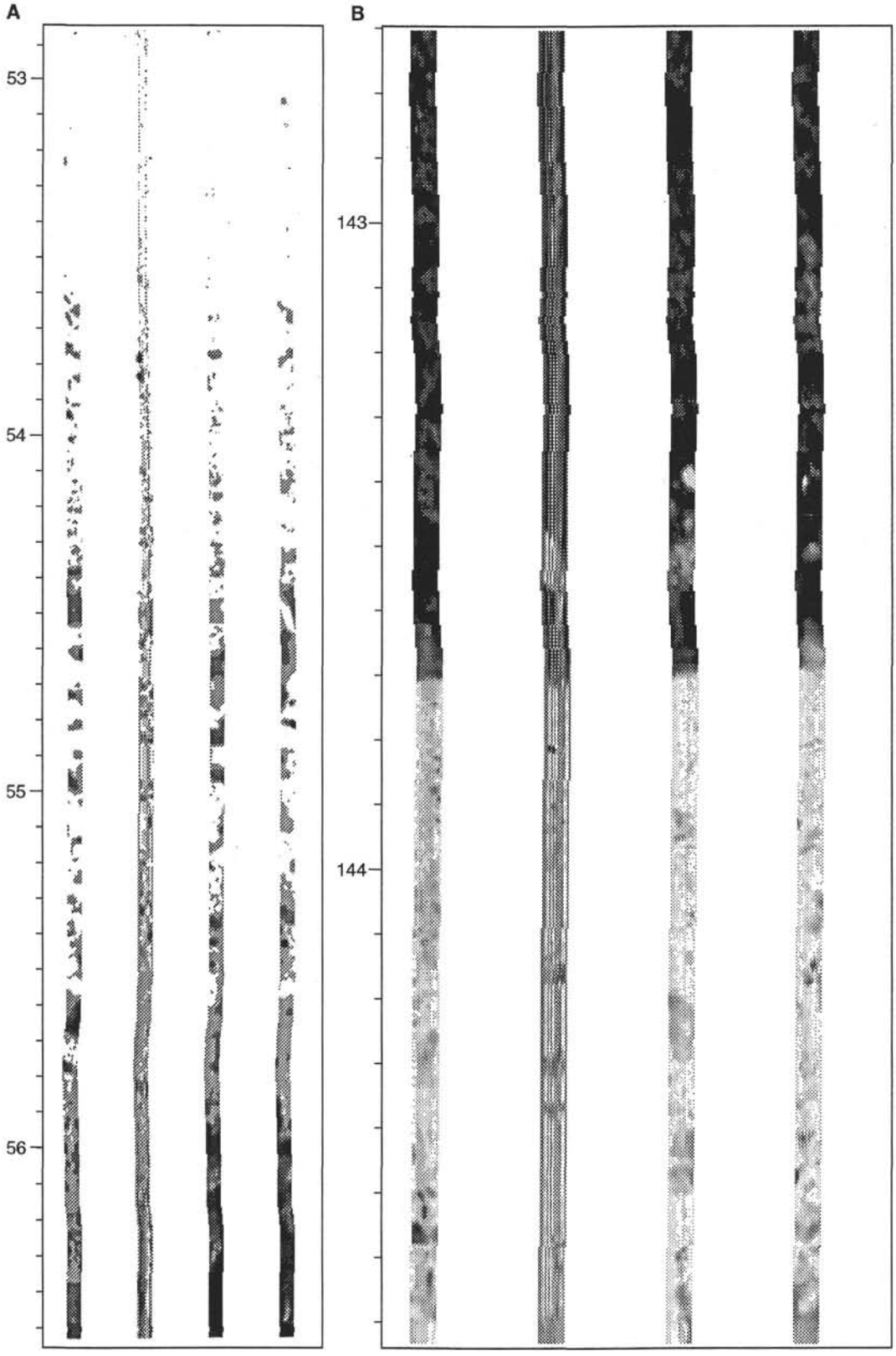

Figure 40. Formation MicroScanner high-resolution, high-contrast resistivity imagery of the borehole wall of Hole 874B. **A.** High-resistivity (displayed as light shaded) upper portion of a typical cycle with a sharp contact to overlying low-resistivity (displayed as dark shaded) material. This interval from 52.8 to 56.6 mbsf corresponds to the lower part of Core 144-874B-6R (Lithologic Subunit IIC), which recovered algal rudist rudstone and boundstone. These features probably represent shoaling-upward carbonate deposition cycles. **B.** Sharp contact of high-resistivity (10 Ωm), well-cemented, rhodolith-rich algal grainstone facies (Lithologic Subunit IIF) to overlying porous grainstone (Lithologic Subunit IIE). A peak in natural gamma intensity (60 AGI units) caused by anomalous uranium concentrations (over 7 ppm) at 139.5–140.5 mbsf appears to correspond to the top of this algal-rich subunit. This uppermost anomalous uranium concentration is partially a diagenetic feature produced by enhanced uranium precipitation at the redox boundary between the algal-rich facies to the overlying oxidized grainstone facies.

Hole 874B: Resistivity-Velocity-Natural Gamma Ray Log Summary

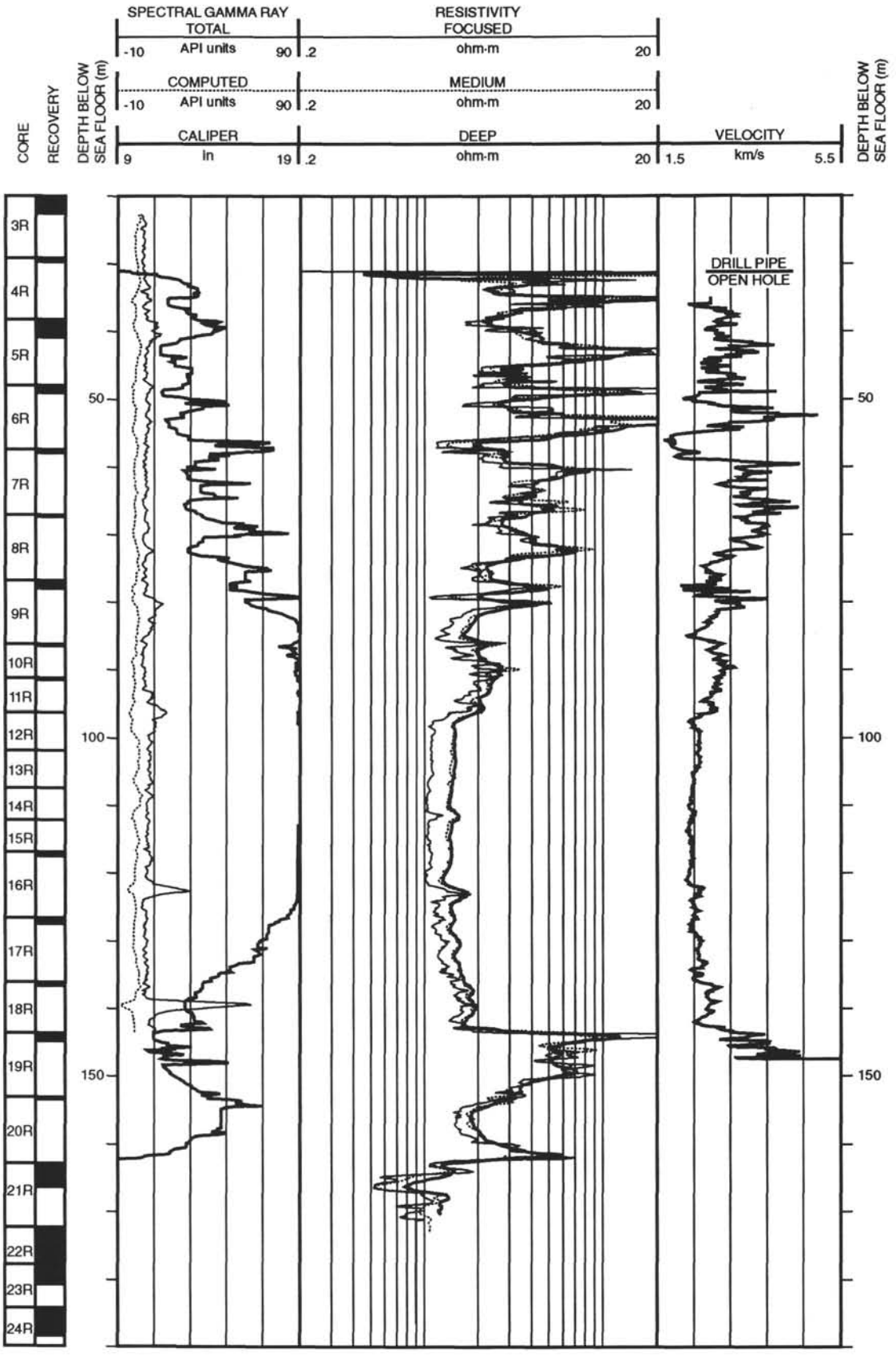

Hole 874B: Density-Porosity-Natural Gamma Ray Log Summary

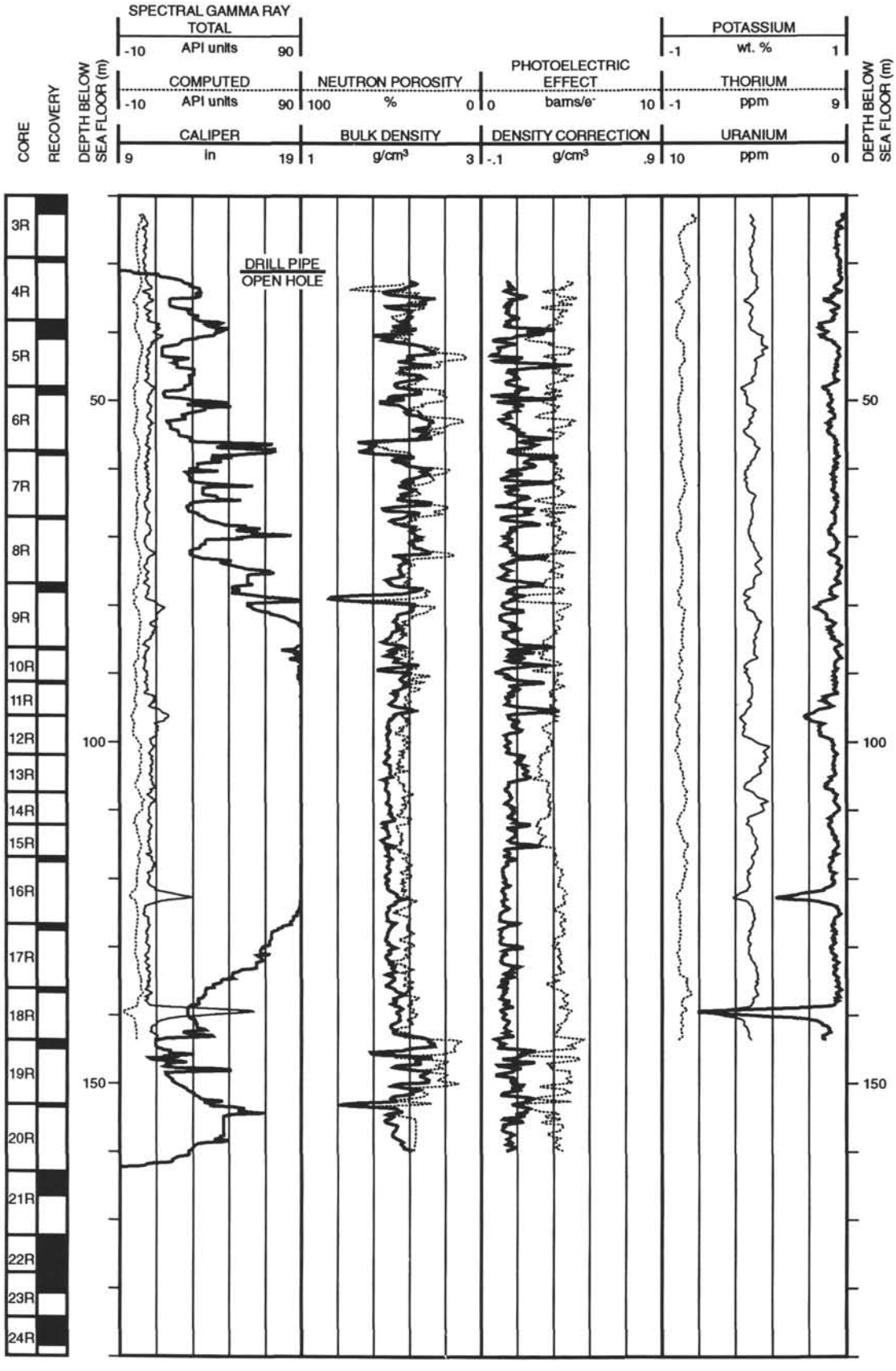

Hole 874B: Geochemical Log Summary

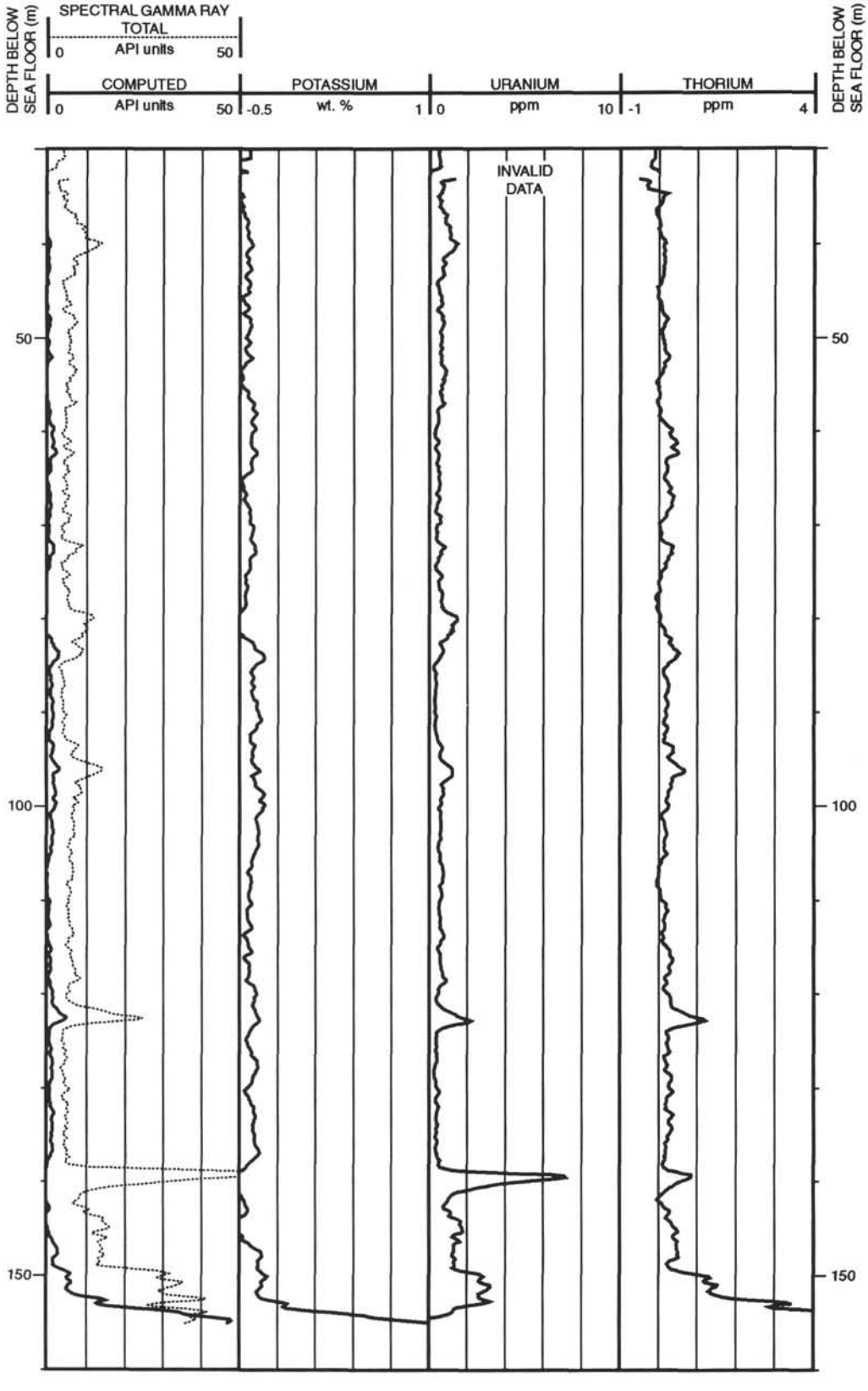

Hole 874B: Geochemical Log Summary